Catalytic on-board hydrogen production from methanol and ammonia for mobile application

vorgelegt von

Dipl.-Ing. Hary Soerijanto

aus Situbondo, Indonesien

Von der Fakultät II – Mathematik und Naturwissenschaften
der Technischen Universität Berlin
zur Erlangung des akademischen Grades
Doktor der Ingenieurwissenschaften
Dr.-Ing.

genehmigte Dissertation

Promotionsausschuss:

Vorsitzender: Prof. Dr. rer. nat. Martin Lerch, Anorganische Chemie der TU Berlin

Berichter/Gutachter:

Prof. Dr. rer. nat. Reinhard Schomäcker, Technische Chemie der TU Berlin

Prof. Dr. rer. nat. Thorsten Ressler, Analytische Chemie der TU Berlin

Tag der wissenschaftlichen Aussprache: 16. November 2007

Berlin 2008

D 83

Acknowledgement

At the beginning of my Ph.D. phase I did not even understand why a technician should be called as a Philosophiae Doctor. But let me tell you some interesting insights and understanding which were confessed during doing my Ph.D. thesis in order to show you, what is due to the people who allowed me to do and finish my Ph.D. Each of them enrich me in their own ways not only in scientific dimension.

I try to mention the thanks chronologically. In this point I would like to warn you, there are a lot of people to mention: beside nine people whom I lead into their scientific work and my four Professors, there is another Professor who is not my supervisor, but if he did not give me a job after I had my diploma, might be happended that the aliens department Ausländerbehörde would kicked me out before I started my Ph.D.

Professor Ziessow thought physical chemistry. He recomended me for a price because I had once the most points in a written test. As I rejected his nomination he told me: Let the others make the evaluation. Okay, then I did not tell him that I could just use Hamilton operator, but actually not more than that. In the phase during the project MOSES (mobile service for student) within the framework of Notebook University, I had also the chance to supervise laboratory experiments in physical chemistry. It was very interesting to find that the students complained about insufficient time for reading the theoretical preparation of the experiment while a supervisor has to handle with at least four experimental sets in one day. Professor Ziessow, I thank you for all these things.

I've written my diploma at TU Berlin in the work group of Professor Schomäcker. It is my demand that I work on a topic which is touchable and useful for the public. Biofuel was the first thing which came in my mind. Insofar hydrogen production for fuel cell application is a very welcome topic for me. At the beginning of my Ph.D. I've once told Prof. Schomäcker: at the end of my Ph.D. I would like to have a reformer prototype. He made a grin. I have to recognize that he was right!

One very pronounced character of Prof. Schomäcker is his attitude towards verification. Each measurement and study must be verified at least once more by another person in the next future. Furthermore: if there is something new written in the literature, it should be proven as far as possible. Such way to work prevent us from invalid conclusion. We accularate this approach unconsiously and prove our measuring instrument with simple methods.

Besides so many things that I learned during the last years, I would like to thank you deeply for your trust, for your help if I had problems with Ausländerbehörde (the foreign students know that such things put really stress each time) and for your care. I can barely say how much I thank you! It is not a farewell letter, but I would like to let you know that even the barbeque party at your home calls in a special way a nice feeling. There is nothing special talking about horn or making your kitchen entropically some degree higher, but it was precious moments which I enjoyed very much.

Without the financial support from Fritz Haber Institute and the supervision by Professor Schlögl my Ph.D. were impossible and much less invaluable. FHI is definitely an enrichment in many terms. I learned another administration system which is very well organized. The literature access is fantastic and allows an own class of literature culture. The legendary Fachbeirat, Ph.D.-Day, Conferences, Project Meeting, Group Meeting are some distinctive aspects which in their intensity and quality distinguishes FHI from other scientific institutes. The infrastructure at FHI Berlin is really enviably. If I made my poster at FHI, my TU colleagues were jealous if they see the surface and the print quality of FHI posters. In scientific area FHI Berlin exhibits an excellent hightech laboratory equipments and there are qualified experts as permanent employess! Professor Schlögl leads on the top of the Department of Inorganic Chemistry the scientific research and provides for competitive capability. One thing impresses me very much: whatever I tell Prof. Schlögl – even a quite special thing from technical chemistry – he knows everything!

In the end of my Ph.D. phase I could not interprete an experimental result. Prof. Schlögl solved my problem easily in seconds. He could see correlations quickly. Finding an evidence by unconventional - sometimes indirect - ways is one of his remarkable spezialised skills. This required a lot of knowledge, but at least the creative approach can be kept in mind.

First of all I thank you Professor Schlögl of course for the financial support and for all the scientific opportunity at FHI Berlin, for the discussion and the supervision. But it would not be complete if I would not mention the other sites of FHI Berlin: Weihnachtsfeier, Sommerfest, Weißwurst-Essen and Betriebsausflug. I am one of the people who noticed that boat trip last year was facilitated spontaneously. Thank you very much!

As mentioned above there is group meeting which at my case caused a shuttle trip between TU and FHI weekly. A move and latter a change in group name which was combined with a change of group leader and group affiliation were occured. A rearrangement has its nice sites. I got to know the members of the new work group better and since the number of the group member became bigger, we must not so often give a presentation. Since we are members of Department of Inorganic Chemistry of FHI, we knew actually each other. I knew the group leader Dr. Trunschke already from the previos organisation of Ph.D.-Day. She is a pragmatical and friendly person. The meeting atmosphere was comfortable and as a new member of the group I felt in a short time beein integrated in the group! Thanks a lot!

My former group leader at FHI had applied for a position as professor at TU Berlin, so at least I had one more professor as supervisor. Since the group meeting of my first work group at FHI Berlin took place once a week, Professor Ressler the one with the most meeting time with me. I very much appreciate the way he discusses the literature which was something new for me. I learned from him how to read a paper critically. And in point of writting a paper I would like to express my thanks. Since I am not the one who can good explain things in a convicing way, his help was very meaningful. One important thing to

say “thanks you” to Professor Ressler is that he supported me in the end phase of my Ph.D. as I meant I should present more data as evidences. In this context I would like to especially thank to Rolf Jentoft who showed interest in my work, tried to understand the problem and took time to discuss how to solve the problem or which investigations need to be done. Thank you Rolf! Generally I thank the member of previous Ressler-Group. Normally near the end phase of Ph.D. a longer talk was possible. Benjamin, Alexandra, Jürgen, Olga, Eva and also Patrick all of you merit my thanks!

As I signed my contract at FHI Berlin I was wondering that the project sounded somehow new for me. Surprise, surprise! I had an extra supervisor: Professor Lerch. The testing of zirconia oxynitride was at the beginning not easy. There were problems refered to the compability of equipments and catalyst insufficiency. There were not to many publication about ZrON and the existing papers had reference to the papers of Prof. Lerch. Prof. Lerch is definitely leading in this topic. It was so frustating that I was moved to tears after a talk at FHI because I did not get the support which I needed. But as the project would be given up and new devices were installed, it worked. I still remember: it was almost 2 am and I danced around the laboratory table twice before informed Prof. Schomäcker per Email: “It jumps!” In the course of time a patent was applied from this study. I do not know how to rate a patent, but my parents were very happy. This means much for me. That is why I would like to speak a special thanks for you Prof. Lerch. My thanks apply also to Chistoph Rödel and Nancy Frenzel who sythetized the ZrON catalysts.

I would thank Professor Antonietti and his co-workers from the MPIKG Golm for the preparation of $Cu/CeO_2/ZrO_2$ catalysts which were used in tested for the Steam Reforming of Methanol.

Having a status of shuttle student is at the beginning a little bit confusing: the focus of interest at TU Berlin is the application of catalyst at preferably high conversion while at the FHI the areas of small structures are investigated to gain the correlation of a defined change of a factor to the reaction. But at least it was a big advantage for me moving over the lines and received more than an impression. If I now

read a paper, I see the data more critically because a result from a microreactor could not always be taken as a reference for a reactor system near industrial scale which could easily had a heat accumulation which could impact to the catalyst features. Comparison of internal measurements had shown this aspect clearly.

It is very helpful knowing how the preparation-people think and to learn which factors have impact on the performance of a catalyst. The result can be better interpreted and understood.

During the past years I was responsible for following persons whom I at least leaded into their scientific work in the work group of Prof. Schomäcker: Benjamin, Agnes, Ada, Natalie, Stéphane, Yücel, Sebastian, Thorsten, Anne. Thanks for the cooperation, for the questions and discussions.

Thanks also to the former and actual members of work group of Prof. Schomäcker. It is nice to hear the greetings, to play bowling, to cook and eat together or go to conference together. I do not know if I mean anything for my colleagues, but I enjoy every claps from Oliver, the guys accept that I have no interest on playing table soccer, I could speak my mind about some manner and anyhow they said sometimes that they were happy to see me. It is a quite congenial circumstances. Even a master student from abroad could within three months fool around with us and deliver his report on time. Especially I thank Gabriele Vetter for her help to repair and maintain the experimental devices and purchase the technical equipments and chemicals. And also for the talks & invitations. In this opportunity I would like also distinguish Benjamin and Marian. A lot of thanks for Benjamin especially for the team work and helpful suggestions. Thank you Marian for the data recovery and generally for your support. Many thanks to Prof. em. Hugo for your kindness to help me & to revise my Ph.D.-presentation.

One of the reasons why I wrote a Ph.D. thesis besides the curiosity and interest on the meaningful topic is the feeling that I knew to little about my subject. I could not say that I have sufficient knowledge now since the small wish at the beginning to develop a reforming prototype is not achieved. But having the experience to implement an absolute new

laboratory experiment well, to handle a new research topics, to develop a new reaction arrangements helps me to build a moderate self-confidence up. Moreover I developed a sense of a purpose and integral point of view. The CO_2 problem is based on the fact that the produced CO_2 are more than the capacity of plant to convert and there is no other system which can recover oxygen from carbon dioxide just by means of sun light. The approach to reduce the production of CO_2 like the european emission trading is a good idea. In contrast: storing CO_2 underground like the EU-aided CO_2SINK project is not a solution and that is not just because this method eludes inevitably oxygen from the atmosphere. But who cares about this easy mathematical balance? The dinosaur which need more oxygen content for their living are already died off. But precisely this paradigm and the emotional aspect provide in real terms a pragmatical solution. New driving feeling of fuel cell cars and moderate speed or power have more chance to be heard as a simple mathematical ballance. Discovering the truth is actually an attribute of scientist, but at a point the adventure ends. I am finally very happy to have Professors in such diversity who show me the beauty of scienctific matter and the reference to the application with all its aspects. Daring act to put anything basic if into question, asking whether something makes sense, and dealing with crises are critical atitudes which I owe to my supervisors. My sincere thanks Prof. Schomäcker, Prof. Schlögl, Prof. Ressler and Prof. Lerch!

I doubt if my brothers, my sister or my parents understand why I did not prioriate the time in finishing my Ph.D., but they pray for me and at least I have the time to prove my data and to give the conclusion more base by furhter experiments. It is very important for me, that I do not write what I am not commited to. Knowing that someone else pray for me is a beautiful feeling. Dad, Mom, dear brothers and sister: Thank you for everything! May God bless you and give me chance to make you very happy. I dedicate this work to my parents and my sister Ita.

Hary Soerijanto
Berlin, September 2007

Table of Contents

Acknowledgement i

Table of Content vii

Abstracts x

1. Introduction 1

1.1. Fuel Cells 4

1.2. Reformer 8

1.3. Heterogeneous catalysis 9

1.4. Kinetics 17

1.4.1. The power law rate equations 18

1.4.2. Langmuir-Hinselwood and Eley-Rideal rate laws 20

1.5. References 23

2. Steam Reforming von Methanol

2.1. Kinetic study of SRM over Cu/ZrO_2/CeO_2 catalysts 25

2.1.1. Introduction 26

2.1.2. Experimental 28

2.1.2.1. Catalyst Preparation 28

2.1.2.2. Catalyst Characterization 30

2.1.2.2.1. X-ray fluorescence analysis (XFA) 30

2.1.2.2.2. N_2 adsorption-desorption 30

2.1.2.2.3. N_2O decomposition 30

2.1.3.2.4. X-ray diffraction (XRD) 32

2.1.2.3. Catalytic test reaction 32

2.1.3. Results and Discussion 34

2.1.3.1. Catalyst characterization and long-term stability 34

2.1.3.2. Kinetic model 40

2.1.4. Conclusions 56

2.1.5. References 57

2.2. Autothermal reactor concept for SRM 61

2.2.1. Introduction 61

2.2.1.1. Autothermal reforming of methanol 64

2.2.1.2. Knudsen membrane 66

2.2.2. Experimental 73

2.2.2.1. First experimental set up 73

2.2.2.2. Second experimental set up 74

2.2.2.3. Third experimental set up 75

2.2.3. Result and discussion 78

2.2.4. Outlook 81

2.2.4. References 82

3. CO free Hydrogen Production from Ammonia over Zirconia Oxynitride

3.1 Introduction 84

3.2. Experimental 85

3.2.1. Catalyst Preparation 85

3.2.2. In situ XRD 86

3.2.3. Catalyst testing 87

3.2.4. X-ray photoelectron spectroscopy (XPS) 90

3.3. Result of catalyst testing and catalyst characterization 91

3.5. Kinetic study 99

3.6. Result of kinetic study 99

3.7. Reaction mechanism 102

3.7.1. The role of anion vacancies, nitrogen concentration and ion conductivity 103

3.7.1.1. Catalyst preparation & characterization 105

3.7.1.2. Catalyst pretreatment 106

3.7.2.3. Result of catalyst testing and mechanismus study 108

3.7.2. TPR study 109

3.8. Reaction kinetics 112

3.9. Conclusion 120

3.10. References 121

4. Summary 123

5. Appendix 126

5.1. Madonna – Simulation (450 °C) / mechanistic model 126

5.2. List of Abbreviations & Greek Symbols 127

5.2.1. List of Abbreviations 127

5.2.2. List of Greek Symbols 129

Abstract

This PhD thesis deals with the catalytic hydrogen production for mobile application, for example for the use in fuel cells for electric cars. Electric powered buses with fuel cells as driving system are well known, but the secure hydrogen storage in adequate amounts for long distance drive is still a topic of discussion. Methanol is an excellent hydrogen carrier. First of all it has a high H:C ratio and therefore a high energy density. Secondly the operating temperature of steam reforming of methanol is comparatively low (250 °C) and there is no risk of coking since methanol has no C-C bond. Thirdly methanol is a liquid, which means that the present gasoline infrastructure can be used.

For the further development of catalysts and for the construction of a reformer it is very important to characterize the catalysts very well. For the dimensioning and the control of an on-board production of hydrogen it is essential to draw accurately on the thermodynamic, chemical and kinetic data of the reaction. At the first part of this work the mesoporous $Cu/ZrO_2/CeO_2$-catalysts with various copper contents were characterized and their long-term stability and selectivity were investigated, and the kinetic data were determined.

Carbon monoxide is generated by reforming of carbon containing material. This process is undesired since CO poisons the Pt electrode of the fuel cell. The separation of hydrogen by metal membranes is technically feasible and a high purity of hydrogen can be obtained. However, due to their high densitiy this procedure is not favourable because of its energy loss. In this study a concept is presented, which enables an autothermal mode by application of ceramic membrane and simultaneously could help to deal with the CO problem.

The search for an absolutely selective catalyst is uncertain. The production of CO can be neither chemically nor thermodynamically excluded, if carbon is present in the hydrogen carrier. Since enrichment or separation are unfavourable for energetic and economic reasons, it is reasonable to investigate another reaction system, which is free of carbon. At the last part of this study the catalytic production of hydrogen from ammonia cracking was investigated. Ammonia is an interesting alternative: it has a high hydrogen densitiy, it is available and cheap. Since the Pt electrode is sensitive to reactive substances, it must be ensured, that for example no hydrazine is produced during the ammonia cracking .

A new type of ammonia cracking catalyst was investigated in this study, which unlike the conventional catalyst is not based on metal. Four different zirconium oxynitrides: ß' ZrON, ß" ZrON, Zr_2ON_2 and $Zr_{0.88}Y_{0.12}O_{1.72}N_{0.15}$ (Y_2O_3 doped ZrON) were prepared by various methods and subsequently tested for their activity in ammonia cracking. A long-term study was carried out on the best catalyst and no hydrazine was detected. On the basis of the data from the accomplished investigations a reaction mechanism is proposed. The result provides a basis for the further improvement of the catalyst.

Zusammenfassung

Diese Doktorarbeit befasst sich mit der katalysierten Herstellung von Wasserstoff für Anwendungen in Brennstoffzellen, genauer gesagt für mobile Einsätze. Elektroautos mit Brennstoffzellenantrieb sind keine Neuheit mehr, nur die Frage, wie Wasserstoff in ausreichender Menge und sicher gespeichert werden kann, ist Gegendstand einer regen Diskussion. Methanol gilt als ein hervorragender Wasserstoffsträger. Erstens weist Methanol mit seinem hohen H:C Verhältnis eine hohe Energiedichte auf. Zweitens ist die Betriebstemperatur bei der Reformierung von Methanol um die 250°C vergleichsweise niedrig und es besteht keine Verkokungsgefahr, da Methanol keine C-C-Bindung enthält. Drittens ist Methanol flüssig, so dass man nicht in neue Infrastruktur investieren müsste.

Für die weitere Entwicklung von Katalysatoren im Allgemeinen und für die Auslegung eines Reformers ist es von großer Bedeutung, dass man den verwendeten Katalysator gut kennt. Für die Dimensionierung und Regelung einer on-board Produktion von Wasserstoff müssen die thermodynamischen, chemischen und kinetischen Daten herangezogen werden. Im ersten Teil dieser Arbeit wurden mesoporöse $Cu/ZrO_2/CeO_2$-Katalysatoren mit verschiedenen Kupfergehalt charakterisiert, auf ihre Langzeit-Stabilität und Selektivität untersucht, und ihre kinetischen Daten ermittelt.

Bei der Reformierung von kohlenstoffhaltigen Ausgangsstoffen wird immer Kohlenmonoxid gebildet, das schädlich für die Pt-Elektrode in Brennstoffzelle ist. Die Abtrennung von Wasserstoff mittels Metallmembranen kann zwar für hochreinen Wasserstoff sorgen, aber wegen ihrer hohen Dichte ist diese Maßnahme mit hohen Energieverlusten verbunden. In dieser Arbeit wird ein Konzept vorgestellt, das unter Anwendung von Keramikmembranen autothermalen Betrieb ermöglichen und gleichzeitig die CO-Problematik bewältigen helfen könnte.

Die Suche nach einem völlig selektiven Katalysator ist ungewiss. Chemisch und thermodynamisch gesehen ist die CO Bildung nicht auszuschließen, falls in der Wasserstoffquelle Kohlenstoff enthalten ist. Da eine Anreicherung oder Trennung energetisch und wirtschaftlich ungünstig ist, ist es einen Versuch wert, ein anderes System zu erforschen, das keinen Kohlenstoff enthält. Im letzten Teil dieser Arbeit wird die Gewinnung von Wasserstoff aus dem katalysierten Abbau von Ammoniak untersucht. Ammoniak ist eine interessante Alternative: es hat eine hohe Wasserstoffdichte und ist bereits gut verfügbar. Da Platinelektroden sensitiv gegen reaktive Stoffe sind, ist zu gewährleisten, dass z.B. kein Hydrazin beim Abbau Ammoniak entsteht.

In dieser Arbeit wurde eine neue Art von Ammoniakkatalysatoren erprobt, die im Gegensatz zu herkömmlichen Katalysatoren nicht auf Metal basieren. Vier verschiedene Zirconiumoxidnitride: ß' ZrON, ß" ZrON, Zr_2ON_2 and $Zr_{0,88}Y_{0,12}O_{1,72}N_{0,15}$ (Y_2O_3 dotierter ZrON) wurden auf verschiedene Weise synthetisiert und getestet. Eine Langzeitstudie an dem besten Katalysator wurde durchgeführt und dabei kein Hydrazin detektiert. Ein Reaktionsmechanismus wird anhand der Daten der durchgeführten Untersuchungen vorgeschlagen. Das Ergebnis dient als Grundlage für die weitere Optimierung des Katalysators.

1. Introduction

One of the biggest challenges of our century is an adequate energy supply, which is important for our living standard, especially for our mobility and security. On the first sight, it could be said that there are still big amount of oil and natural gas resources in the world and some oil reserves turned into oil resources since the oil price became higher and higher. The high price of oil and new technical progress allowed the exploration in difficult regions by means of expensive methods. Furthermore: in consequence of global warming the arctic ices would melt away and we can explore gas reservoirs in this region. But it would be a great pity, if the next generations could not take a walk in Venice anymore or the polar bears just could be seen in zoos. But fact is that everyone can really see a result of global warming clearly: potatoes can cultivated in Greenland since some areas are not covered with ice any longer and the climate gets milder. It does not sound like a bad news, isn't it? But some degree higher could cause a terrible drouth at the other side of the earth. And that is in no case a good news.

In the recent years USA sells the wars in middle east as a campaign against terorism and while the people still can keep smiling watching the Ice Age II, we must begin to think about a new energy strategy due to provide the economic growth and to maintain the security stability in our countries. Please keep in mind that the golden dragon and the king cobra in Asia keep grazing the unrenewable fossil fuel all over the world and supplementary the conflicts in oil regions drive the petroleum price high and higher, and at least Russia greeted the New Year 2006 by turning the gas valve for the people in Ukraine off. All of these political and economical aspects constrain the politicans to appreciate renewable energies better. For the sake of ecological correctness: the ones with zero CO_2 balance.

Sure: the atomic energy doesn't produce carbon dioxide (if we neglect the energy intensive enrichment of Uran), it is economically excellent and technically secure. But what about the atomic waste and

don't 9/11 and the actual Iran conflict show us clearly the problematic of this kind of energy?

Depend on the geographical nature of a region, we should create and use respectively the best and suitablest techniques to answer the energy affairs. Geothermal or hydroelectric power plants, wind generator, solar cells etc. could be implemented if the resources available. Prof. Antonietti from Max-Planck-Insitut für Kolloid- & Grenzflächenforschung reported recently the production of coal powder from biomass by hydrothermal carbonization. Biomass was heated to 180°C with water and citrid acid or iron as catalyst in a hermetically closed reactor under exclusion from pressure and air for 12 h. Sure, it is a way to create renewable fuel with zero CO_2 balance, which actually was invented for the first time by Max-Planck-Insitut für Kohlenforschung some years before. But for mobile application there are indeed just two alternatives: gas or fluid fuell from bioproducts. The following Table 1.1 shows a litte overviews of the bio fuels for the mobile application – the main topic in this work:

Biofuel	**Annual Yield / ha**	**Cruising Range**	**Efficiency**
Biodiesel - RME	1300 Liter	23660 km	91% of petro-diesel
Bioethanol	2500 Liter	33000 km	66% of gasoline
SundDiesel (BtL)	4050 Liter	75330 km	93% of petro-diesel
Biomethane	3650 kg	99600 km	140% of gasoline

Table 1.1: Comparison of some green fuels; BtL = Biomass to Liquid

Germany has produced 1,3 millions tons Rapeseed Methyl Ester (RME) in 2005, using 10% of his agricultural area. It is biggest biodiesel producer of the world. But even if Germany use the maximal area of the available field for this purpose, the maximal exploitation would just gain 3 million tons RME since the annually need are 130 millions tons petro oil. The only country which prosperously uses biofuel in appreciable amount is Brazil: its bio ethanol production covers 40% of its fuel need. SunDiesel and biomethan have a better prospect, but in all cases, we should not just think about the zero CO_2 ballance, but also the ethical and other ecological aspects. A massive cultivation of palm trees due to produce bio diesel would destroy the biodiversity and the wildlife habitat.

There is another fuel medium, which is ethically, ecologically and energically very excellent: hydrogen. It could be produced electro-chemically for example by solar cells. The combustion of hydrogen in fuel cell produces just water. But the storage of hydrogen is very expensive: either it must be liquefied at -253 °C or be compressed at 700 bar. For this purpose we can not use the infrastructure of natural gas stations which compress methan just at 200 bar. Natural gas is ecologically cleaner and economically cheaper than gasoline, but however these two arguments are not sufficient to promote natural gas to achieve acceptance in politics and society.

A new energy carrier could have a real chance to get acceptance if it is in liquid form and has a good efficiency. Methanol meets these requirements. It is a liquid and no investments for infrastructure are necessary. After reforming into hydrogen, it could supply the fuel cell, which has an outstanding efficieny. Who drives a hybrid car knows how great the new driving feeling in a fuel cell car could be: noiseless driving comfort, and don't forget: BMW has showed that a fuel cell car could break the 300 km/h limit. Methanol has indeed excellent properties: it has a high hydrogen density, it has no C-C-bond and its reforming temperature is moderate.

However there are still problems to solve: CO as byproduct at methanol steam reforming could harm the Pt-electrode in the fuel cell unit. A less sensitive Pt-electrode or more selective catalysators need to be found. A chemical solution is hard to find, but we can try to minimize the CO production or solving this problem by reaction engineering.

Another interessting hydrogen carrier is ammonia. Since it is gaseous, it doesn't fullfill the first criteria and is not suitablle for automobile application, but it contains no carbon (also: no CO production) and could be use for small mobile application like laptop battery. And since ammonia could be produce from urea, which is a non explosive material, it is interresting for some deployments.

It is truly not a big news: "Fossil fuels are not renewable". It's as breathtaking as „Smoking kills" which is written over every pack of cigarettes. But they have no meaning untill one gets really sick or petroleum gets really shorter and it became so rare and so expensive. And even I believe that we should solve the energy problem regionally and we should save energy where we can, we have to find an alternative to replace the gasoline for mobile sector. More than the half of world fuel consumption is burned on the streets by cars.

In this study the production of hydrogen from methanol and ammonia is investigated. The kinetic data of the reaction systems and the properties of the used catalysts are determined. They provide a basis for the construction of technical application and for the further studies. An autothermal reactor concept for SRM and the reaction mechanism of ammonia decomposition over zirconia oxynitride are proposed in this study.

1.1. Fuel Cells

Some business people doubt the efficiency of fuel cell cars by asking why we should first convert the fuell into hydrogen then oxidize it into water instead of burning the fuell from the begining. But we should know that burning fuel in a furnace or an internal combustion machine and converting this thermal energy to mechanical energy in a piston or turbine – then a dynamo or generator produces electricity - is an inefficient process: only to 30-40% efficiency. All fuel cells convert the chemical energy into electric energy with a higher efficiency, since they are not constrained the maximum of the Carnot cycle because they do not operate with a thermal cycle like the heat or combustion engines do. Moreover fuel cells combine highly efficient generation of electrical energy with low emissions.

Any exothermic reaction can be converted into electicity if suitalbe electrodes and an electrolyte supporting the reaction can be found. The most used membrane in PEMFC is Nafion (a sulfonated polytetrafluorethylene, 400 Euro/m^2) which was discovered and produced by the french company DuPont. Ballard Power Systems uses Solupor (a porous sulfonated polyethylene) which is produced by Dutch State Mines. The low priced membrane is produced by a company ITM Power PIc in UK. The ITM Power membrane (a hydrocarbon polymer) costs just 4 Euro/m^2 and it should have three times ionic conductivity than Nafion.

A PEMFC unit produces a voltage of 0.6-0.7, which is quite low. In order to yield higher voltage the units must be combined in series. Parallel circuits of PEMFC allow to produce a stronger current. For the application the units are arranged to form a fuel cell stack which can deliver the desired amount of energy. Beside the power and the operating efficiency, an automotive fuel cells should perform a durability of 5,000 hours (the equivalent of 150,000 miles).

An overview of common technical fuel cells is listed on Table 1.2.

	PEMFC	AFC	PAFC	MCFC	SOFC	DMFC
Fuel supply	H_2/ reformate	H_2/NH_3	H_2/ reformate	H_2 /CO/ reformate	H_2 /CO_2/ CH_4/ reformate	reformate ($MeOH+H_2O$)
Electrolyte	Polymer	KOH(l)	H_3PO_4-Gel	molten Li/Na-Carbonat	Y/ZrO_2 ceramic	PEM-unit
Charge carrier	H^+	OH^-	H^+	CO_3^{2-}	O^{2-}	H^+
Reformer	external	NH_3-cracker	external	external/ internal	external/ internal	external
Oxidant	O_2/Air	O_2/Air	O_2/Air	CO_2/O_2/ Air	O_2/Air	O_2/Air
Operating temperature	60 -120°C	60 - 200°C	150 - 220°C	600 - 700°C	800 - 1000°C	60 -120°C
η	40-50%	60-70%	40-50%	50-60%	40-80%	40% (<1kW)

able1.2: Comparison of technical fuel cell systems (PEMFC = Polymer Electrolyte Membrane Fuel Cell, AFC = Alkaline Fuel Cell, PAFC = Phosphoric Acid Fuel Cell, MCFC = Molten Carbonate Fuel Cell, SOFC = solid Oxide Fuel Cell, DMFC = Direct Methanol Fuel Cell)

The general scheme of a fuel cells contains two electrodes where the electrochemical reaction take place separated by an ion conducting electrolyte. At PEMFC Pt or Pt-alloys deposited on carbon particles (10-50 μm) act as the electrodes and nafion as the proton-conducting membrane (electrolyte, 50 – 200 μm). Pt could be poisoned by carbon monoxide. Due to its high affinity to Platinum CO can block the active

surface and therefore make the adsorption of hydrogen on anode or oxygen on the cathode impossible. A purification step is absolutely required if the hydrogen is produced by on board/on site reforming and the formed CO in the product gas is higher than 50 ppm. The new generation of fuel cell electrodes are less sensitive for CO but it is still desirable and necessary to remove the carbon monoxide to keep the performance of the fuel cell at a high level.

The electrode reactions are: Anode: $H_2 \longrightarrow 2H^+ + 2e^-$ (1)

Cathode: $O_2 + 4H^+ + 4e^- \longrightarrow 2H_2O$ (2)

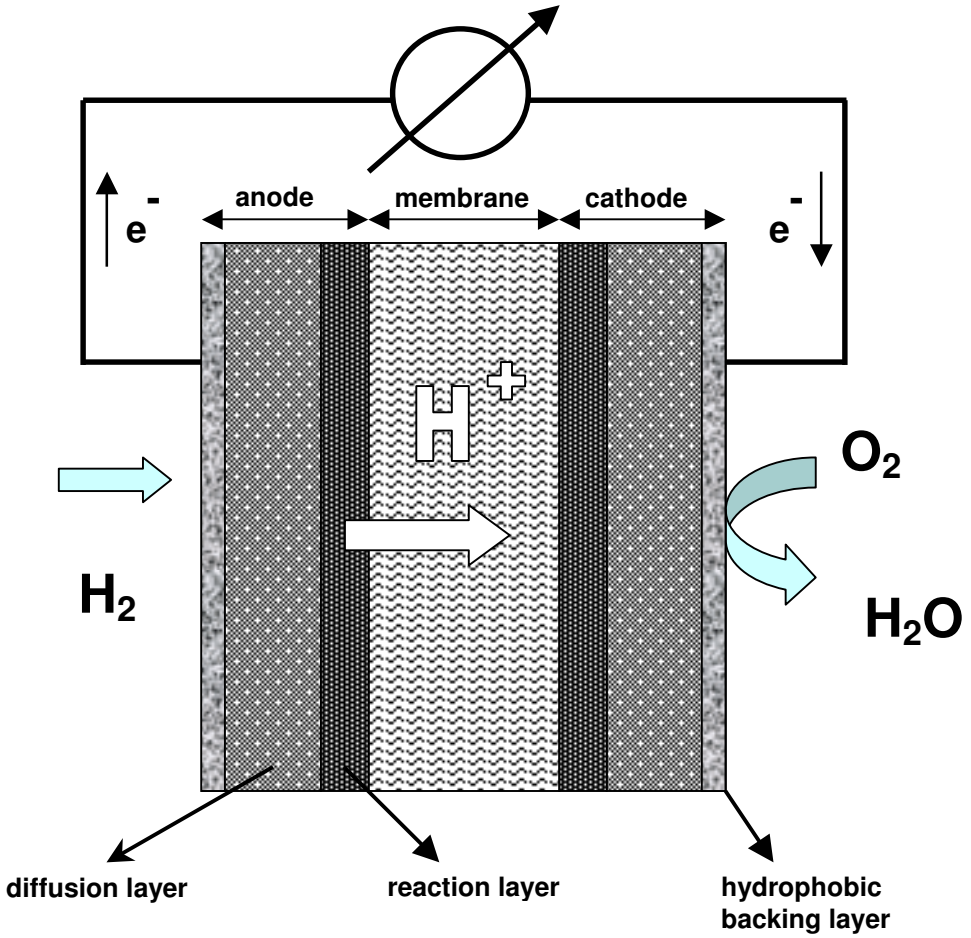

Figure 1.1: Scheme of a PEMFC

1.2. Reformer

Hydrogen can be supplied directly as gas in fuel cell cars or it can be produced on board from various hydrogen containing chemicals. The petrochemical companies produce hydrogen from methane, which has the highest hydrogen-to-carbon ratio among the carbon based materials. But the production of hydrogen from methane with nickel catalyst must be carried out at high tempertures of 900°C. This aspect and the fact that we have to invest much money for new infrastructure, make this alternative not attractive for fuel cell vehicles. Dimethylether (DME) as fuel source fullfill the requirement that it is in liquid form at ambient temperature and its energy content is higher than bioethanol, but as hydrogen source it is a weak candidate because dimethylether is a product of dehydration of methanol:

$$2\ CH_3OH \rightleftharpoons CH_3OCH_3 + H_2 \qquad \Delta H_R = 23{,}4\ kJ.mol^{-1} \qquad (3)$$

and on its refoming it must be in the first step hydrolized to methanol by using solid acid catalyst [1]:

$$CH_3OCH_3 + H_2O \rightleftharpoons 2\ CH_3OH \qquad \Delta H_R = 37\ kJ.mol^{-1} \qquad (4)$$

then in the second step converted to hydrogen in SRM [2]. It has really no sense to convert methanol to dimethyl ether and subsequently reconverts it backwards to methanol at DME-SR. The most suitable candidate is therefore methanol itself. It has high hydrogen density, it is a liquid, and its reforming process to hydrogen occurs at quite low temperatures.

The main focus of this study was first the hydrogen production from methanol and subsequently we introduce an approach to handle the carbon monoxide problem.

Since the reforming of methanol is a endothermic process, it needs a heat supply. Latest constructions of reformers were designed for an autothermal process. Folded or plate-fin reformer (PFR) combine evaporator, combustion and reforming component into a compact device. The feed is not driven to full conversion. A fraction of methanol would be burned due to heat supply for evaporating the feed and keeping the refoming part at SRM temperature. In fact for the start period the reformer needs an external heating source, which can be overcame by an electrical heater [3].

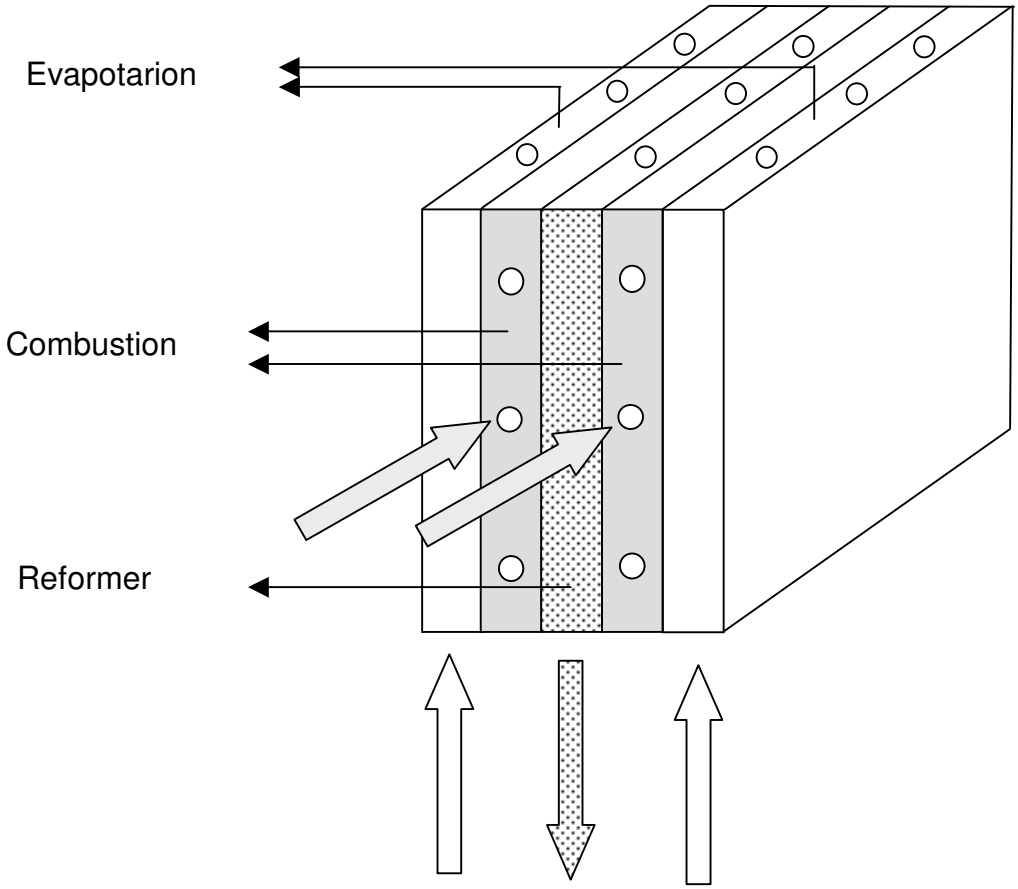

Figure 1.2: Scheme of a plat-fin reformer (PFR)

1.3 Heterogeneous Catalysis

Many reactions are kinetically inhibited even if they are thermodynamically allowed. A reaction cannot occur - even if it is an exothermic reaction – if its activation energy is too high. In such cases we need a catalyst which can lower the activation energy by providing

energetically favourable pathways in which the activation barriers of all intermediate steps are low compared to the activation energy of the gas phases reaction. This fact has two consequences:

1. Depending on how much a catalyst can lower the activation energy or respectively increase the reaction rate, the conversion of the catalysed reaction at certain conditions can be very different. But for reversible reactions it can only accelerate the rate of the reaction until the equilibrium state is achieved. The composition of the equilibrium state is thermodinamically predefined.
2. Depending on which reaction path ways a catalyst prefers, the selectivity of the reaction could strongly differ. An example of this case is the mechanism of methanol steam reforming [4].

The energy diagram in following figure gives an impression of the function of a catalyst, whereas the consecutive reaction steps are simplified just as a single reaction.

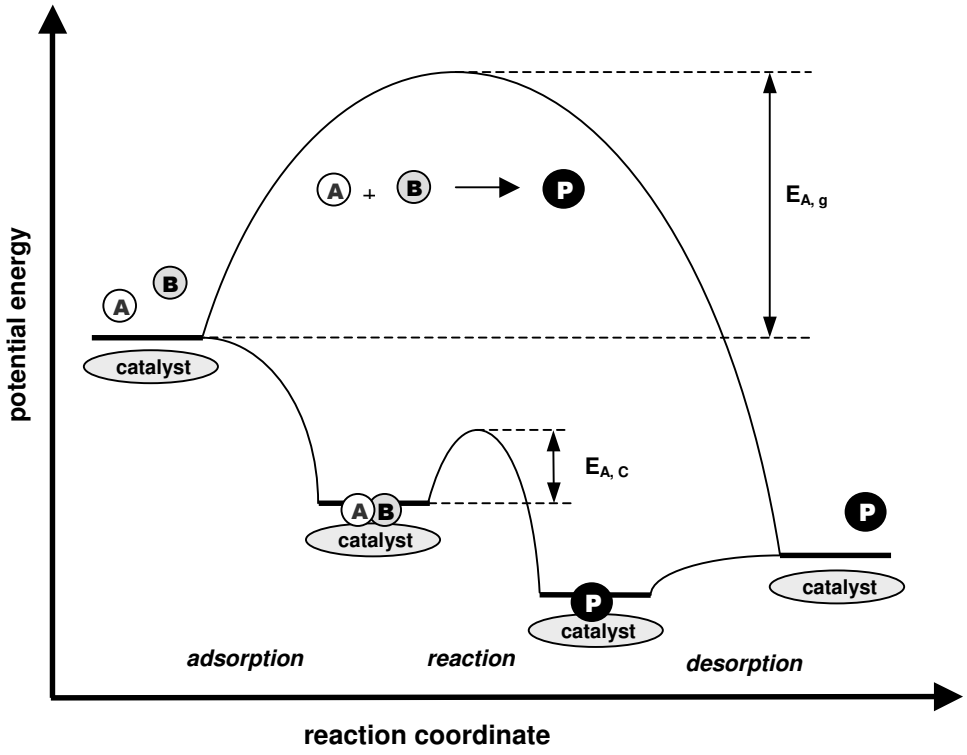

Figure 1.3: Potential energy diagram of a heterogeneous catalysis with gaseous reactants and products over a solid catalyst. $E_{A,g}$ = activation energy of gas phase reaction; $E_{A,C}$ = activation energy of catalysed reaction

Heterogeneous catalysis begins with the adsorption – this is always an exothermic process – of at least one of the gases whose intramoluecular bond are broken or weakened and after reacting with the other species in several consecutive steps at the surface of the catalyst, the products desorb into the gas phase and thereby generate the active sites for the following catalytic cycle. A catalyst should therefore have a high affinity to adsorb the reactans but a low affinity for the products in order to enable the desorption of the products and generation of free active sites. If we use a diluting gas, we should choose one which has a low affinity to the catalyst or its support material.

The following figure shows the synthesis of ammonia over iron catalyst schematically. Nitrogen (big spheres) and hydrogen (small, dark spheres) undergo first a dissociative adsorption, then nitrogen and hydrogen combine in a series of consecutive reactions to form ammonia at the surface of catalyst, and at least the ammonia molecule will be desorbed into the gas phase and this simultaneously regenerates the active sites. More details about the mechanism of ammonia synthesis will be presented in the chapter about the ammonia cracking.

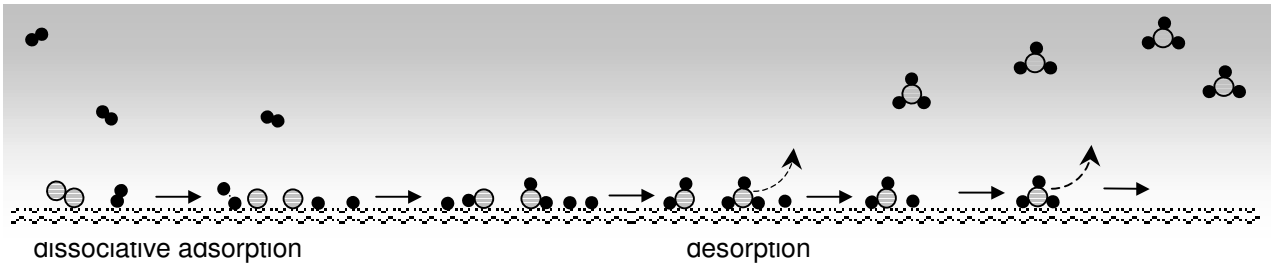

Figure 1.4: Scematic presentation of ammonia synthesis over iron catalyst

As the catalitic reactions occur at the surface, it is desirable to produce catalysts with high specific surface area. This can be achieved by synthezing catalysts with small partical sizes or high porosity. The fine catalyst particles can be achieved by various techniques, for

examples: spray dry or by generating nano particles via ultrasonic vibration. But fine powders can cause an undesired pressure gradient over the catalyst bed or it could be blown out of the reaction zone which means catalyst lost and the need to separate it from the product. Impragnation or dispersing active species on inert particles such as carbon, alumina, titania, porous silica or zeolith are common methods to obtain a high fraction of surface atoms. It must be mentioned that carbon has a disavantage, because its layer structure allows carbon not to be pressed to an extrudates or bigger particles in order to avoid the mentioned pressure problem. Some catalysts are produced by means of spongelike polymer templates which are burned away in the calcination step and thus generate a catalyst with high porosity. But the porosity has to meet two challenges:

1. If the pores are too small for the reactants, there is no efficient mass transfer of the reactants and second: the resulting difussion limitation is not desired, because it results in losses in activity and selectivity.

2. As showed for ammonia synthesis which is carried out at 500 °C and 200 bar, the catalyst must have a stability against high temperature and pressure. Accurately, a catalyst must stable against large temperature and pressure fluctuations, and further it must possess a high mechanical strenght.

The second challenge can be solved by using stable chemical support. Zirconia for example is a good candidate because it is robust and inert. A good method to exclude the diffusion limitation is impragnating the catalyst on a inert dense material. Such materials are refered to as egg-shell catalysts, which contain the catalyst just at the outer surface of the inert support materials.

The requirements for a good catalyst are defined by its activity, selectivity and stability against hight temperatures and pressures. But high surface area, big pores and thermal or pressure stabiltiy are just physical and mechanical aspects of the catalyst. To design a good

catalyst, we have to understand how the catalysis works at atomic scale: the microscopic level of research in catalysis.

At microscopic level, we have to look more precisely at the adsorption at the surface and the reaction mechanisms. First we should know the surface and bulk composition, its morphology and crystal structure. The ammonia synthesis can be carried out with a unsupported iron catayst. This system is comparatively simple in contrast to more complex catalyst systems, such as MoVTeNb catalyst for propane oxidation to acryl acid. In such cases we develop a model catalysts, then try to use in situ techniques to investigate the mechanism of the reaction. But this approach still has a material and pressure gap. Nevertheless we could get informations which help to understand catalysis and finally help us to develop or optimize a catalyst. However the question about the active center and which species are the real catalysts is not trivial.

The methanol steam reforming is catalysed by copper based catalyst. The fresh copper oxide systeme must first be activated by reduction and even at the end of the reaction we still find copper metall. This reduced species is directly active for methanol steam reforming. But we know exactly that it doesn't work if we use just copper powder. There must be some reasons why the atoms at the surface are active or more active than the atoms in the bulk and why copper powder does not catalyse methanol steam reforming.

Between the atoms at the surface and in the bulk there are differences in the electronic and vibrational properties. The atoms in the bulk have saturated coordination shells while the atoms at the surface have fewer neighbours and unsaturated coordination spheres. The number of missing neighbours is denoted as Z_s. An atom in the face-centered cubic (111) or hexagonal closed-packed (001) surface has 6 neighbours in the surface and 3 below, but misses 3 neighbours above. Such atoms have also $Z_s = 3$.

The unsaturated coordination is the reason why the electronic and vibrational features and in some cases also the crystalographic

positions of surface atoms differ from those of the bulk atoms. These are also the reasons why an element in various crystalographic position could have very different sticking coefficient, which is responsible for the first step of the catalysis process: the adsorption. We could also say that the sticking coefficient expresses the affinity beetween the gas and the atoms at the surface of the catalyst. The more an atom has unsaturated coordination, it has more potential to be a reactive center for catalysis. But if the sticking coefficient is to high, the reactant wil just sticks on the surface and there will be no further reaction.

Surface position	Z_s	N
hcp (001)	3	12
fcc (111)	3	12
fcc (100)	4	12
fcc (110)	5	12
bcc (110)	2	8
bcc (100)	4	8
bcc (111)	4	8

Table 1.3: Number of unsaturated coordination of surface species in depedency of its surface position. Z_s: number of missing neighbours on the surface; N: number of neigbours in the bulk at saturated coordinatio; bcc: body-centerd cubic, fcc: face-centered cubic, hcp: hexagonal closed-packed

Microscopically, surface species are less active than edge atoms. Furthermore, the atoms at corners are more active, but the best ones are atoms in kink position. It seems that atoms in this position have the perfect properties that they are attractive enough for the reactants and do not bind the intermediates strongly that the reaction steps can occur easely. An example for an illustration is the structure sensitive reaction

of NO and CO over Rhodium, whose structure is fcc. The Z_s of Rh(111) is just 3 and Rh(100) has a higher number of missing neigbours: $Z_s = 4$, so even both of them adsorb in relatively similiar amount of NO and CO, the Rh(100) is the more reactive one because it has higher number of unsaturated coordination. And it is observed that Rh(100) already oxidize CO to CO_2 at 300 K, since most of CO on Rh(111) desorbs unreacted and the CO_2 formation does not begin under 400 K [5]. But if we summarize the activation energy of the dissosiation of adsorbed NO, the reaction of CO_{ads} and O_{ads} to CO_2 and the E_A of nitrogen production from adsorbed nitrogen atoms, we can see clearly that Rh(111) with totally 250 kJ/mol is the better one than Rh(100) with accordingly its 355 kJ/mol [6]. It is the reason why the N_2 formation occurs faster on Rh(111) and at least the Rh(111) is the better catalyst.

If we take a look at cooper powder and reduced cooper at a support materials or oxide system, they are not only different in chemical circumstances, but they have also distinctive different structure and surface morphology. Macroscopicly we could say that amorphous and big copper particles have bad catalyst performance in comparison to more ordered species, for example: nanostructured catalyst. This matter was already studied by B. Kniep [7]. In his study about the performance of Cu/Zn-catalysts which were prepared with different ageing time, a clear correlation between molecular structure, strain and its catalyst performance was reported. But perfectly ordered atoms and perfect crystal structure are commonly not active. Strained distorted structures and defects are the better catalyst candidates.

Most cataysts are based on metals of the groups VIII- and I-B of the periodic systems. Due to enhance the catalyst performance, we could use chemical promotors. They could play various roles:

1. Adding a dopant with similiar size is expedient if this could act as a second reactive center, for example Zn in Cu/Zn-catalyst plays a important role as a center for hydrogen spill over in methanol steam reforming.

2. Adding atoms with different size or different oxydation state and respectively different coordination number could create defects or strain in the more distorted structure of the catalyst.
3. Adding some alkali metalls could have a big impact on the electronic structure of a catalyst.

Although the reactivity of a catalyst belongs to the important features, we should keep in mind another very substantial aspect in catalysis: the selectivity. The study of the Ga/Pd catalyst for ethylen oxidation shows that it is possible to design a catalyst with high selectivity. If the byproduct is a result of dimerisation or the products of the reaction could be influenced wether the reactant are adsorbed on its π or σ bonding, the principle of site isolation could be used [8]. If such solution is not possible, we can try to solve the problem, for example by using various reactor modules or operation modes.

Summary: to develop a good catalyst we should recognize following aspects:

1. Surface properties:

- well dispersed nanostructured particles with strained structure and much defects.
- high fraction of active atoms at the surface.
- fine dispersion of active material over inert support material with high porosity without diffusion limitation.

2. Long term stability: stable against temperature and pressure, low abrasion, slow deactivation or at least it should easily be regenerated.
3. Promoted with suitable dopants to enhance the reactivity and structure designed to achieve high seletivity.
4. The preparation must give reproducible product.
5. Concerning the financial issues: the catalyst should have a low production cost.

Some materials need to be activated, for example by a reduction or oxidation. Since as per definition catalyst after participation on the reaction must be recovered in ist original form at the end of the cycle, some catalyst is actually just a precursor.

1.4. Kinetics

Reastion kinetics handles the rates of chemical reactions and enables us to relate the rate to a reaction mechanism. In the beginning of 20th century it was simply an emprical description of reaction rate, determined by studying just the macroscopic process parameters such as concentrations, pressures and temperatures. But as the spectrum of tools was extended widely in the second half of the 20th century we can study the microscopic level of reactions by investigating how the molecules react, which intermediates are detected and which species of the catalyst work as the active centers. Nowadays there are some in-situ techniques, which can investigate the molecular processes at the reaction conditions. These measurements allow us to follow the dynamic structure evolution and the formation of intermediate species in catalytic processes. Hence, kinetics is a key discipline for catalysis. It provides us with its tools to link the microscopic level of reacting molecules to the macroscopic world of industrial reaction engineering.

The understanding of the microscopic level is very important for the design and improvement of a catalyst. And the reaction mechanisms of the formation of the main product or byproduct have to be understood before we develop a reactor concept. But in a practical situation and at the production level we are not interrested any longer in a single event but what happens in a large ensemmble of molecules. This is expressed for example by the conversion, reaction rate and the energy development of the running processes during a reaction at specific conditions. Temperature is the parameter which describes the energy content of the molecules in the reaction.

1.4.1. The power law rate equations

The rate of a reaction is definied as the rate of disappearance of the reactants or the rate of the formation of products. For the schematic chemical reaction:

$$\nu_A\ A + \nu_B\ B \underset{k_r}{\overset{k_f}{\rightleftharpoons}} \nu_C\ C + \nu_D\ D \qquad (5)$$

with A, B = reactants; C, D = products

ν_i = stochiometric coefficient of component i

k_f = rate constant of forward reaction

k_r = rate constant of reward reaction

the reaction rate is defined as:

$$r = \frac{-dc_A}{\nu_A \cdot dt} = \frac{-dc_B}{\nu_B \cdot dt} = \frac{dc_C}{\nu_C \cdot dt} = \frac{dc_D}{\nu_D \cdot dt} \qquad (6)$$

with c_i = concentration of component i [mol.L^{-1}]

t = time [s]

If the reaction occurs in the gas phase, we can replace the concentration c_i by partial pressure of the gases p_i/p_0, where p_0 = 1 bar is the reference pressure:

$$r = \frac{-dp_A}{\nu_A \cdot p_0 \cdot dt} = \frac{-dp_B}{\nu_B \cdot p_0 \cdot dt} = \frac{dp_C}{\nu_C \cdot p_0 \cdot dt} = \frac{dp_D}{\nu_D \cdot p_0 \cdot dt} \qquad (7)$$

It is quite usual not to include the p_0 at the equation, but implicitly assume that the p_i represents partial pressures of the gases.

If a reaction occurs in a single step which can not be divided into further sub-steps and proceeds exactly by the reaction equation, it is called an elementary reaction. If the reaction in equation (1) is elementary, we can express its rate as:

$$r = k_f \cdot c_A^{\nu_A} \cdot c_B^{\nu_B} - k_r \cdot c_C^{\nu_C} \cdot c_D^{\nu_D} = r_f - r_r \qquad (8)$$

A reaction mechanism is a series of elementary steps involving a number of intermediates. These steps mean in the heterogeneous catalysis reactions, including the adsoption at the surface and desorption step. We have to take diffusion into account if the processes are inhibited by this mass transfer limitation.

An elementary step has an integer order. But for industrial and ingeneering purpose it is often enough if we could get the reaction order of overall reaction. The power law rate equation could deliver this data. For the purpose of parameterization, we could write the reaction rate formally as a function of concentration or pressures, in the form of a power law:

$$r = k \cdot c_A^{n_A} \cdot c_B^{n_B} \cdot c_C^{n_C} \cdot c_D^{n_D} \quad \text{or} \quad r = k \cdot p_A^{n_A} \cdot p_B^{n_B} \cdot p_C^{n_C} \cdot p_D^{n_D} \qquad (9)$$

with n_i = reaction order of component i.

where the orders of n_i may take virtually all values: integer, fractional, positive, zero or negative. The reaction order of the overal reaction (forward and reserve reactions) is then the sum of n_i (:n_A+n_B+ n_C+n_D).

1.4.2. Langmuir-Hinselwood or Eley-Rideal rate laws

In the first step of many heterogeneous reactions, the reactants are adsorbed at the catalyst surface, and after some consecutive reaction steps the products are desorbed from the surface. Hence we can express the reaction rate for the heterogeneous gas phase catalysis with a term of surface coverage, as Langmuir and Hinselwood kinetic does if all species are adsorbed and adsorption equilibirum is established before the reactions occur. If it is not necessary, for example if one of the reactants could directly react from the gas phase without being chemisorbed at the surface, the species undergo the so called Eley-Rideal mechanism. Both these mechanisms have a significant implication for the kinetic description, as in case of Eley-Rideal mechanism free sites are not required for all reaction species [6].

The decomposition of ammonia over iron based catalysts is a simple heterogenous catalysis with just one compound as reactant. It is given as $2NH_3 \rightleftharpoons N_2 + 3H_2$. But even this simple system conceals a certain complexity. All possible elementary steps of ammonia decomposition over metal based catalysts are described by following equations:

I: $NH_{3(g)} + * \rightleftharpoons *\text{-}NH_3$

II: $*\text{-}NH_3 + * \rightleftharpoons *\text{-}NH_2 + *\text{-}H$

III: $*\text{-}NH_2 + * \rightleftharpoons *\text{-}NH + *\text{-}H$

IV: $*\text{-}NH + * \rightleftharpoons *\text{-}N + *\text{-}H$

V: $2*\text{-}N \rightleftharpoons *\text{-}N_2 + *$

VI: $*\text{-}N_2 + * \rightleftharpoons *\text{-}N_2\text{-}*$

VII: $*\text{-}N_2\text{-}* \rightleftharpoons *\text{-}N_2 + *$

VIII: $*\text{-}N_2 \rightleftharpoons N_{2(g)} + *$

IX: $2*\text{-}H \rightleftharpoons *\text{-}H_2 + *$

X: $*\text{-}H_2 \rightleftharpoons H_{2(g)} + *$

XI: $2{*}\text{-}NH_2 \rightleftharpoons {*}\text{-}N_2H_4 + *$

XII: ${*}\text{-}N_2H_4 \rightleftharpoons N_2H_{4(g)} + *$

XIII: $2{*}\text{-}NH \rightleftharpoons {*}\text{-}N_2H_2 + *$

XIV: $2{*}\text{-}N_2H_2 \rightleftharpoons N_2H_{2(g)} + *$

The reactions steps I-X are reported in many literatures about synthesis or decomposition of ammonia [9, 10, 11, 12], the other steps which form hydrazine and diazene are barely reported. The corresponding rate for each step is formulated by following equations:

$$r_I = k_{I,f} \cdot p_{NH_3} \cdot \theta_* - k_{I,r} \cdot \theta_{*-NH_3} \quad (10)$$

$$r_{II} = k_{II,f} \cdot \theta_{*-NH_3} \cdot \theta_* - k_{II,r} \cdot \theta_{*-NH_2} \cdot \theta_{*-H} \quad (11)$$

etc. and the overall reaction **r** is defined as follows:

$$\frac{1}{r} = \sum_i \frac{1}{r_i} \quad (12)$$

The ballance of the surface species is expressed by folowing equation (13):

$$1 = \theta_* + \theta_{*-NH_3} + \theta_{*-NH_2} + \theta_{*-NH} + \theta_{*-N} + \theta_{*-N_2} + \theta_{*-H} + \theta_{*-H_2} + \theta_{*-N_2H_2} + \theta_{*-N_2H_4}$$

$\theta_i = \dfrac{c_i}{\sum_i c_i}$ = coverage of species i

$*$ = free active site

According to the principle of microkinetic reversibility, we can describe the desorption of nitrogen (step V and VIII) by means of the achieved results from ammonia synthesis [9] in details:

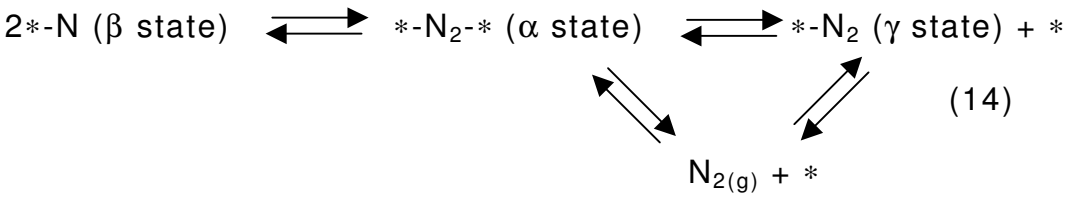

(14)

The existence of the various states of the nitrogen species was detected by XPS measurements. The positions of the XPS signals are listed in the table 1.4.

XPS peak	Nitrogen species
397 eV	β state
399 eV	α state
400 & 405 eV	γ state

Table 1.4: XPS peaks of nitrogen species involving at ammonia synthesis on the surface of Fe(111)

Based on high resolution EELS data, the α–state is attributed to bridge-bonded nitrogen and γ–state is assigned to terminally-bonded nitrogen [9]. In the ammonia synthesis exists also a route to α–state directly from the gase phase without first form the γ–state (terminally-bonded species). Therefore the desorption of nitrogen directly from α-state could not be excluded: $*\text{-}N_2\text{-}* \rightleftharpoons N_{2(g)} + 2*$

The previous description of ammonia decomposition in twelve possible elementary steps is hardly usefull for kinetic calculation and we actually do not know how it really works, for example wether the

hydrogen abstraction from ammonia occurs subsequently and really requires three free sites for the available hydrogens etc. Vitally important for the kinetic description is just the rate determining step (rds) which has the slowest reaction rate. The fast reactions do not contribute a significant part to the overall reaction rate (see equation 12) and can often be neglected in the description of the overall process. And the short-lived intermediates which undergo fast reactions can also be neglected in the description of coverage ballance. The reactants of the rds have a longer lifetime since the rds is the slowest step. They are therefore the **m**ost **a**bundant **r**eaction **i**ntermediates at the catalyst surface, abbreviated *mari*. For the calculation we could simplifiy the ballance of surface species as just the sum of free sites and *mari*. It must be mentioned that the *mari* is not necessarily the most abundant species at the catalyst surface, since some species could cover the surface but they do not take part in the reaction.

1.5. References

[1] T.A. Semelberger, K.C. Ott, R.L. Borup, H.L. Greene, Generating hydrogen-rich fuel cell feed from DME using physical mixtures of commercial Cu/Zn/Al2O3 catalyst and several solid acid catalysts, Applied Catalysis B: Enviromental 65 (2006) 291-300.

[2] T.A. Semelberger, R.L. Borup, H.L. Greene, Dimethyl ether as an alternative fuel, Journal of Power Soruces 156 (2006) 497-511.

[3] Jung Yeon Won, Hee Kwon Jun, Min Ku Jeon, Seong Ihl Woo, Performance of microchannel reactor combined with combuster for methanol steam reforming, Catalysis Today 111 (2006) 158-163.

[4] B. Frank, F. Jentoft, H. Soerijanto, J. Kröhnert, R. Schlögl, R. Schomäcker, Steam reforming of methanol over copper-containing catalysts: influence of support material on microkinetics, Journal of Catalysis, submitted.

[5] M.J.P. Hopstaken, J.W. Niemandsverdriet, J. Vac. Sci. Technol. A 18 (2000) 1503.

[6] I. Chorkendorff, J..W. Niemandtsverdriet, Concepts of Modern Catalysis and Kinetics, Wiley-VCH, 2003, ISBN: 3-527-30574-2.

[7] B.L. Kniep, F. Girgsdies and T. Ressler, Effect of precipitate aging on the microstructural characteristics of Cu/ZnO catalysts for methanol steam reforming, Journal of Catalysis, Volume 236, Issue 1, 15 November 2005, Pages 34-44.

[8] Patent: J. Osswald, K. Kovnir, M. Armbrüster, R. Giedigkeit, R.E.

Jentoft, T. Ressler, Y. Grin, R. Schlögl, Hydrogenation Process using Catalyst comprising Ordered Intermetallic Compound (Max Planck Society, Germany), EP 06005310.5 (2006).

[9] L.M. Aparicio, J.A. Dumesic, Ammonia synthesis kinetics: surface chemistry, rate expressions and kinetic analysis, Topics in Catalysis 1 (1994) 233-252.

[10] G. Djéga-Mariadassou, C-H. Shin, G. Bugli, Tamaru's model for ammonia decomposition over titanum oxynitride, Journal of Molecular Catalysis A: Chemical 141 (1999) 263-267.

[11] J. Zhang, H. Xu, W. Li, Kinetic study of NH_3 decomposition over Ni nanoparticles: The role of La promoter, structure sensitivity and compensation effect, Applied Catalysis A: General 296 (2005) 257-267.

[12] P. Stoltze, J.K. Norskov, The surface science based ammonia kinetics revisited, Topics in Catalysis 1 (1994) 253-263.

2.1. Kinetic study of SRM over $Cu/ZrO_2/CeO_2$ catalysts

2.1.1. Introduction

In the past decade, considerable attention has been focused on the reduction of the significant emissions originating from mobile sources, such as internal combustion engines [1-4]. For environmental reasons, the development of proton-exchange membrane fuel cells (PEMFCs) has gained in increasing importance [5,6]. As compared with conventional heat engines, several advantages of fuel cell application have been established, including a higher efficiency and a more convenient operation, the absence of moving parts and the low emission of hazardous compounds [1,5]. The combustion of hydrogen in a fuel cell is regarded as a clean process, releasing energy and providing only water as an exhaust material [4,7,8]. However, hydrogen is not a natural energy source and must be generated by consuming a large amount of energy, either from natural gas or via the electrolysis of water [4]. Furthermore, for a fuel cell vehicle, the storage and the supply of hydrogen, a volatile and explosive gas, imposes mechanical problems and safety hazards on a commercial level [1,4,8].

Several liquid fuel candidates have been discussed for on-board reforming, including methanol, ethanol, gasoline and diesel [1], of which methanol is considered the most favourable alternative [1,9]. Although mostly produced from natural gas, methanol can also be obtained from renewable sources, thus lowering the production of carbon dioxide [5,9]. Moreover, via methanol synthesis from hydrogen and carbon dioxide, methanol can be employed as a storage and transport medium for hydrogen. In addition to its good availability and low boiling point, methanol possesses a high hydrogen to carbon ratio (4:1) and contains no carbon-carbon bond, which considerably reduces the risk of coke formation during its reactions [1,5,6].

The most important processes to produce hydrogen from methanol (Eqs.1-3) are decomposition (MD), steam reforming (SRM), and partial oxidation (POM) [1]. The combined or oxidative reforming of methanol (CRM or OSRM), a combination of (2) and (3), has also been investigated [2,6,10,11]. The decomposition of methanol is a strongly endothermic reaction producing a high CO yield, which makes it rather unsuitable for fuel cell applications [1]. The steam reforming reaction is also endothermic, however, it typically affords a substantial H_2 yield of 75%, while maintaining high carbon dioxide selectivity (~ 25%) [1,4,8]. The partial oxidation of methanol is an exothermic reaction with a rapid start-up and a dynamic response [4]. Nevertheless, the formation of hot spots in the reactor may result in sintering of the Cu particles, which tends to decrease the catalytic performance [8,11]. Furthermore, this reaction produces a considerably lower amount of hydrogen than SRM [1,8,9].

$$CH_3OH_{(g)} \underset{k_{RMD}}{\overset{k_{MD}}{\rightleftharpoons}} 2H_2 + CO \qquad \Delta H^0 = 91\ kJ.mol^{-1} \qquad (1)$$

$$CH_3OH_{(g)} + H_2O \underset{k_{RSRM}}{\overset{k_{SRM}}{\rightleftharpoons}} 3H_2 + CO_2 \qquad \Delta H^0 = 50\ kJ.mol^{-1} \qquad (2)$$

$$CH_3OH_{(g)} + 0{,}5O_2 \underset{k_{RPOM}}{\overset{k_{POM}}{\rightleftharpoons}} 2H_2 + CO_2 \qquad \Delta H^0 = -192\ kJ.mol^{-1} \qquad (3)$$

As the highest hydrogen yield may be achieved by the steam reforming of methanol [1], the latter reaction was investigated within the framework of the present study. The major drawback of SRM is the formation of CO as a by-product, which, even at a low concentration of 100 ppm, decreases the fuel cell performance by poisoning the Pt electrode [2,6,12]. Currently, second stage catalytic reactors are being used to remove CO by the water-gas shift reaction, oxidation or methane formation [6,10]. However, this CO clean-up unit is rather inconvenient as it occupies a large volume and decreases the efficiency of the fuel cell through hydrogen

consumption [8]. In order to eliminate the need for gas purification, high performance catalysts are required that provide substantial methanol conversion and H_2 selectivity, together with the lowest possible amount of CO [10,12]. The complete absence of CO in the product gas may be difficult to achieve under SRM conditions.

Several studies have been reported in the literature on the applications of Cu- and Pd-based catalysts for SRM [1-6,8-12,13-18], of which Cu containing catalysts are clearly preferred because of their high activity and selectivity at lower temperatures [1,12,19]. Although Cu catalysts are also regarded as susceptible to thermal deactivation, their sintering abilities may be considerably reduced by the addition of one or more oxide species, such as ZnO, Al_2O_3 or Cr_2O_3 [20]. The most efficient catalysts for SRM, including the traditional Cu/ZnO and Cu/ZnO/Al_2O_3 systems, have been investigated in detail [1,3,6,9,15,16,21-25]. The in situ characterization of Cu/ZnO under SRM activation and operating conditions revealed that the interaction of the Cu and ZnO phases has a pronounced effect on the catalytic activity [22,23]. For Cu/ZnO/Al_2O_3 catalysts, high methanol conversions and low CO selectivities have been obtained [1,5,8,9,16] and kinetic analysis provided important information on the overall reaction mechanism [5,6,16,21,25,26]. Compared to the conventional ZnO or Al_2O_3-supported Cu catalysts, ZrO_2-containing samples have shown increased activities and reduced CO levels for the SRM reaction [3,5,12,27-29]. The promoting effect of ZrO_2 has been attributed to an improved reducibility of CuO, which tends to increase the Cu dispersion [29]. ZrO_2 has also been reported to prevent the sintering of Cu crystallites under reaction conditions [5,12,29] and thus may be regarded as a structural stabilizer. Likewise, the application of CeO_2, as either a support material or a promoter, has been found to improve the efficiency of Cu-based catalysts [11,30,31]. CeO_2 has been found to increase the thermal stability and the activity of Al_2O_3-supported Cu catalysts through a synergetic effect and favour the conversion of

CO via the water-gas shift reaction [30]. Moreover, CeO_2 has a high oxygen storage capacity [32,33] and the partially reduced CeO_2 sites formed under reductive conditions produce mobile oxygen, which tends to have a beneficial effect on the catalytic performance [31,32]. For ZrO_2-CeO_2 supported catalysts, the interaction between the oxide phases, leading to the formation of a thermally stable solid solution, has been reported to increase the mobility of oxygen in both phases [32].

The aim of the current work was the structural and catalytic investigation of novel Cu/ ZrO_2/CeO_2 catalysts prepared by co-precipitation. In order to increase the specific surface area, highly porous polymer beads were employed as template for the preparation of the solid catalysts [34]. Samples with different Cu loadings were examined for the steam reforming of methanol and their catalytic properties are discussed, including long-term stability and CO production. Furthermore, the reaction mechanism was studied and a kinetic analysis was undertaken to determine the rate constants and the activation energies for the model reactions.

2.1.2. Experimental

2.1.2.1. Catalyst preparation

The Cu/ZrO_2/CeO_2 (CZC) catalysts were synthesized from metal sols, prepared from the appropriate amounts of the mixed precursors $(NH_4)_2Ce(NO_3)_6$, $ZrO(NO_3)_2 \cdot H_2O$ and $Cu(NO_3)_2 \cdot 2.5\ H_2O$ (all Aldrich products of > 99% purity), dissolved in 40 ml of distilled water. The total metal content of the resulting sol was $5 \cdot 10^{-3}$ mol. Co-precipitation of the metal sols as metal hydroxides was accomplished by increasing the pH above 10 through addition of a NaOH solution. The resulting precipitate was repeatedly washed with distilled water until pH=7 was obtained, and then suspended in a mixture of 5 ml of distilled water and a calculated amount of 90% HNO_3. Depending on the sample composition, the HNO_3:metal molar ratio was varied

between 1:1 and 1.5:1. Ultrasonic treatment of the suspension for 45-60 min resulted in the formation of a transparent sol [35].

Templating was carried out by using XAD-16 non-functionalized polystyrene beads (a Sigma product), with a specific surface area of 800 m^2g^{-1} and an average pore diameter of 10 nm. 1.5 ml of the wet beads and 0.005 mol of the metal sol were mixed together and then heated in an oven at 333 K for 2 days in order to ensure solvent evaporation. The beads were subsequently dried at 373 K for another day and then washed with distilled water to remove any excess deposit from their surface. After drying at 333 K for 1 day, the samples were calcined in an oven at 773 K in a N_2 stream of 100 ml/min for 2.5 h and then for an additional 8 h in air. Upon calcination grey-green materials were obtained (see Fig. 2.1.1). Due to the mean particle diameter (500 µm) and the regular character of the polymer beads, the resulting CZC samples could be conveniently applied as catalysts in fixed bed reactors.

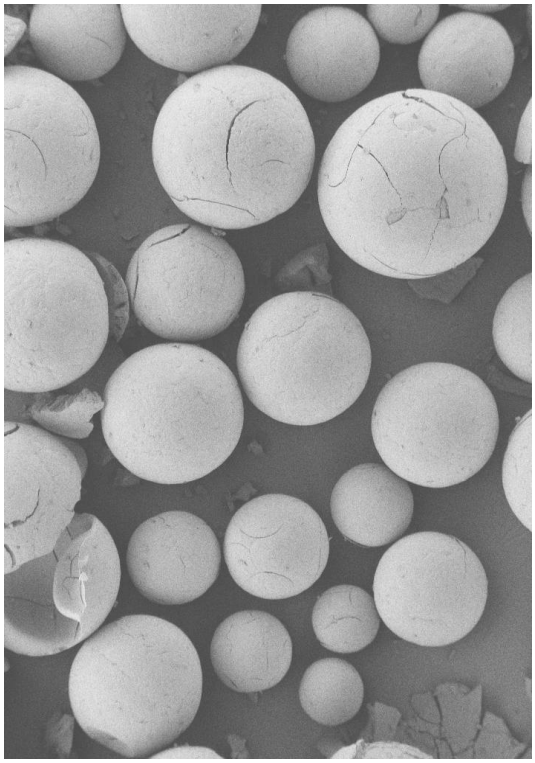

Figure 2.1.1: Scanning electron micrograph of a $Cu/ZrO_2/CeO_2$ catalyst (CZC5) after calcination.

Four representative CZC samples were synthesized by the above method, with Cu contents 5, 15, 25 and 35%, denoted as CZC5, CZC15, CZC25 and CZC35, respectively, to be characterized and tested for the steam reforming of methanol. The molar ratio ZrO_2:CeO_2 = 1:1 for the support materials was maintained in each case.

2.1.2.2. Characterization

2.1.2.2.1. X-ray fluorescence analysis (XFA)

The results of the elementary analysis of the CZC samples, performed by a Seiko (SEA 2010) instrument, are shown in Table 1. The amount of Cu detected in the samples was found to be only slightly lower than that expected from the preparation conditions and the ratio ZrO_2:CeO_2 = 1:1 proved to be well adjusted.

2.1.2.2.2. N_2 adsorption-desorption

The specific surface areas of the CZC samples were determined from N_2 adsorption-desorption data obtained at the temperature of liquid N_2 (77K), by using a Micromeritics 2375 BET apparatus equipped with a Vacprep 061 degasser. In order to remove traces of water and impurities from the surface, all samples were degassed before measurement at 13 Pa and 393 K for 12 h. The specific surface areas were calculated from the BET equation and the average pore diameters d_p were obtained by the BJH method from the desorption branches of the adsorption isotherms.

2.1.2.2.3. N_2O decomposition

The specific Cu^0 surface areas of the samples were measured by N_2O decomposition, by using the reactive frontal chromatography (RFC) method introduced by Chinchen et al [36].

The method is based on the oxidation of the exposed Cu^0 surface atoms of a reduced sample by switching the feed from an inert gas stream to a mixture containing N_2O as an oxidizing species. The Cu^0

surface area can then be determined from the amount of N_2O consumed in the reaction, as given below (Eq.4).

$$2Cu + N_2O \longrightarrow \text{“}Cu_2O\text{”} + N_2 \qquad (4)$$

Before measurements, the CZC samples were activated in a stream of MeOH:H_2O = 2:1, with a flow rate of 36 cm^3min^{-1} at 523 K. In order to diminish the amount of adsorbed molecules on the Cu surface, the samples were subsequently purged in pure He (50 cm^3min^{-1}) at 523 K for 1 h and then cooled down to 313 K, where the measurements were performed in a 0.5% N_2O/He stream of 15 cm^3min^{-1}. The catalysts were diluted with boron nitride to provide a sample bed of ca. 25 mm height, with a thermocouple positioned directly inside the powder bed. The material was placed onto a quartz frit in a tubular quartz reactor.

For the RFC method described by Chinchen et al., the area under the ion current trace (m/e = 28 for N_2) has been directly used to determine the Cu^0 surface area. For the current experiments, however, the same MS signal obtained from the amount of N_2 produced for the CZC samples was found to be insufficient for evaluation. Therefore, the amount of N_2 formed during decomposition was indirectly estimated from the retarded evolution of N_2O (m/e = 44), as compared with blank experiments performed with boron nitride. Earlier investigations for Cu/ZnO samples revealed a good agreement between the Cu^0 surface areas determined by N_2O RFC with those obtained from the Cu crystallite size [23,37]. The Cu^0 surface area was calculated by assuming a stoichiometry of N_2O/Cu = 0.5 and a value of $1.47 \cdot 10^{19}$ Cu atoms/m^2 for the surface density [5,29,36].

2.1.2.2.4. X-ray diffraction (XRD)

Ex situ XRD measurements were performed on a STOE STADI P transmission diffractometer (CuK_α radiation, Ge monochromator), equipped with a position sensitive detector (PSD, internal resolution $2\Theta = 0.01°$). The CuO crystallite diameters were calculated from the Scherrer equation [38]. The full width at half maximum (FWHM) was determined by fitting a Lorentzian profile function to the CuO (111) and (200) diffraction peaks at $2\Theta = 38.371$ and $38.923°$, respectively.

2.1.2.3. Catalytic test reaction

The steam reforming of methanol was studied in a fixed bed tubular reactor (stainless steel, id = 10 mm), by utilizing a 3-channel set-up, which ensured that 3 catalysts could be investigated at the same time, under exactly the same conditions. In order to achieve an efficient heat transfer, the reactors were placed in an aluminium heating block. The temperature of the reactor was regulated by PID control of the cartridge heaters situated inside the aluminium block. Time-on-stream investigations were performed at 523 K and the mass of catalyst was varied between 0.100 and 0.770 g, depending on the Cu content, in order to keep the amount of CuO constant for all samples (0.0225 g). For kinetic measurements, the mass of catalyst was increased by a factor of 2.6, corresponding to a CuO content of 0.0584 g for each sample, to achieve full conversion in the temperature range investigated (503-573 K). The catalyst was supported inside the reactor by a stainless steel grid. For flow conditioning, inert Pyrex beads (d = 500 μm) were placed below and on top of the catalyst bed. The reactant mixture of MeOH (HPLC grade, 99.9% purity) and distilled water, with a molar ratio MeOH:H_2O = 1:1, was introduced into the reactor by means of a Dionex HPLC P 580 pump. Both reactants were degassed before use at 20 kPa. For time-on-stream measurements, the flow rate for a single channel was 0.07 cm^3min^{-1}, whereas for kinetic investigations, it was varied

between $3.33 \cdot 10^{-3}$ and 0.67 cm^3min^{-1}. Kinetic measurements were performed by using fresh catalysts to eliminate aging effects and experimental data were collected after 5 days time-on-stream. In order to achieve steady-state conditions, experimental data at low flow rates were collected 60 min after the flow rate had been adjusted. Before measurement, the catalysts were activated in situ in a MeOH:H_2O = 1:1 stream of 0.07 cm^3min^{-1} at 523 K for 16 h [15,16,25].

The reaction products consisting of effluent gases (H_2 and CO_2 as main products and a minor amount of CO), together with unreacted methanol and water, were passed through a condenser at 268 K, which removed most of the liquid from the product gas stream. Complete removal of the condensed reactant mixture was achieved by applying an additional condenser at 253 K. The liquid composition was analyzed by using an Intersmat gas chromatograph (GC), equipped with a thermal conductivity detector (TCD), operated with a 50m x 0.53 mm CP-Wax column at 363 K. The composition of the dry product gas mixture was determined on-line, by means of a Varian 3800 GC with a TCD. Helium was applied as a carrier gas and separation was achieved by using a 25 m x 0.53 mm CarboPLOT P7 column at 304 K. For quantitative analysis of the product gas stream, a calibration gas mixture, containing 0.5% CO, 4.5% N_2, 25% CO_2 and 70% H_2 (a Messer Griesheim product), was employed. Under the present experimental conditions, no evidence for the formation of the by-products methane, methyl formate and dimethyl ether was found [27,39].

2.1.3. Results and Discussion

2.1.3.1. Catalyst characterization and long-term stability

The results obtained for the CZC samples from N_2 adsorption-desorption and N_2O decomposition are summarized in Table 2.1.1.

Sample	Cu [%]	Zr [%]	Ce [%]	BET area [m^2g^{-1}]	d_p [nm]	Cu^0 area [$m^2g^{-1}_{catalyst}$]	Cu^0 area [$m^2g^{-1}_{Cu}$]
CZC5	4.4	44.6	51.0	96	12.3	0.9	51.4
CZC15	12.1	44.3	43.6	102	11.5	1.8	25.8
CZC25	23.9	37.6	38.5	94	12.7	1.8	12.2
CZC35	31.0	32.7	36.3	83	13.0	1.5	7.6

Table 2.1.1: Characteristic data of the CZC catalysts

The BET surface areas obtained for the CZC samples were higher than those reported for ZnO supported Cu catalysts [39] and of a similar order as those published for Cu/Al_2O_3 samples by Cheng et al. [19]. A decreasing BET surface area with increasing Cu loadings [19] was observed only for the samples with Cu contents exceeding 5%. As seen in Table 1, the values for the average pore diameter were very close for each sample (11.5-13 nm). Although the Cu^0 specific surface areas for the CZC materials proved to be lower than expected from the internal surface areas and the Cu contents [29], the values exhibited a similar trend as the BET results. The highest Cu^0 surface area per gram copper was obtained for CZC5. An increasing Cu content resulted in a decreasing Cu^0 surface area roughly in agreement with an increasing Cu particle size. The net

decrease of the Cu^0 specific surface area with increasing Cu content, observed for CZC15, CZC25 and CZC35, is in correlation with earlier results reported in the literature for supported Cu catalysts [5,19].

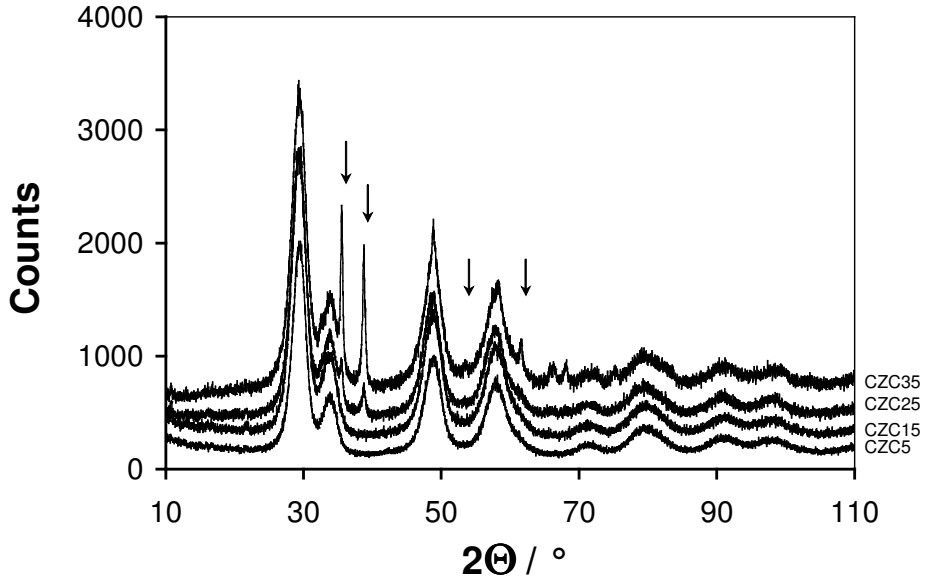

Figure 2.1.2: X-ray diffraction patterns of four CZC catalysts with a nominal copper concentration of 5 % (CZC5), 15 % (CZC15), 25 % (CZC25), and 35 % (CZC35) with a constant ZrO_2/CeO_2 ratio of about 1. Arrows indicate CuO phase

The XRD patterns of the CZC samples displayed in Fig. 2.1.2 revealed that the characteristic CuO peaks could be distinguished only for the samples with the highest Cu contents. The absence of CuO signals for CZC5 and CZC15 may be attributed in part to their lower Cu loadings. Furthermore, the Cu crystallite size for the above samples may be too small to be detected by XRD, as related to a pronounced line broadening [5]. The broadening of the peaks also renders it difficult to establish whether the Zr, Ce and O atoms are arranged in one single mixed phase or in separate phases. For the same reason, the corresponding crystal structures (cubic and/or tetragonal) cannot be reliably determined. The Cu crystallite sizes obtained from the diffraction peaks for CZC25 and CZC35 were 12.4 and 15.3 nm, respectively. The slight increase in the particle size

observed for the latter sample is in line with the decrease of the Cu^0 specific surface area obtained from N_2O decomposition. Further structural data of the $Cu/CeO_2/ZrO_2$ catalysts obtained under reaction conditions and corresponding structure-activity relationships will be presented elsewhere.

'n order to make a comparison between the long-term stabilities of the CZC catalysts, the methanol conversions obtained during a continuous operation of 16 days under standard conditions were plotted as a function of time-on-stream (Fig. 2.1.3).

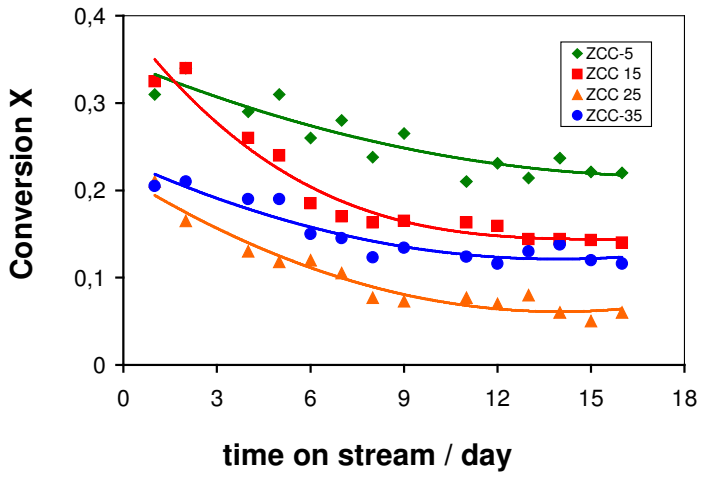

Figure 2.1.3: Methanol conversions during SRM of four CZC catalysts as a function of time-on-stream (m_{CuO} = 0.0225 g, T = 523 K, p = 10^5 Pa, w = 0.07 cm^3min^{-1}, MeOH:H_2O = 1:1)

It can be seen that no linear correlation exists between the catalytic activity depicted in Fig. 2.1.3 and the Cu surface area (Table 2.1.1). Evidently, the catalytic activity of the CZC samples is not only determined by the the Cu surface area, but also by the particular microstructure of the Cu particles, which may be similar to the microstrain in Cu/ZnO catalysts [23]. The catalytic activities of all the samples were found to diminish considerably for a period of 5 days, although to a different extent, which displayed no systematic variation with the Cu content. The conversions determined after 5 days approached a constant value, except for CZC5, which exhibited

a further decrease. After an initial period of deactivation, the CZC samples with Cu contents exceeding 5% displayed good long-term stabilities and, hence, these samples may be suitable for extended operation. The relatively poor thermal stability of CZC5 may be related to the small Cu particle size, considering that small particles tend to be more susceptible to thermal sintering under reaction conditions [40], even at temperatures lower than 523 K [41]. In addition to the CZC samples, a copper-free CeO_2/ZrO_2 sample was prepared by using the same procedure as described above. This material did not exhibit any detectable activity in the steam reforming of methanol under the reaction conditions employed. Hence, the differences observed for the CZC catalysts in the steam reforming of methanol can be mainly attributed to the bulk and surface properties of the Cu phase in these materials.

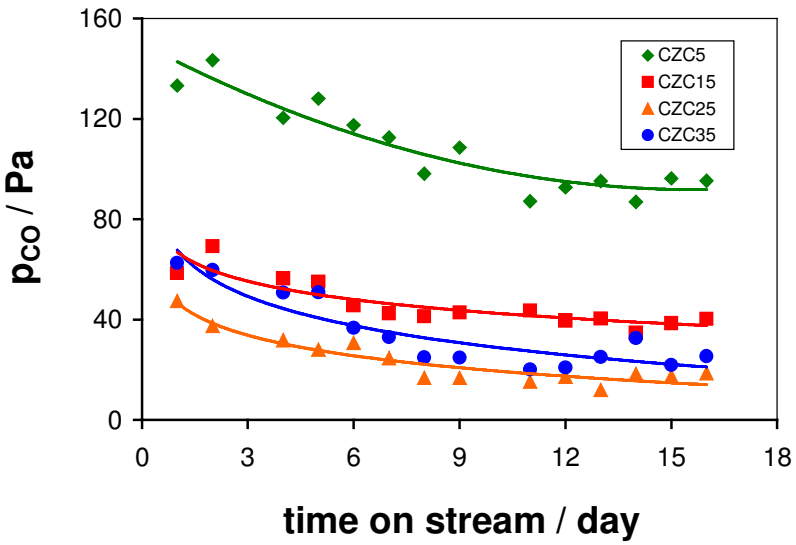

Figure 2.1.4: CO formation during SRM of four CZC catalysts as a function of time-on-stream (m_{CuO} = 0.0225 g, T = 523 K, p = 10^5 Pa, w = 0.07 cm^3min^{-1}, MeOH:H_2O = 1:1)

The CO partial pressures determined during the above measurements are depicted in Fig. 2.1.4. As mentioned above, the sample masses were adjusted to provide the same Cu content. For this reason, the mass of CZC5 considerably exceeded those of the other samples, and this may accounted for the amount of CO detected for CZC5 being substantially higher than those for the samples with higher Cu contents. Moreover, following a pronounced decrease for about 5 days, the CO levels were stabilized and did not exhibit any significant difference. This finding is consistent with the results of N_2O decomposition, indicating that the active Cu contents of these samples were very similar. It may be concluded from Figs. 2.1.3 and 2.1.4 that an increase of the Cu content from 5 to 15% has a beneficial effect on the catalytic performance of CZC through improving the long-term stability and suppressing the CO production. Although the effect of a further increase of the Cu loading proved to be less important for the stability of the catalyst, it resulted in lower CO levels. Nevertheless, the CO production is also dependent on the conversion of methanol [29], as the activity order of the CZC samples (Fig. 2.1.3) is in correlation with the order of the CO levels throughout the entire time-on-stream interval (Fig. 2.1.4). Accordingly, under the present experimental conditions, the samples with increased Cu contents may be regarded as more efficient catalysts for SRM, with respect to the formation of CO in particular.

Considering that the CZC catalysts are porous materials and the methanol conversions in Fig. 2.1.3 displayed no systematic variation with either the Cu loading or the Cu^0 surface area, the effect of mass transport limitations on the catalytic performance was additionally investigated. It was previously observed that the CZC samples were not uniform in size. Thus, for each material, three fractions with different particle diameters could be obtained by sieving. Moreover, a Cu/CeO_2 sample containing 25% of Cu, prepared by the same method, was found to slightly deteriorate during SRM, as a small amount of the original catalyst beads (3.3%)

was transformed into a fine powder after reaction. On the other hand, the Zr-containing beads of the CZC samples remained essentially unchanged after catalytic investigations, which confirms that ZrO_2 is an important structural stabilizer [12,29]. The methanol conversions obtained for the different sieve fractions of CZC15 under the same conditions are plotted in Fig. 2.1.5 as a function of the reactant flow rate.

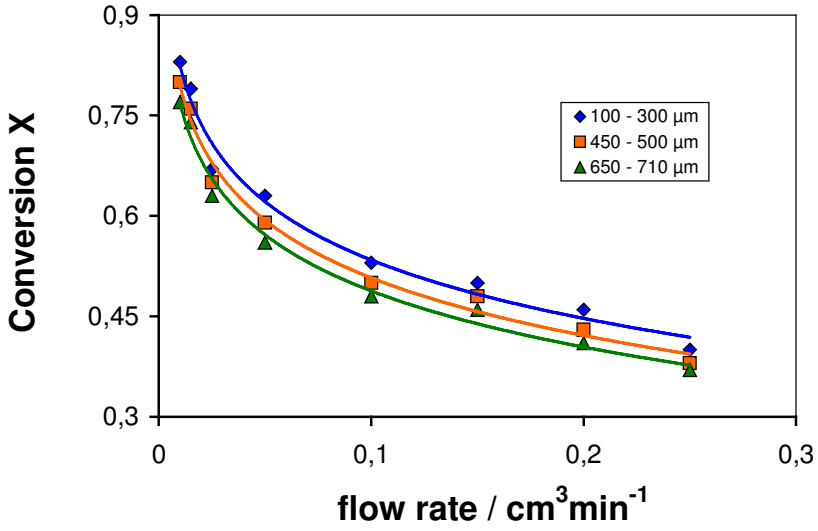

Figure 2.1.5: Methanol conversions during SRM as a function of the reactant flow rate, determined for various sieve fractions of CZC15 (m = 0.5500 g, T = 523 K, p = 10^5 Pa, MeOH:H_2O = 1:1)

On increasing the flow rate, the conversions for the various sieve fractions declined to the same extent. At a given flow rate, the values obtained slightly decreased with an increasing particle diameter, however, the differences detected are not significant with respect to mass transport limitation. This is corroborated by the dependence of the CO partial pressure on the methanol conversion, as depicted in Fig. 2.1.6.

According to Fig. 2.1.6, the CO levels for the three fractions at the same conversions were very similar and thus all values could be fitted with the same exponential function. It may therefore be

concluded that intraparticle transport phenomena exerted no considerable influence on the CO formation. Hence, because mass transport limitations can be excluded, a reliable kinetic model was suggested for the steam reforming of methanol. The kinetic parameters were determined by fitting the model to the experimental results obtained for the CZC catalysts.

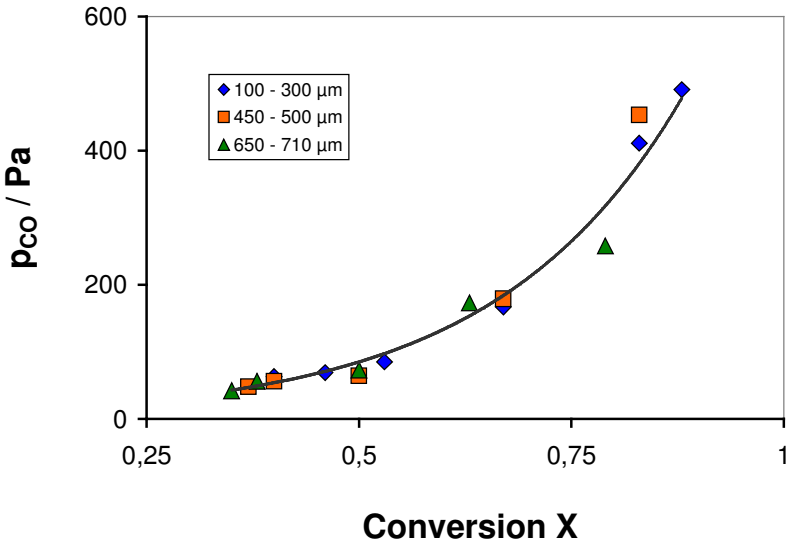

Figure 2.1.6: CO partial pressures determined for various sieve fractions of CZC15 during SRM under standard conditions (m = 0.5500 g, T = 523 K, p = 10^5 Pa, MeOH:H_2O = 1:1)

2.1.3.2. Kinetic model

The individual reactions to be included in the kinetic model of the methanol steam reforming process are still under debate. Earlier studies have suggested that the kinetics could be sufficiently described by using only one or two of the possible overall reactions while assuming that the others were either at equilibrium or their rates were negligible. Initially, SRM was supposed to proceed by the formation of CO and H_2, followed by the water-gas shift (WGS) reaction [15,42]. The formation of CO_2 by the direct reaction of methanol and steam has also been proposed [43]. Methanol

decomposition was involved in the reaction mechanism in certain studies [14,42,44], whereas in other cases, it was regarded as insignificant [16,21].

An adequate kinetic model for the steam reforming of methanol on a commercial $Cu/ZnO/Al_2O_3$ catalyst, which includes methanol decomposition (Eq.1) and the WGS reaction (Eq.5), in addition to the SRM process (Eq.2), has been recently suggested by Peppley et al [25].

$$CO + H_2O_{(g)} \underset{k_{RWGS}}{\overset{k_{WGS}}{\rightleftharpoons}} CO_2 + H_2 \qquad \Delta H^0 = -41\ kJ.mol^{-1} \qquad (5)$$

Further investigations on SRM revealed that the above model may also apply for other catalysts including Zr- or Ce-containing systems [28-30]. For the present study, it was found that a kinetic evaluation performed by including MD in the reaction scheme afforded a better fit to the experimental data. Accordingly, evaluation of the experimental data obtained for the CZC samples was based on Peppley's model. The kinetic model suggested by Takahashi et al., involving a methyl formate intermediate [45], may be regarded as less suitable for evaluation, given that no methyl formate production was observed under the present experimental conditions. In fact, methyl formate is more likely to be formed when the reaction is conducted in an excess of methanol [3].

CO formation has been generally observed at high methanol conversions and long contact times, indicating that CO is a secondary product, formed by the reverse water-gas-shift (RWGS) reaction [3,6,28]. For the CZC samples, kinetic analysis suggested that the amount of CO produced by MD was considerably lower than that formed by the RWGS reaction and therefore the reaction scheme was simplified by regarding MD as an irreversible reaction. Furthermore, because of the low Hüttig temperature of Cu [46], as reflected in its relatively low melting point (1356 K) [5,6], Cu-based

catalysts tend to undergo thermal deactivation at temperatures exceeding 573-623 K [5,6,47]. In order to eliminate ageing effects, kinetic measurements for the CZC samples were carried out in the temperature range 503-573 K.

According to the above considerations, the reaction scheme utilized for methanol steam reforming on CZC catalysts included the MD, SRM and the RWGS reactions (Eqs.1,2,5). Because SRM is the sum of the other two reactions, the above processes are not independent [26]. The partial pressures of the reactants and products were calculated by assuming that the contribution of MD to the conversion was negligible. If the SRM reaction for an equimolar mixture of methanol and water takes place with a conversion of X, then the total mole number after SRM is $n = n_0(1+X)$. By considering that the RWGS reaction proceeds with a conversion of X_w, the partial pressures of the reactants and products can be expressed as follows:

$$p_{CO} = \frac{X \cdot X_W}{2+2X} \cdot p \qquad (6)$$

$$p_{CO_2} = \frac{X(1-X_W)}{2+2X} \cdot p \qquad (7)$$

$$p_{H_2} = \frac{X(2+X_W)}{2+2X} \cdot p \qquad (8)$$

$$p_{MeOH} = \frac{1-X}{2+2X} \cdot p \qquad (9)$$

$$p_{H_2O} = \frac{1-X(1-X_W)}{2+2X} \cdot p \qquad (10)$$

The partial pressures can be obtained from Eqs. 6-10, given that $p = 10^5$ Pa, and X_w can be calculated from Raoult's law as:

$$X_W = \frac{\varphi_{CO}}{\varphi_{CO} + \varphi_{CO2}} \qquad (11)$$

where φ_{CO} and φ_{CO_2} are the volume fractions for CO and CO_2, respectively, which can be determined from the corresponding GC peak areas after analyzing the calibration gas mixture.

The rate equations for the model reactions (Eqs. 1,2,5) can be described as follows:

$$r_{SRM} = k_{SRM} \cdot p_{MeOH}^{m_1} \cdot p_{H_2O}^{m_2} - k_{RSRM} \cdot p_{CO_2}^{m_3} \cdot p_{H_2}^{3 \cdot m_4} \quad (12)$$

$$r_{MD} = k_{MD} \cdot p_{MeOH}^{m_5} \quad (13)$$

$$r_{RWGS} = k_{RWGS} \cdot p_{CO_2}^{m_6} \cdot p_{H_2}^{m_7} - k_{WGS} \cdot p_{CO}^{m_8} \cdot p_{H_2O}^{m_9} \quad (14)$$

Accordingly, the differential equations for the single components (obtained by the Maple V software, release 4.00c) are given below.

$$\frac{\partial p_{MeOH}}{\partial t} = -(r_{SRM} + r_{MD}) \cdot \frac{2}{1+X} \quad (15)$$

$$\frac{\partial p_{H_2O}}{\partial t} = -(r_{SRM} + r_{RWGS}) - (r_{SRM} + r_{MD}) \cdot \frac{p_{H_2O}}{p_{MeOH,0}} \quad (16)$$

$$\frac{\partial p_{CO}}{\partial t} = (r_{MD} + r_{RWGS}) - (r_{SRM} + r_{MD}) \cdot \frac{p_{CO}}{p_{MeOH,0}} \quad (17)$$

$$\frac{\partial p_{CO_2}}{\partial t} = (r_{SRM} - r_{RWGS}) - (r_{SRM} + r_{MD}) \cdot \frac{p_{CO_2}}{p_{MeOH,0}} \quad (18)$$

$$\frac{\partial p_{H_2}}{\partial t} = (3 \cdot r_{SRM} + 2 \cdot r_{MD} - r_{RWGS}) - (r_{SRM} + r_{MD}) \cdot \frac{p_{H_2}}{p_{MeOH,0}} \quad (19)$$

The increased mole numbers during SRM (4 mole of products formed from 2 mole of reactants) were taken into account via expressing the conversion X by the partial pressures of methanol as

$$X = \frac{p_{MeOH,0} - p_{MeOH,t}}{p_{MeOH,0} + p_{MeOH,t}} \quad (20)$$

Likewise, the contact time τ was determined by considering the increase of volume in the catalyst bed during conversion. It was calculated by integrating the progress of conversion $X(\ell)$ as a function of the reactor length ℓ inside the catalyst bed, as described in Eq. 21:

$$\tau = \frac{1}{\ell}\int_0^{\ell} \tau(\ell)\, d\ell = \frac{A}{w_0}\int_0^{\ell} \frac{1}{1+X(\ell)}\, d\ell \quad (21)$$

where A is the cross section of the reactor and w_0 is the initial flow rate of the reactants. Further, $X(\ell)$ may be sufficiently well approximated by an exponential function (Eq.22):

$$X(\ell) = 1 - e^{-\varpi\ell} \quad (22)$$

and the parameter ω can be obtained from the values of the final conversion X_f and the final length of the catalyst bed ℓ_f (Eq.23).

$$\varpi = -\frac{\ln(1-X_f)}{\ell_f} \quad (23)$$

The kinetic evaluation was performed by means of the Berkeley Madonna 8.0.1. software. A Runge Kutta method was used to solve the differential equations (Eqs. 15-19) and the experimental data were fitted by a least-squares method. The rate constants for the model reactions were determined by fitting the simulation to the experimental data by varying the reaction orders until a good agreement was obtained and this procedure was repeated until an

optimal fit was achieved. According to the previous results of Purnama et al., the total reaction order for SRM (m_1+m_2) was 1, whereas the individual reaction orders determined experimentally for methanol and water were 0.6 and 0.4, respectively [21]. The application of the above reaction orders ensured an optimal fit for the current experimental data. For the components involved in the RWGS reaction, the reaction orders were set to 1 [21], in correlation with those published by Choi and Stenger in their detailed study on the kinetics of the WGS reaction [48], including rate expressions derived from various reaction mechanisms [49]. The rate constants for both the RWGS and the MD reactions were considerably smaller than that of SRM, as revealed by the low CO production, and thus the reaction orders of the components implied in RWGS and MD had no appreciable effect on the fitting results. The reaction orders are summarized in Table 2.1.2.

SRM		RWGS		MD	
component	reaction order	component	reaction order	component	reaction order
MeOH	0,6	CO_2	1,0	MeOH	1,3
H_2O	0,4	H_2	1,0		
CO_2	1,0	CO	1,0		
H_2	1,0	H_2O	1,0		

Table 2.1.2: Reaction orders for the components involved in the kinetic model

The partial pressures for the components of the product stream were determined as a function of the contact time at the temperatures 503, 523, 543 and 573 K for all catalysts. The results obtained for CZC15

are displayed in Figs. 2.1.7-10. Between the respective data for the other CZC samples, no significant differences were observed.

Figures 7-10

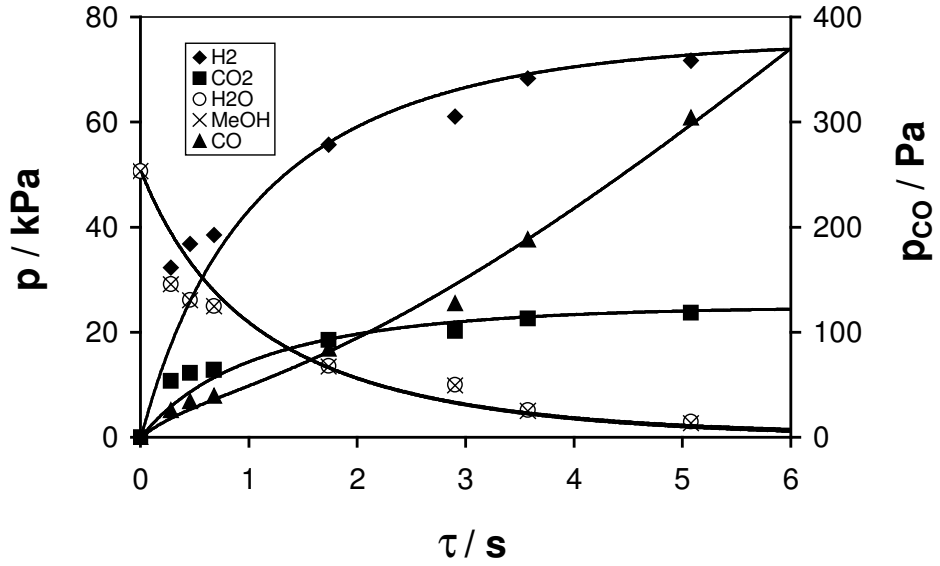

Figure 2.1.7: Partial pressures of the components in the reaction mixture during SRM on CZC15, experimental data and fitting results; m = 0.6726 g, T = 503 K, p = 10^5 Pa, MeOH:H_2O = 1:1

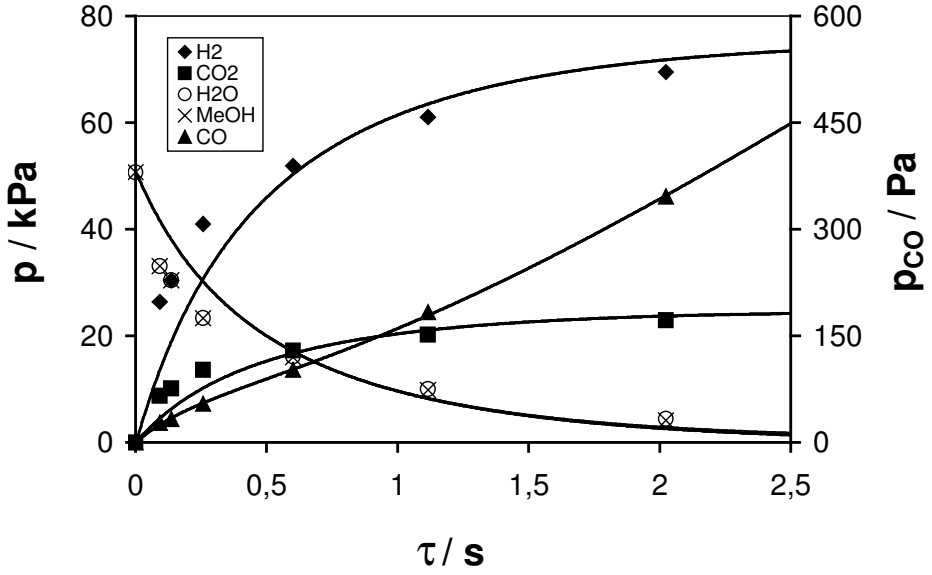

Figure 2.1.8: Partial pressures of the components in the reaction mixture during SRM on CZC15, experimental data and fitting results; m = 0.6726 g, T = 523 K, p = 10^5 Pa, MeOH:H_2O = 1:1

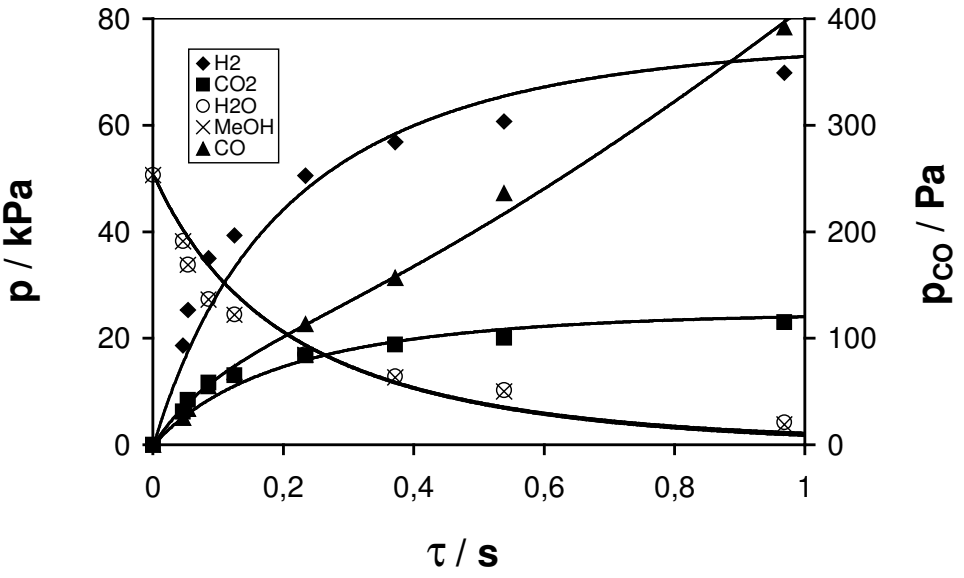

Figure 2.1.9: Partial pressures of the components in the reaction mixture during SRM on CZC15, experimental data and fitting results; m = 0.6726 g, T = 543 K, p = 10^5 Pa, MeOH:H_2O = 1:1

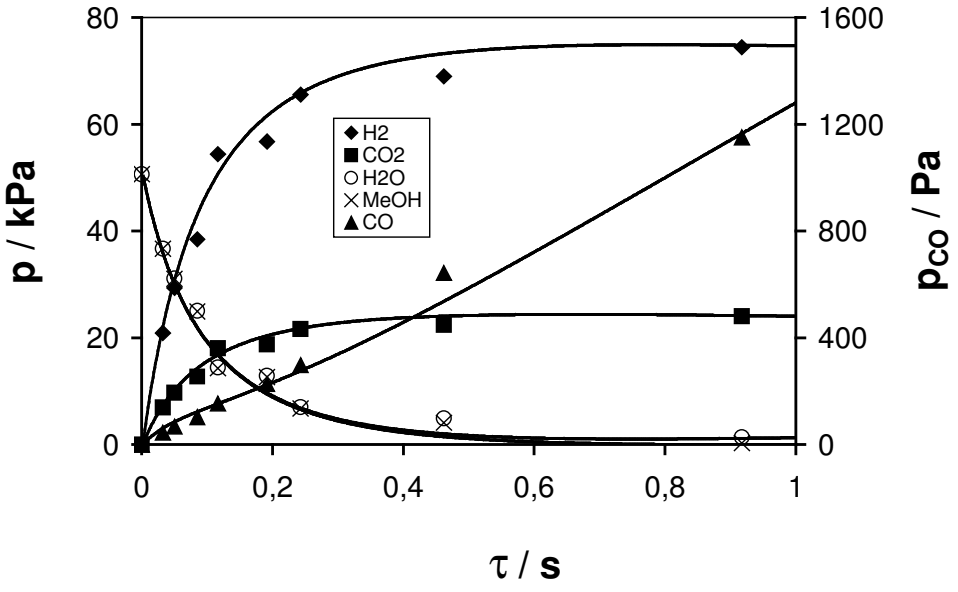

Figure 2.1.10: Partial pressures of the components in the reaction mixture during SRM on CZC15, experimental data and fitting results; m = 0.6726 g, T = 573 K, p = 10^5 Pa, MeOH:H_2O = 1:1

It can be seen from Figs. 2.1.7-10 that the partial pressures of the reactants methanol and water decreased to the same extent with increasing contact times at all temperatures. The most pronounced

decrease can be observed at 573 K, where complete transformation occurred at $\tau < 1$ s. Meanwhile, the partial pressures of the main reaction products H_2 and CO_2 increased steadily during reaction, and could be fitted with saturation curves, for which the limits for H_2 and CO_2 production proved to be 70-75 kPa and 24 kPa, respectively. This implies that the amount of H_2 gained in the reaction at 573 K attains the theoretical maximum of 75%, corresponding to the thermodynamical equilibrium state [4], and approaches it reasonably well at lower temperatures. The differences in the partial pressures of H_2 and CO_2 at various contact times confirm that the amount of H_2 formed in the reaction was 3 times higher than that of CO_2, irrespective of the reaction temperature and the conversion level. By increasing the contact time, CO_2 formation was less affected than H_2 production and the contact time required to reach the saturation value decreased with the reaction temperature to an appreciable extent.

Compared to a commercial $Cu/ZnO/Al_2O_3$ catalyst [21], the H_2 partial pressures obtained for the CZC samples were somewhat lower (74–85% of those reported for the commercial sample between 503 K and 573 K, respectively) at short contact times. Nevertheless, the saturation values observed for the CZC catalysts at long contact times approached 75 kPa at all temperatures.

The minor amount of CO detected in the reaction mixture was found to increase with both the contact time and the reaction temperature. In the temperature range investigated, the amount of CO typically varied between 0.06-0.4%, only exceeding that at 573 K, at contact times longer than 0.4 s. Unlike the main reaction products, the formation of CO can be described with S-shaped curves at each temperature, which may be regarded as a further evidence of CO being a secondary product in the reaction [6,21]. As shown in Figs. 2.1.7-10, the partial pressures of CO could be fitted at all temperatures and contact times when MD was included in the reaction scheme. Nevertheless, it should be noted that the

significance of MD can be observed merely at low contact times and therefore CO production is suggested to occur predominantly by the RWGS reaction. The conversions obtained for CZC15 at different temperatures, plotted as a function of the contact time, are displayed in Fig. 2.1.11.

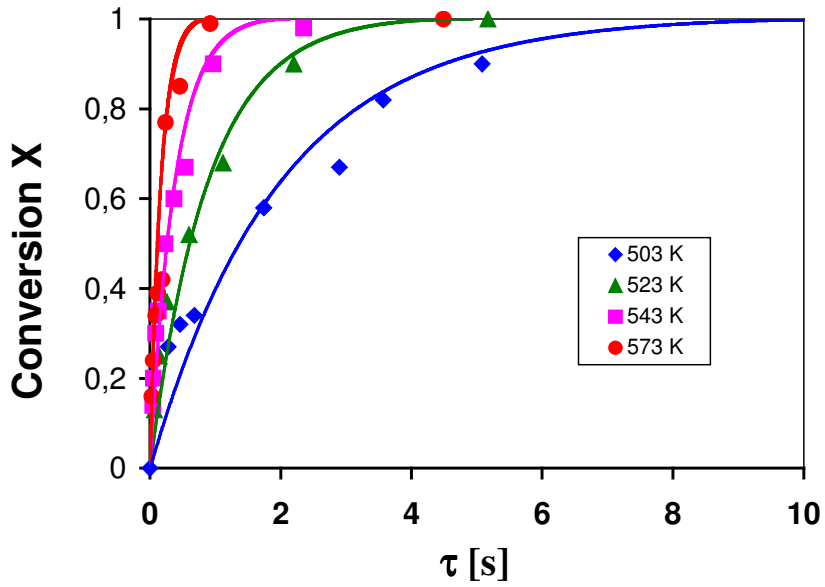

Figure 2.1.11: Methanol conversions during SRM of CZC15 as a function of contact time at different reaction temperatures (m = 0.6726 g, p = 10^5 Pa, MeOH:H_2O = 1:1)

The complete transformation of methanol could be achieved at all reaction temperatures, except for 503 K, at which the contact time corresponding to full conversion was determined by extrapolation (τ ~10 s). It can be seen that an increase in the reaction temperature resulted in a marked decrease of the contact time corresponding to the same conversion level. Accordingly, the full conversion of methanol at 573 K was observed at a contact time of 0.92 s. Although an increase in the reaction temperature proved to be beneficial in terms of the catalytic activity, as suggested by Fig.11, it also resulted in the formation of an increased amount of CO in the product mixture (see Fig. 2.1.12). Furthermore, a prolonged exposure of the catalyst to 573 K was found to result in a moderate deactivation, which may be due to sintering of the active Cu particles [6,47]. For the other

CZC samples, similar observations have been made. Likewise, Lindström and Pettersson reported that sintering of Cu particles of a $Cu/ZnO/Al_2O_3$ catalyst subjected to 613 K resulted in a loss of Cu surface area [50]. Hence, the optimal reaction temperature range for the steam reforming of methanol on CZC catalysts is 523-543 K, at which high methanol conversions can be achieved while maintaining a low CO level.

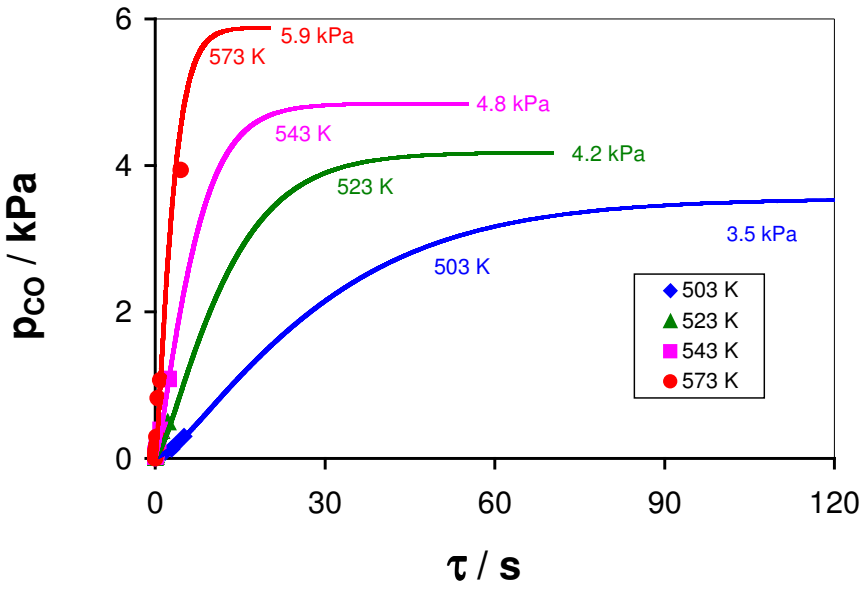

Figure 2.1.12: CO partial pressures during SRM of CZC15 as a function of contact time at different reaction temperatures (m = 0.6726 g, p = 10^5 Pa, MeOH:H_2O = 1:1)

For the CO partial pressures, fitting of the experimental data was performed by setting the final values, calculated at long contact times from the thermodynamical equilibrium constant of the RWGS reaction, as displayed in Fig. 2.1.12. For comparison, these values were also determined experimentally by investigating a large amount of catalyst (m = 3.55 g) at a low flow rate of 0.01 cm^3min^{-1} to ensure an extended contact time for the reaction. The CO partial pressures obtained from repeated runs at different temperatures were in good agreement with the theoretical values. It can be observed in Fig. 2.1.12 that the experimental CO levels are located at the low end of the theoretical curves and, hence, are far below those predicted by equilibrium calculations at all temperatures. It follows that the limiting

CO partial pressures could be attained only at contact times considerably longer than those obtained under the present experimental conditions (see also Figs. 2.1.7-10). Accordingly, it is reasonable to assume that the kinetics of the CO formation is more complex than that described within the framework of this study [21].

Nevertheless, the kinetic model employed provides a good approximation for the experimental data obtained for all components in the contact time region where complete methanol conversion occurs, which may be of major interest for industrial applications.

The reaction rate constants k for the individual reactions, obtained from the simulations performed by applying the reaction orders indicated in Table 2.1.2, are listed below in Table 2.1.3. For a better comparison, all values were referred to a CuO content of 1.0 g.

Sample	k_R [$s^{-1}g^{-1}$]^{a*}				$10^2 \cdot k_{-W}$ [$bar^{-1}s^{-1}g^{-1}$]^{b*}			
	503K	*523K*	*543K*	*573K*	*503K*	*523K*	*543K*	*573 K*
CZC5	0.03	0.12	0.39	0.77	0.04	0.12	0.34	1.25
CZC15	0.76	1.69	3.92	8.97	0.91	2.02	4.28	11.89
CZC25	1.0	2.80	4.0	7.41	1.10	4.81	6.95	15.51
CZC35	2.3	5.29	7.67	14.28	2.68	4.98	9.58	19.92

Sample	k_D [$bar^{-0.3}s^{-1}g^{-1}$]^{c*}			
	503K	*523K*	*543K*	*573K*
CZC5	0.04	0.13	0.66	2.12
CZC15	0.09	0.36	1.02	2.89
CZC25	0.14	0.38	1.13	4.50
CZC35	0.36	0.96	1.54	3.44

Table 2.1.3: Rection rate constants determined for the SRM, RWGS and MD reactions on the CZC catalysts at different reaction temperatures; [a] reaction rate constant of SRM, [b] reaction rate constant of RWGS, [c] reaction rate constant of MD, [*] all values were referred to a CuO content of 1.0 g

For the most active catalyst (CZC35) investigated at the highest reaction temperature (573 K), the Thiele modulus [51] was calculated to be 0.594, from which the mass transfer factor (the actual reaction rate as referred to the ideal reaction rate without transport limitation) was 0.977, indicating that the mass transport limitation was indeed negligible and thus the reaction was kinetically controlled. Given that the reaction rates for the other CZC samples were found to be typically lower, in particular at temperatures below 573 K, the effect of intraparticle transport phenomena on the kinetic parameters can be safely excluded.

The apparent activation energies were determined from the slopes of the Arrhenius plots, as expressed in Eq. 24.

$$\ln k = \ln k_0 - \frac{E_A}{RT} \qquad (24)$$

A typical illustration of the Arrhenius parameters for the model reactions on CZC15 is displayed in Fig. 2.1.13. It may be readily observed from the slopes that the activation energies of SRM and RWGS are comparable and considerably lower than that of MD. The values of the activation energies for the SRM, RWGS and MD reactions, determined for all the CZC samples, are listed in Table 2.1.4.

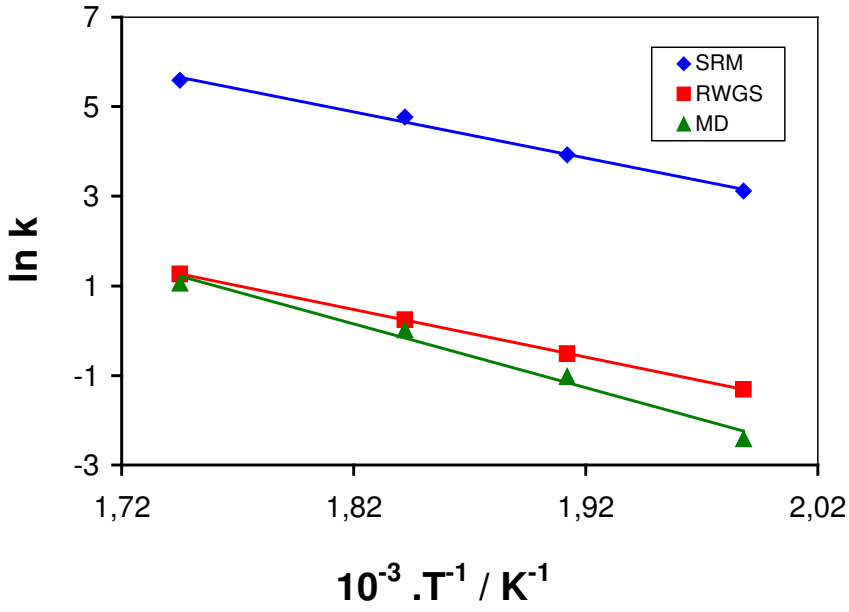

Figure 2.1.13: Arrhenius plots for the SRM, RWGS and MD reactions determined for CZC15

Reaction	E_A [kJmol^{-1}] CZC5	E_A [kJmol^{-1}] CZC15	E_A [kJmol^{-1}] CZC25	E_A [kJmol^{-1}] CZC35
SRM	109.2	85.4	66.1	60.7
RWGS	115.5	88.2	85.7	69.3
MD	142.6	118.7	104.9	75.5

Table 2.1.4 : Apparent activation energies for the SRM, RWGS and MD reactions on the CZC catalysts

According to Table 2.1.4, no significant differences between the activation energies of the SRM and RWGS reactions can be observed, except for CZC25. For the latter sample, the activation energy of the RWGS reaction was considerably higher than that for SRM, which may account for the particularly low CO level observed for this catalyst (see Fig. 2.1.4). On the other hand, the activation energies for MD proved to be considerably higher than those of SRM and RWGS and therefore MD may be regarded as the rate-limiting step for CO formation at short contact times. As mentioned above, the significance of MD in the overall reaction mechanism decreases dramatically at contact times exceeding 0.3-1 s, depending on the reaction temperature. Accordingly, the enhanced CO levels obtained at longer contact times can be attributed to the predominance of the RWGS reaction, which requires a considerably lower activation energy.

For the main reaction (SRM), the apparent activation energies proved to be relatively close for all samples, apart from CZC5, for which the highest value was obtained. For comparison, the Arrhenius plots for all the CZC samples are depicted in Fig. 2.1.14. For CZC5 and CZC15, the apparent activation energies are in good agreement

with those reported in the literature for $Cu/ZnO/Al_2O_3$ catalysts, whereas the values for CZC25 and CZC35 are lower [6,16,21,52].

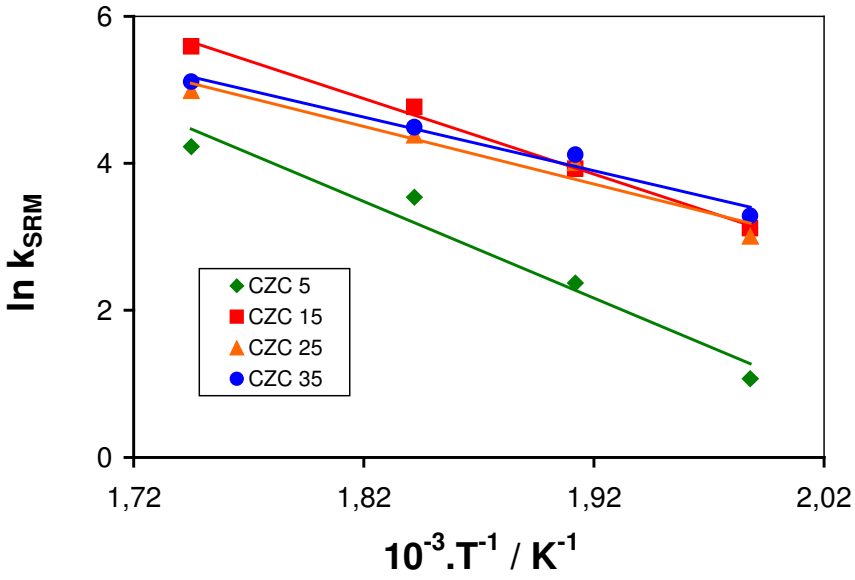

Figure 2.1.14: Arrhenius representation of the reaction rate constants obtained for the SRM reaction on the CZC catalysts

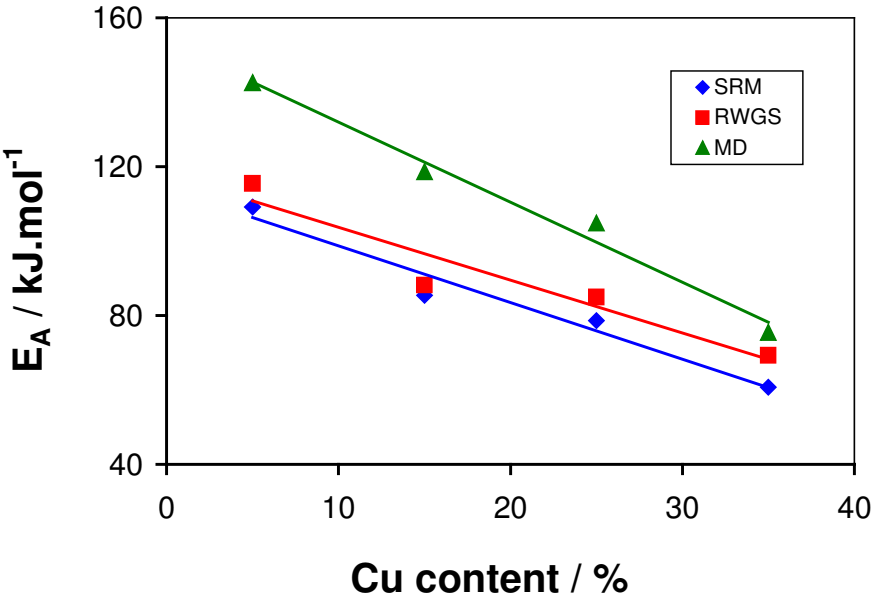

Figure 2.1.15: Apparent activation energies of the model reactions (SRM, RWGS, and MD) as a function of the Cu content of four CZC catalysts

For all the model reactions (SRM, RWGS, and MD), the activation energies determined exhibit a linear correlation with the Cu content, as shown in Fig. 2.1.15. On increasing the amount of Cu, a systematic decrease can be observed for each reaction. The most pronounced decrease can be observed in the activation energy of MD, indicating that at lower Cu loading the contribution of MD to CO formation diminishes. Takeguchi et al. have reported a similar trend for the SRM reaction on two Cu/ZnO catalysts [53], although a potential mass transport limitation was not taken into account and thus their studies cannot be directly compared with the results presented here. Conversely, in the current study, the well-known effect of mass transport limitation on the kinetic studies to result in a reduced apparent activation energy can be excluded. Therefore, it is concluded that the variation of the Cu concentration in the CeO_2/ZrO_2 precursor material gave rise to the formation of CZC samples with significantly different catalytic behaviour. Whereas the chemical complexity in the various CZC catalysts remains the same, the chemical composition adjusted in the preparation procedure results in a significantly altered structural complexity of the materials. These catalysts with vastly different active surfaces exhibit a catalytic behaviour that is not simply correlated to the accessible surface area. Dispersion, Cu particle size, and Cu support interactions have a pronounced influence on the microstructure of the Cu particles and the effect of the microstructure on the active Cu surface. Eventually, both the Cu surface area and the microstructural properties of the Cu particles need to be elucidated in order to fully understand the significantly different catalytic activities and the kinetics described above.

2.1.4. Conclusions

Novel $Cu/ZrO_2/CeO_2$ materials prepared by co-precipitation and polymer templating have been investigated as catalysts in the steam reforming of methanol. Catalytic measurements were performed under continuous operation in a fixed bed reactor at atmospheric pressure. Time-on-stream experiments indicated that following an initial period of deactivation, the conversions for the samples with Cu contents exceeding 5% were stabilized and thus these samples could be suitable for prolonged catalytic applications. An increase in the Cu content from 5 to 15% was found to improve the long-term stability and suppress the CO production considerably, whereas the effect of a further enhancement was less significant. With respect to a reduced formation of CO during SRM, the samples with increased Cu loadings proved to be more efficient catalysts.

Since the effect of mass transport limitations on the catalytic reaction was found to be insignificant, a kinetic analysis was undertaken. The reaction scheme suggested for the overall transformation included the SRM, MD and RWGS reactions. The experimental data obtained in the range 503-573 K could be well fitted by the kinetic model employed. The optimal temperature range for SRM on the CZC catalysts was 523-543 K, for which high methanol conversions and low CO levels were obtained. For the SRM and RWGS reactions, the values of the activation energies were comparable and considerably lower than that of MD. The activation energy of each individual reaction exhibited a systematic decrease with an increasing Cu content of the catalyst. Evidently, the variation in the Cu concentration of the precursor material during preparation altered the microstructure of the Cu particles and, thus the active Cu surface, which considerably affected the catalytic behaviour of the CZC catalysts.

2.1.5. References

[1] B. Lindström, L.J. Pettersson, Int. J. Hydrogen Energy 26 (2001) 923.

[2] S. Velu, K. Suzuki, M. Okazaki, M.P. Kapoor, T. Osaki, F. Ohashi, J. Catal. 194 (2000) 373.

[3] J.P. Breen, J.R.H. Ross, Catal. Today 51 (1999) 521.

[4] P.J. de Wild, M.J.F.M. Verhaak, Catal. Today 60 (2000) 3.

[5] J. Agrell, H. Birgersson, M. Boutonnet, I. Melian-Cabrera, R.M. Navarro, J.L.G. Fierro, J. Catal. 219 (2003) 389.

[6] J. Agrell, H. Birgersson, M. Boutonnet, J. Power Sources, 4654 (2002) 1.

[7] G.A. Olah, Catal. Lett. 93 (2004) 1.

[8] B. Lindström, L.J. Pettersson, J. Power Sources 106 (2002) 264.

[9] J. Agrell, M. Boutonnet, J.L.G. Fierro, Appl. Catal. A 253 (2003) 213.

[10] S. Velu, K. Suzuki, T. Osaki, Chem. Commun. (1999) 2341.

[11] J. Papavasiliou, G. Avgouropoulos, T. Ioannides, Catal. Commun. 5 (2004) 231.

[12] X.R. Zhang, P. Shi, J. Zhao, M. Zhao, C. Liu, Fuel Processing Technol. 83 (2003) 183.

[13] K. Takahashi, N. Takezawa, H. Kobayashi, Appl. Catal. 2 (1982) 383.

[14] E. Santacesaria, S. Carra, Appl. Catal. 5 (1983) 345.

[15] J.C. Amphlett, R.F. Mann, R.D. Weir, Can. J. Chem. Eng. 66 (1988) 950.

[16] C.J. Jiang, D.L. Trimm, M.S. Wainwright, Appl. Catal. A 93 (1993) 245.

[17] N. Iwasa, S. Masuda, N. Ogawa, N. Takezawa, Appl. Catal. A 125 (1995) 145.

[18] C. Cao, G. Xia, J. Holladay, E. Jones, Y. Wang, Appl. Catal. A 262 (2004) 19.

[19] W.H. Cheng, I. Chen, J. Liou, S.S. Lin, Top. Catal. 22 (2003) 225.

[20] M.V. Twigg, M.S. Spencer, Top. Catal. 22 (2003) 191.

[21] H. Purnama, T. Ressler, R.E. Jentoft, H. Soerijanto, R. Schlögl, R. Schomäcker, Appl. Catal. A 259 (2004) 83.

[22] M.M. Günter, T. Ressler, R.E. Jentoft, B. Bems, J. Catal. 203 (2001) 133.

[23] B.L. Kniep, T. Ressler, A. Rabis, F. Girgsdies, M. Baenitz, F. Steglich, R. Schlögl, Angew. Chem. Int. Ed. 43 (2004) 112.

[24] T. Shishido, Y. Yamamoto, H. Morioka, K. Takaki, K. Takehira, Appl. Catal. A 263 (2004) 249.

[25] B.A. Peppley, J.C. Amphlett, L.M. Kearns, R.F. Mann, Appl. Catal. A 179 (1999) 21.

[26] S.P. Asprey, B.W. Wojciechowski, B.A. Peppley, Appl. Catal. A 179 (1999) 51.

[27] H. Purnama, F. Girgsdies, T. Ressler, J.H. Schattka, R.A. Caruso, R. Schomäcker, R. Schlögl, Catal. Lett. 94 (2004) 61.

[28] J.P. Breen, F.C. Meunier, R.H. Ross, Chem. Commun. (1999) 2247.

[29] P.H. Matter, D.J. Braden, U.S. Ozkan, J. Catal. 223 (340) 2004.

[30] X. Zhang, P. Shi, J. Mol. Catal. A 194 (2003) 99.

[31] Y. Liu, T. Hayakawa, K. Suzuki, S. Hamakawa, T. Tsunoda, T. Ishii, M. Kumagai, Appl. Catal. A 223 (2002) 137.

[32] H.S. Roh, K.W. Jun, W.S. Dong, S.E. Park, Y.S. Baek, Catal. Lett. 74 (2001) 31.

[33] M.F. Luo, J. Chen, L.S. Chen, J.Q. Lu, Z. Feng, C. Li, Chem. Mater. 13 (2001) 197.

[34] B.C. Gates, Catalytic Chemistry, Wiley, New York, 1992.

[35] A.S. Deshpande, N. Pinna, P. Beato, M. Antonietti, M. Niederberger, Chem. Mater. 16 (2004) 2599.

[36] G.C. Chinchen, C.M. Hay, H.D. Vandervell, K.C. Waugh, J. Catal. 103 (1987) 79.

[37] M.M. Günter, T. Ressler, B. Bems, C. Büscher, T. Genger, O. Hinrichsen, M. Muhler, R. Schlögl, Catal. Lett. 71 (2001) 37.

[38] R.A. Young, The Rietveld Method, Oxford University Press, New York, 1993.

[39] Y. Choi, H.G. Stenger, Appl. Catal. B 38 (2002) 259.

[40] J. Agrell, M. Boutonnet, I. Melian-Cabrera, J.L.G. Fierro, Appl. Catal. A 253 (2003) 201.

[41] E.D. Schrum, T.L. Reitz, H.H. Kung, Stud. Surf. Sci. Catal. 139 (2001) 229.

[42] J.C. Amphlett, M.J. Evans, R.F. Mann, R.D. Weir, Can. J. Chem. Eng. 63 (1985) 605.

[43] J.C. Amphlett, R.F. Mann, B.A. Peppley, Stud. Surf. Sci. Catal. 81 (1994) 409.

[44] H. Kobayashi, N. Takezawa, C. Minochi, Chem. Lett. (1976) 1347.

[45] K. Takahashi, N. Takezawa, H. Kobayashi, Appl. Catal. 2 (1982) 383.

[46] M.S. Spencer, Nature 323 (1986) 685.

[47] M.V. Twigg, M.S. Spencer, Appl. Catal. A 212 (2001) 161.

[48] Y. Choi, H.G. Stenger, J. Power Sources 124 (2003) 432.

[49] N. Amadeo, M. Laborde, Int. J. Hydrogen Energy 20 (1995) 949.

[50] B. Lindström, L.J. Pettersson, Catal. Lett. 74 (2001) 27.

[51] O. Levenspiel, Chemical Reaction Engineering, Wiley, New York, 1972.

[52] K. Geissler, E. Newson, F. Vogel, T.B. Truong, P. Hottinger, A. Wokaun, Phys. Chem. Chem. Phys. 3 (2001) 47.

[53] T. Takeguchi, Y. Kani, M. Inoue, K. Eguchi, Catal. Lett. 83 (2002) 49.

2.2. Autothermal reactor concept for SRM

2.2.1. Introduction

The new generation of fuel cells is less sensitive against carbon monoxide and many new catalyst synthezised in the past years have better long term stability and selectivity. But since CO is produced always either as byproduct or consecutive product, it still needs to be removed or separated otherwise the performance of the fuel cells over the time would be affected.

In the steam reforming process, methanol would is converted to hydrogen and carbon dioxide. During this process it depends on the reaction path way at the used catalyst which specific intermediates are favoured. In our in situ DRIFT measurements [1] we could see that the catalyst which favours *methylformate* as intermediate produced carbon monoxide in a large ammount. The better catalyst which produced less carbon monoxide prefer the reaction path way with *dioxomethylene* as intermediate which decomposes to carbon dioxide. The steam reforming of methanol at this second type of catalyst produce the carbon monoxide as a consecutive product by reverse water gas shift reaction, preferentially.

The involved reactions are listed here as an overview for further discussion:

$$\text{SRM: } CH_3OH_{(g)} + H_2O \underset{k_{RSRM}}{\overset{k_{SRM}}{\rightleftharpoons}} 3H_2 + CO_2 \qquad \Delta H^0 = 50\ kJ.mol^{-1} \qquad (1)$$

$$\text{MD: } CH_3OH_{(g)} \underset{k_{RMD}}{\overset{k_{MD}}{\rightleftharpoons}} 2\,H_2 + CO \qquad \Delta H^0 = 91\ kJ.mol^{-1} \qquad (2)$$

$$\text{POM: } CH_3OH_{(g)} + 0{,}5O_2 \underset{k_{RPOM}}{\overset{k_{POM}}{\rightleftharpoons}} 2H_2 + CO_2 \qquad \Delta H^0 = -192\ kJ.mol^{-1} \qquad (3)$$

$$\text{WGS} \quad CO + H_2O_{(g)} \underset{k_{RWGS}}{\overset{k_{WGS}}{\rightleftharpoons}} CO_2 + H_2 \qquad \Delta H^0 = -41\ kJ.mol^{-1} \qquad (4)$$

$$\text{MO:}\ CH_3OH_{(g)} + 1{,}5O_2 \underset{k_{RMO}}{\overset{k_{MO}}{\rightleftharpoons}} 2H_2O + CO_2 \qquad \Delta H^0 = -725\ kJ.mol^{-1} \qquad (5)$$

The main reaction is the Steam Reforming of Methanol (SRM). The Methanol Decomposition (MD) is a parallel reaction which appears negligible at good catalysts. The Partial Oxidation of Methanol (POM) could be carried out on Cu/Zn-catalysts and it occurs also during Preferential Oxidation (PROX) which could be arranged if about 1% oxygen is added to steam reforming feed. In the Oxidative Steam Reforming of Methanol (OSRM) both SRM and POM take place. Velu et all [2] found that a oxygen/methanol ratio more than 0.3 leads to a decrease of hydrogen production as some hydrogen is consumed by oxygen over that ratio. If OSRM is carried out near to autothermal condition, it could be called as Combined Reforming of Methanol (CRM). Agrell et al [3] suggested an oxygen to methanol ratio of 0,2 for a CRM at 260°C and a construction of consecutive reactors because a simultaneous combining of oxygen and SRM feed in the inlet did not resilt in a parallel process of SRM and POM and therefore had no effect in minimizing the CO content.

There are some strategies to minimize the carbon monoxide concentration in the reformate gases or to purify the hydrogen from carbon monoxide. For example: a WGS reactor can be subsequently attached to the reformer or prevential CO oxidation (PROX) can reduce the carbon monoxide content. A study of Pan et al [4] reported that they reduced the CO concentration to less than 50 ppm by using of four prefential oxidation reactor. A study of Pozdnyakova et all [5] reported the advantages of a Pt/CeO_2 catalyst which has oxygen storage capacity (OSC) and showed an excellent activity at lower temperatures.

However, the downstream aftertreatments need an extra heating and some hydrogen lost.

In case that the carbon monoxide is a product of a consecutive reaction [6, 7], a membrane reactor can be used. At least the higher pressure in a membrane reactor could suppress the methanol decomposition and since back mixing in a reactive membrane is excluded, the product gases have a limited time for the consecutive reaction. A comparison between traditional PFTR and a reactive membrane reactor in our former study [6] confirmed this. But the reactive membrane still produced to much carbon monoxide, even it was definetely less than the CO concentration from PFTR. The produced hydrogen still had to be purified for the application in fuel cells.

Hydrogen purification by metal membranes is very selective. A CO-free hydrogen can be achieved by this method. But it needs high pressure, is quite expensive and its yield is far from satisfying. A study of the application of dense metal membranes by Basile et al succesfully produced a CO-free permeate, but the recovered yield of hydrogen was under 30% [8]. A better recovery rate can be achieved by setting higher temperatures but this requires more energy.

Doohwan Lee reported in his thesis [9] about a highly hydrogen permeable silica membrane supported on porous alumina. After 12 h silica deposition the pore diameter became smaller and the permeance of the gases was not controlled by Knudsen diffusion anymore, but because of the size of the gases, a high operating pressure and temperature were necessary. The study on alumina membrane, after 12 h silica deposition, achieved at 70 kPa and 873 K a hydrogen selectivity for CO was over 2000 and a hydrogen permeance in order of 10^{-7} $mol.m^{-2}.s^{-1}.Pa^{-1}$. The recovery rate was not reported, but it is a public secret that the recovery rate of dense materials is not satisfying.

Since the new PEMs are less sensitive to carbon monoxide, we just need to enrich the hydrogen and respectively surpress the CO content of permeate to the acceptable limit or if better catalysts were developed and the CO concetration in product gas is already under der acceptable concentration, the main task is to separate unconverted methanol which will be combusted for providing an autothermal operating mode. In order to realize this approach we developed a new aftertreatment concept which requires low energy demand. In the first step we use the optimized condition for the reforming process. Using good catalyst, water excess in feed and operating the reaction at moderate methanol conversion, which provide a low CO content in product gas.

2.2.1.1. Autothermal reforming of methanol

For the first approach of a steady state of an ATR, following assumption was made: The energy requirement consists just of the energy needed for evaporation and heating the reactants from 25°C to reaction temperature of 250°C and the energy needed for the steam reforming of methanol. The heat supply comes from the combustion of methanol and there are no energy loses due to an ideal isolation.

The sum of energy requirement is equal to heat supply from methanol combustion; this expression is formulated in following equation:

$$\int_{25}^{100} Cp(H_2O_{(l)})\,dT + \Delta H^0_{vap}(H_2O) + \int_{100}^{250} Cp(H_2O_{(g)})\,dT + \int_{25}^{100} Cp(CH_3OH_{(l)})\,dT + \Delta H^0_{vap} + \int_{100}^{250} Cp(CH_3OH_{(g)})\,dT + \left(\int_{25}^{250} Cp(O_{2(g)})\,dT + \Delta H_{SRM}\right)\cdot X = (1-X)\cdot \Delta H_{MC} \quad (6)$$

$Cp\ (H_2O_{(l)}) = 75{,}24\ J.mol^{-1}.K^{-1}$

Cp ($H_2O_{(g)}$) = 34,88 $J.mol^{-1}.K^{-1}$

Cp ($CH_3OH_{(l)}$) = 85,76 $J.mol^{-1}.K^{-1}$

Cp ($CH_3OH_{(g)}$) = 58,46 $J.mol^{-1}.K^{-1}$

Cp ($O_{2(g)}$) = 16,56 $J.mol^{-1}.K^{-1}$

ΔH_{vap}^0 (H_2O) = 40,66 $kJ.mol^{-1}$

ΔH_{vap}^0 (CH_3OH) = 35,28 $kJ.mol^{-1}$

Cp = heat capacity of water

ΔH_{vap}^0 = standard enthalpy of evaporation

ΔH_{MC} = enthalpy of Methanol combustion

X = conversion of SRM

The calculation gives a conversion of 0,8 for an authothermal process with the assumed conditions. A schematically construction of the proposed configuration is showed in Figure 2.2.1.

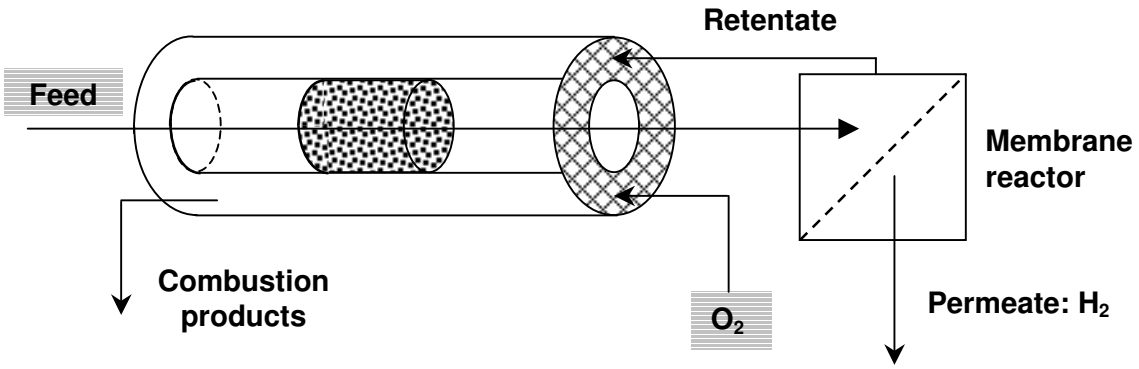

Figure 2.2.1: Autothermal reactor system for steam reforming of methanol. The feed (CH_3OH + H_2O) would be to 80% converted in the inner reactor and the retentate of membrane modul with 20% remaining methanol would be combusted with O_2/air in the outer shell of the reactor.

A thermal loss of energy can be barely be avoided at practical application. More methanol must be combusted for maintaining of an autothermal mode. Therefore the SRM must be operated at lower conversion than 0,8. For example, at conversion of 0,7 the CO concentration in the product gas is much less in comparison to the value at higher conversion, as can be seen clearly at Figure 2.2.2.

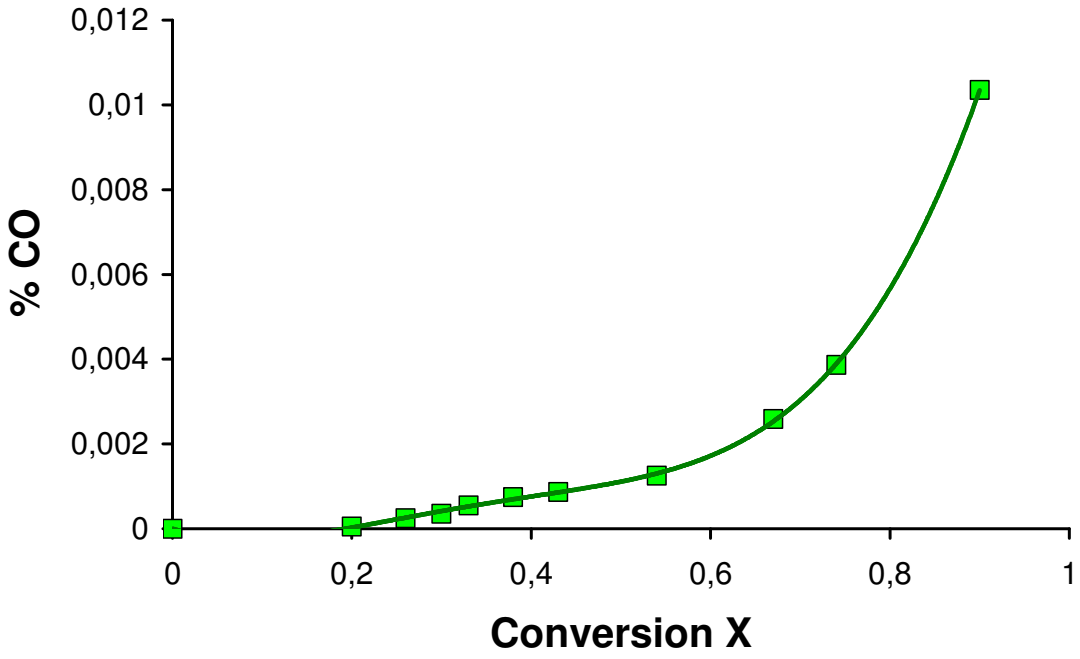

Figure 2.2.2: Depedency of carbon monoxide concetration on conversion of SRM at 250 °C over 200 mg MeOH1 + 1 g BN.

2.2.1.2. Knudsen membrane

In the second step the product gases would be fed into a membrane modul, in which the residual methanol as retentate will be redirect to the outer shell of the reactor for the combustion. The enrichment of hydrogen and the reduction of carbon monoxide content in permeate should be achieved by the Knudsen mechanism. Knudsen diffusion occurs when the mean free path of a gas is large compared to the pore size, so that the gas molecules collide

frequently with the pore wall. In Oirder to understand the enrichment process, kinetic gas theory is applied.

In the kinetic gas theory the properties and behaviour of ideal gases are assumed. The gas particles or moleculs are small hard spheres, they move randomly, collide perfectly elastic with the wall and each other frequently without any interactions, and their average kinetic energy depends only on the temperature of the system. The mean velocity of such small elastic gas particles or moleculs is:

$$\left\langle v^2 \right\rangle = \frac{3 \cdot k \cdot T}{m} \tag{7}$$

k = the Boltzmann constant = 1.38×10^{-23} $J.K^{-1}$

T = temperature of the system in K

m = mass of a single gas particle or molecule

The kinetic energy of a hard sphere gas is then:

$$E_k = \frac{1}{2} \cdot m \cdot \left\langle v^2 \right\rangle = \frac{3}{2} \cdot k \cdot T \tag{8}$$

Since gases in a thermodinamic equilibrium posess the same kinetic energy, we can express the ration of the mean velocity of two gases in this state by the following equation:

$$\left(\frac{\left\langle v_A^2 \right\rangle}{\left\langle v_B^2 \right\rangle} \right)^{1/2} = \sqrt{\frac{m_B}{m_A}} = \sqrt{\frac{M_B}{M_A}} \tag{9}$$

The movement of the gases undergo a random Brownian motion. But in case that the gases go through a turbular channel whose pore diameter smaller as their mean free path, we could make a quite accurate prediction, because the gases would always collidate with the pore wall and make forward movement. This case is the region of Knudsen diffusion. The gas molecules with a lower molecular weight have a higher velocity and will be transported faster to the other end of the turbular channel and therefore enrich in comparison to the molecules of the heavier gases.

In order to fulfil the precondition of Knudsen diffusion the pore diameter of the membrane must be smaller than the mean free path of the concerned gas.

$$\bar{\lambda} = \frac{1}{\sqrt{2} \cdot \pi \cdot \sigma^2} \cdot \frac{V}{N_A} \qquad (10)$$

$\bar{\lambda}$ = mean free path in m

N_A = Avogadro number = $6{,}023.10^{23}$ particles/mol

V = mol volume of the gas under the current pressure in m^3

σ = cross section of the molecule in m

The Knudsen diffusion occurs predominantly in pores with pore diameters between 2 and 50 nm [10]. The gases involved in SRM have a σ in a range of some Angstrom. The calculation gives a corresponding mean free path of 40 nm for the heaviest molecule at an operating temperature of 100°C.

The Knudsen diffusion coefficient of a ideal gas i in a cylindrical pores is giving by following equation:

$$D_{K,i} = \frac{d_p}{3} \cdot \sqrt{\frac{8RT}{\pi \cdot M_i}} \quad [m^2.s^{-1}] \qquad (11)$$

d_p = pore diameter

R = universal gas constant

T = temperature

M_i = molar mass of gas i

For a porous solid material we have to introduce a structure factor κ_0. The effective Knudsen diffusion coefficient is expressed by following equation:

$$D^e_{K,i} = \frac{\varepsilon_p}{\tau_K} \cdot \frac{d_p}{3} \cdot \sqrt{\frac{8RT}{\pi \cdot M_i}} = \kappa_0 \cdot \sqrt{\frac{8RT}{\pi \cdot M_i}} \qquad [m^2.s^{-1}]$$

(12)

ε_p = relative pore volume, characteristic value for solid materials: 0,2 < ε_p < 0,7

τ_K = tortuosity factor, typical values: 0,3 < τ_K < 7

The flux density of Knudsen diffusion of an ideal gas in porous solid materials j_i is then described by the first law of Fick:

$$j_i = -D^e_{K,i} \cdot \frac{\Delta c_i}{\Delta y_i} = -K_0 \cdot \sqrt{\frac{8RT}{\pi \cdot M_i}} \cdot \frac{\Delta c_i}{\Delta y_i} \quad [mol.m^{-2}.s^{-1}] \qquad (13)$$

Δc_i = concentration gradient of gas i between feed and permeate

Δy_i = thickness of pore membrane

The selectivity which can be achieved by Knudsen diffusion depends strictly on the molar mass of the involved gases. The separation factor at the beginning of Knudsen domain - pore diameter in sizes near of the mean free path - is indeed close to the value of the square root of the quotient of molecular mass of the gases. But on closer inspection the pore size plays also a role, especially in the range of small pore diameters. A more precise equation for the separation factor is given by following expression:

$$\alpha_{i,j} = \frac{j_i}{j_j} = \sqrt{\frac{M_j}{M_i}} \cdot \left(\frac{d_p - d_j}{d_p - d_i} \right)^3 = \frac{\beta_i}{\beta_j} = \frac{\left(x_{i,P} / x_{i,F} \right)}{\left(x_{j,P} / x_{j,F} \right)} \qquad (14)$$

α = separation factor

j_i = flux of gas i through the membrane

d_p = pore diameter of the membrane, d_i = molecule diameter of gas i

β_i = enrichment factor of gas i

$x_{i,P}$ = mol fraction of gas i in permeate, $x_{i,F}$ = mol fraction of gas i in feed

$$\beta_i = \frac{\alpha_{i,j}}{1 + (\alpha_{i,j} - 1) \cdot x_{i,F}} \qquad (15)$$

The curiosity of the equation of the separation factor is that $\alpha_{i,j}$ decreases with increasing pore diameter of the membrane. But if we just look at the diffusion by the Knudsen mechanism, we can understand why the separation due to the Knudsen diffusion has a higher value at larger pore diameter. The reason is that the light molecules with their higher mean free path already undergo a

Knudsen diffusion and therefore are enriched while the heavy molecules collide with each other and must undergo a Brownian molecular motion which means a longer route.

A plot of the separation factor for H_2/CO system is presented in Figure 2.2.3. Doohwan Lee [9] has measured in his study a separation factor of 3.25 for H_2/CO and a separation factor of 4.67 for the H_2/CO_2 system for a aluminium membrane with a pore diameter of 4.5 nm. This experimental result is in good agreement with the calculated value of 3.74 and 4.80 using the equation (9). The calculation by the corrected equation (14) gives 3,51 and 4,55, respectively. The results are calculated based on the data in PhD Thesis of Lee [9], which specified the diameter of H_2 = 2.89 Å, CO = 3.76 Å, CO_2 = 3.3 Å. It is also reported that the enrichment order of the gases by a denser membrane did not obey the Knudsen prediction anymore. In the range of smaller pore diameters carbon dioxide would be more enriched than carbon monoxide, even though the particle size of CO is bigger than the particle size of CO_2.

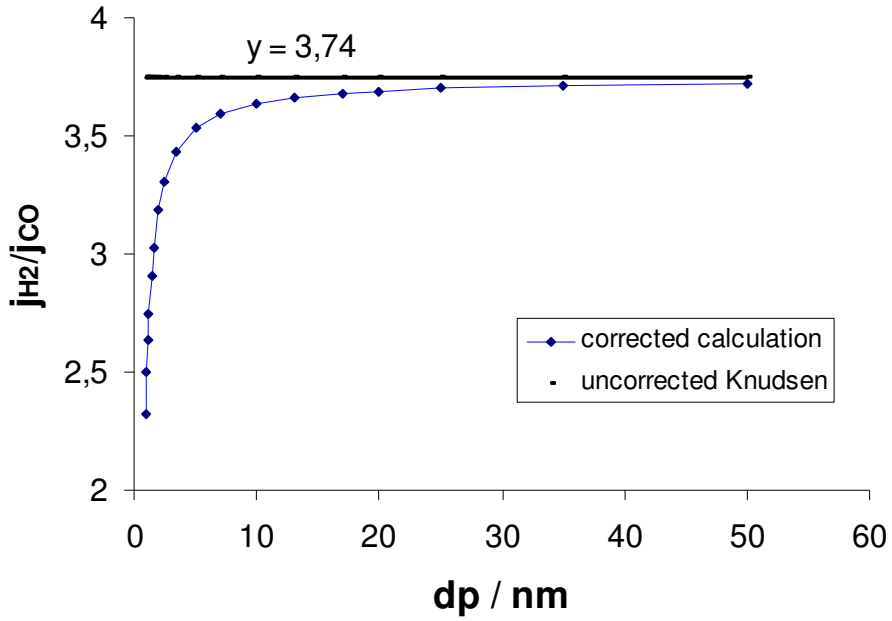

Figure 2.2.3: Separation factor of hydrogen to carbon monoxide in dependency of the pore diameter of the membrane

Since the permeance of the gases is proportional to d_p and the dependency of the Knudsen diffusion constant is just proportional to the square root of the temperature, the first experimental measurements were carried out over ceramic membrane with d_p = 5 nm at room temperature. The membrane module was connected to the outlet of the PFTR for SRM as described. Schematically the configuration of the experimental set up is displayed in Figure 2.2.4.

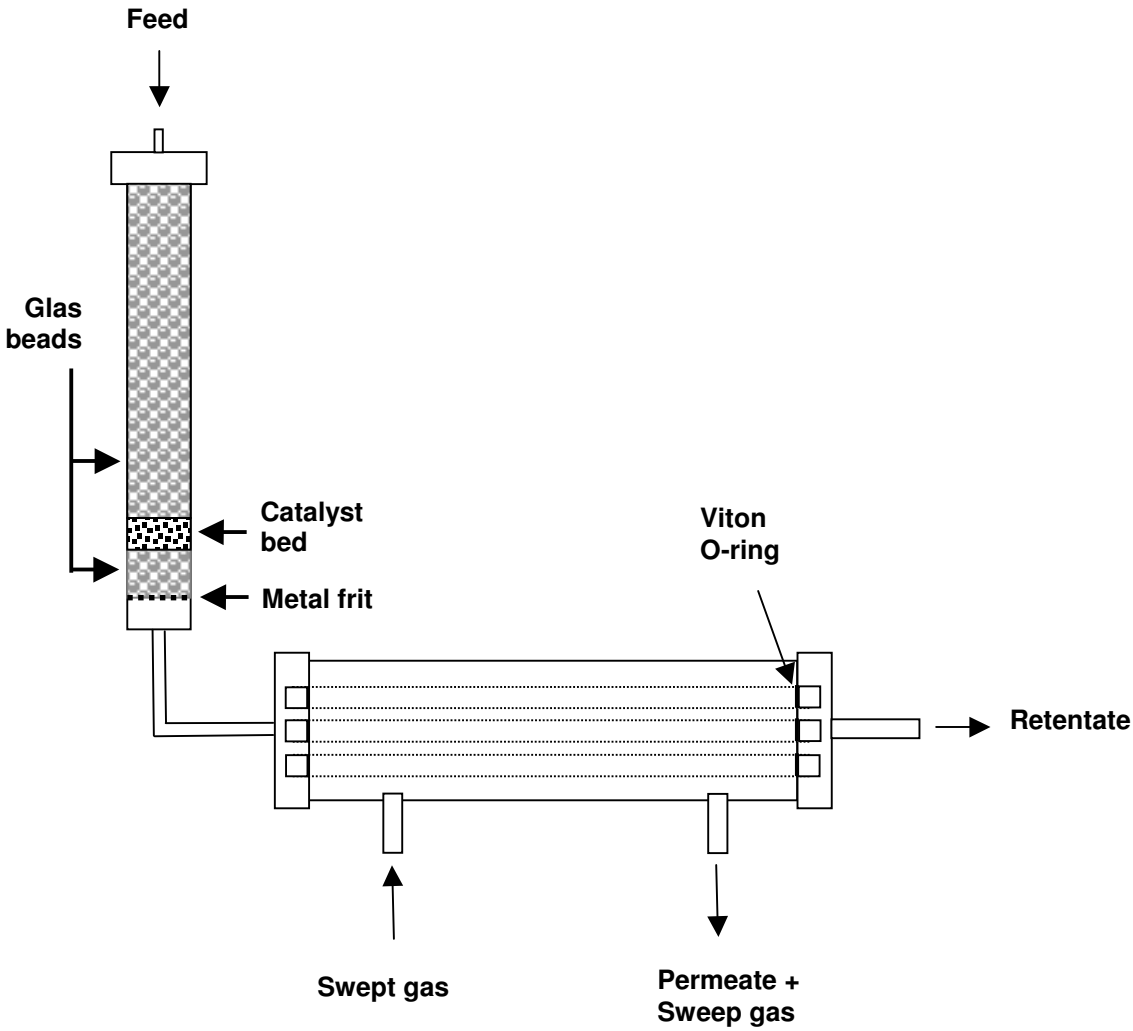

Figure 2.2.4: Membrane reactor with sweep gas

2.2.2. Experimental

2.2.2.1. First experimental set up

The first membrane studied was a 25 cm long cylindrical membrane with an outer diameter of 2,9 mm and inner diameter of 1,9 mm. The thickness of the TiO_2 membrane was 0,5 mm. The active layer of the membrane was about 100 µm with an average pore diameter of 5 nm. The inlet of membrane module was connected to the product gas from the SRM reactor and the retentate at the other end was led into a condenser, then after passing a heat exchanger of -10°C they were analysed by a GC. Since no gas went through the nano-membrane in absence of a pressure gradient, a reduced pressure (setting: 600 mbar, lumen site) as the driving force was generated. For this purpose the permeate site was connected with pressure regulator and vacuum pump (Divac 0.6).

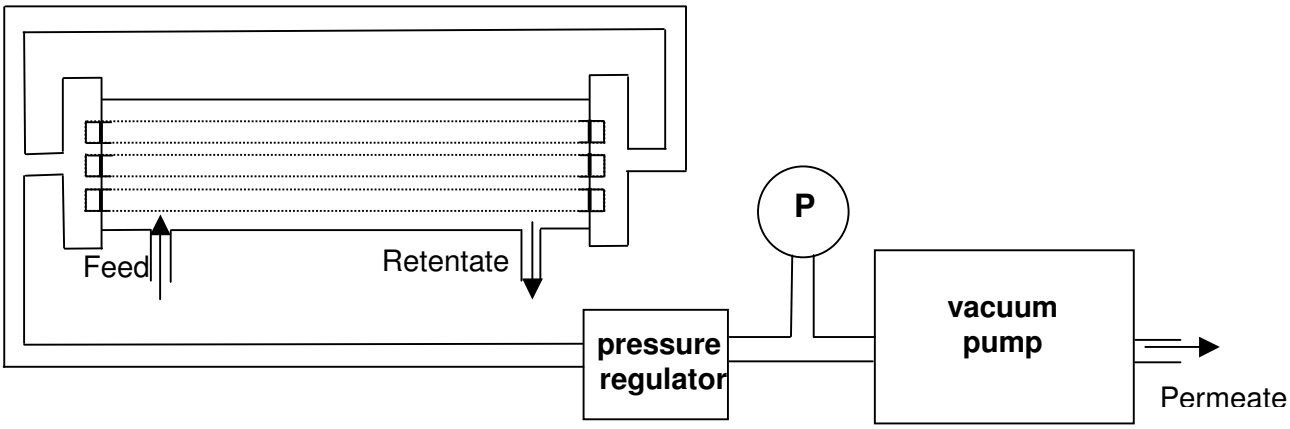

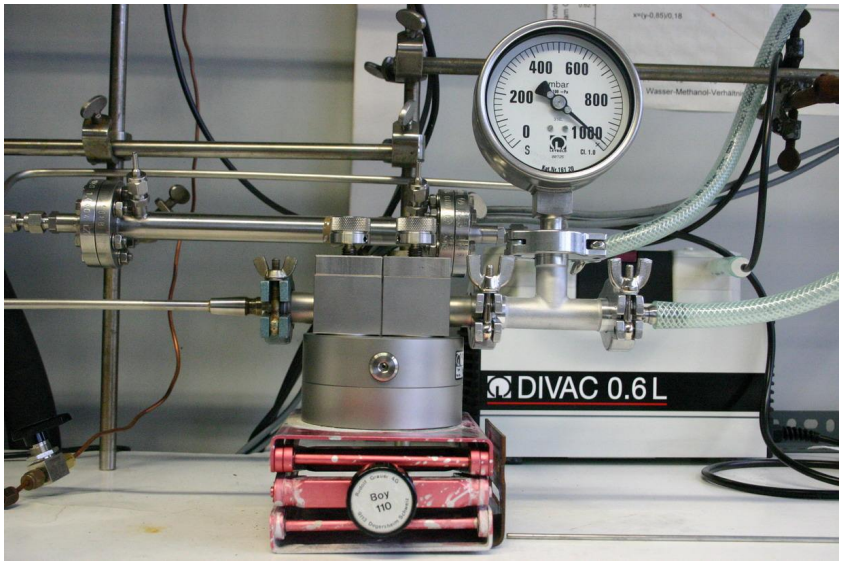

Figure 2.2.5: Membrane module with pressure regulator and vacuum pump

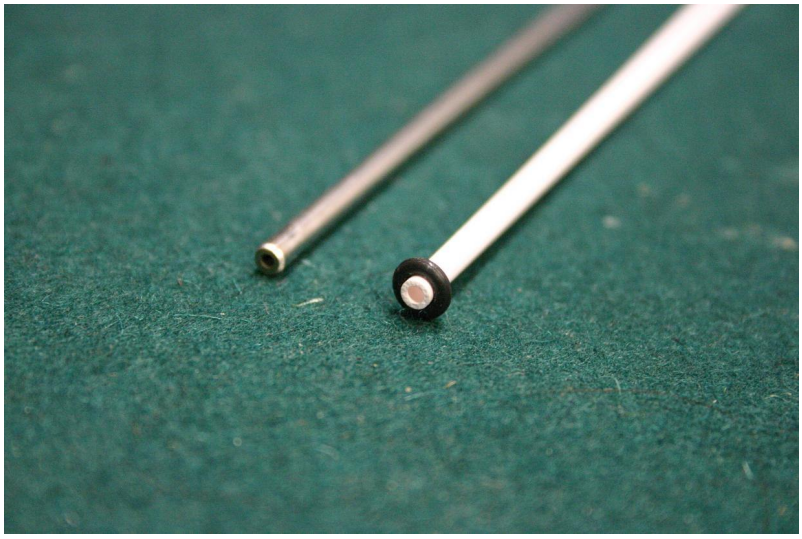

Figure 2.2.6: A small ceramic membrane (outer diameter: 2,9 mm, inner diameter: 1,9 mm) with an inserted Viton O-ring and a 1/8' metal tube as a size comparison

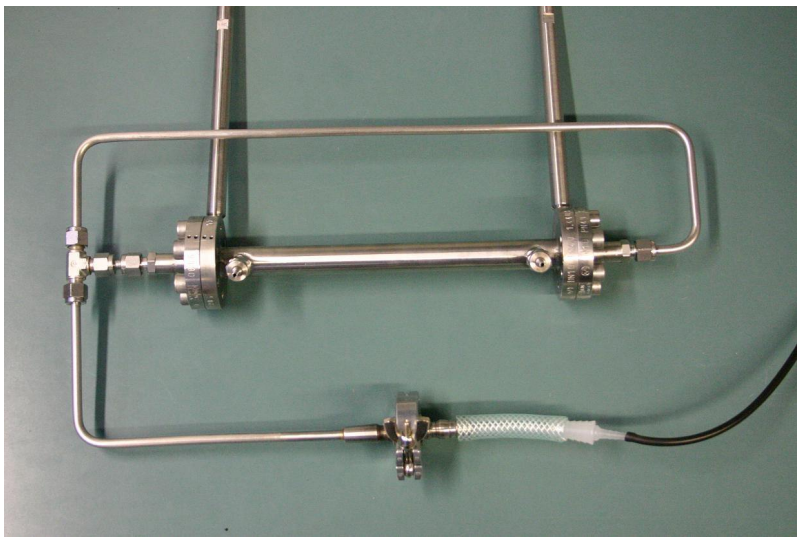

Figure 2.2.7: Basis device of membrane module without technical support. No gas passed over the ceramic membrane (d_p = 5 nm) in the absence of pressure gradient

2.2.2.2. Second experimental set up

In this set up the same membrane module and the same membrane with 5 nm pores as described above were used, but instead a vacuum device, a higher pressure in the retentate side was built up by adjusting a needle valve in the exit end. Two other

changes were implemented: the membrane module was heated to 80°C to avoid fluid condensation and the membrane module was positioned vertically.

The hot gas from the SRM reactor was introduced to the lumen site and went to a condenser to collect unreacted feed while the gas exit was connected to a needle valve due building an overpressure which acted as the driving force for the permeation of gases through the ceramic membrane. Retentate and permeate were analyzed by gas chromatograph after passing a -10°C heat exchanger to ensure the dryness of the gases.

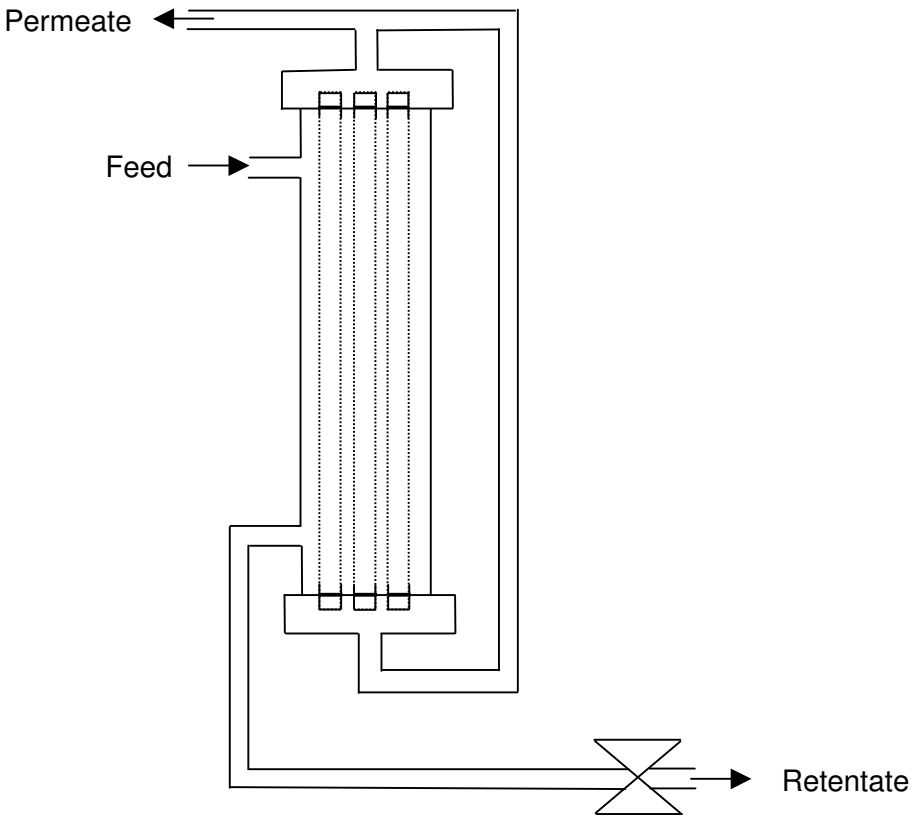

Figure 2.2.8: Membrane module with needle valve in exit end of retentate gas

2.2.2.3. Third experimental set up

The ceramic membrane with a pore diameter of 0,9 nm has an outer diameter of 10 mm and inner diameter of 8 mm. Its length is 25 cm. The construction of the membrane module is the same, but it has

a larger dimension, since the used ceramic membranes have a bigger size. The membrane module was heated particularly to temperatures between 140 °C and 80 °C and in this experimental nitrogen was used as swept gas.

During the series of experiments the inlet of the hot reaction gas and sweep gas were exchanged to inspect if a relocation between lumen and shell site has an effect, since the 0,9 nm pore diameter exists just as a thin layer on the shell site.

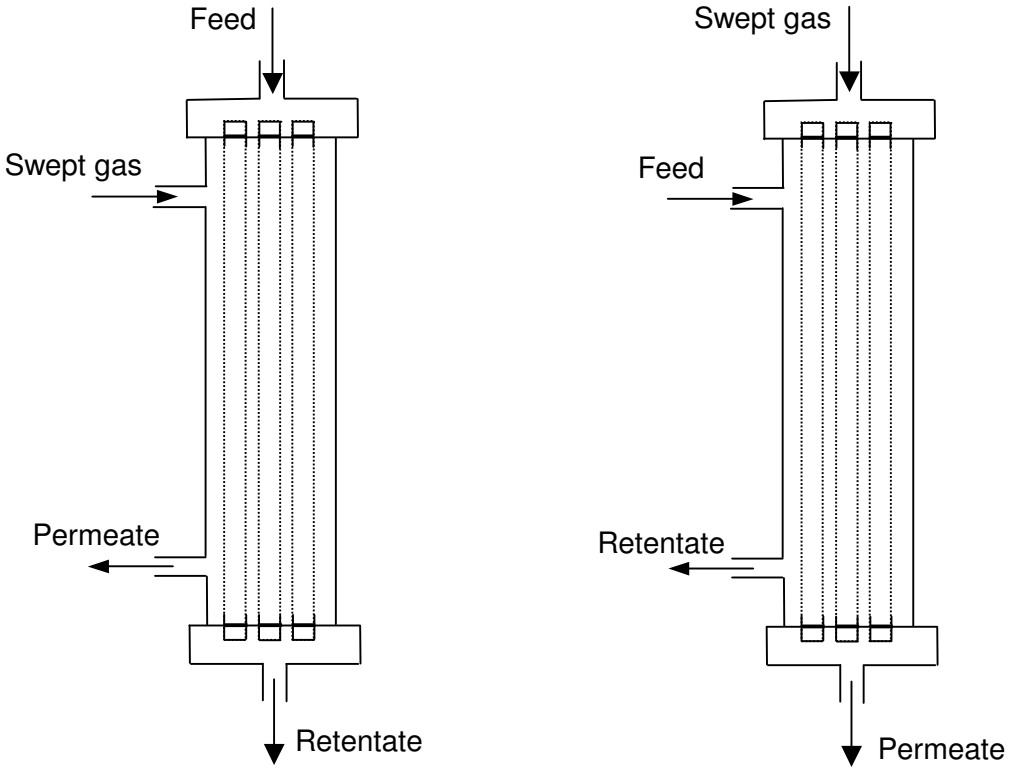

Figure 2.2.9: Membrane module with nitrogen as swept gas; left configuration: feed in lumen site; right configuration: Feed in shell site.

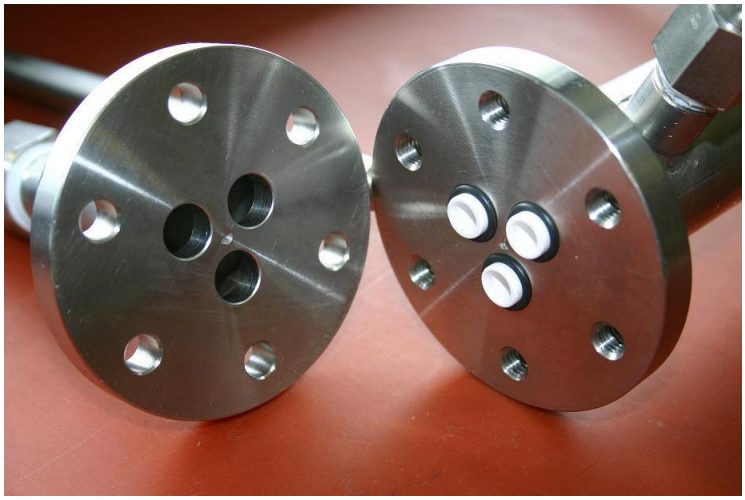

Figure 2.2.10: The head of the membrane module with three nano membrane and Viton O-rings

Figure 2.2.11: Configuration of membrane module with feed inlet in shell site (left picture in figure 8. The three ways valve in the feed inlet allowed to switch the feed either in shell site of membrane module or a direct feed to the GC.

2.2.3. Result and discussion

The theoretical calculation said that the Knudsen effect must be seen for diffusion through membranes with a pore diameter of 50 nm downwards. The first experiment was carried out with a ceramic membrane from Hermsdorfer Institut für Technische Keramik with a pore diameter of 5 nm. The first experimental set up was technically unsuitable since the vacuum devices were to powerful which was not match with the low production of the produced gases from the SRM reactor. As a result of this mismathc a too low pressure was adjusted in the membrane modul and all gas passed the membrane.

The second experimental set up with its vertically positioned membrane module could separate a dry gas fraction which could pass the membrane to the shell site and a wet fraction (product gases and residual feed) for a while but no enrichment of hydrogen was observed.

The third experimental set up with a larger membrane module and denser ceramic membrane (d_p = 0,9nm) used nitrogen as swept gas which was regulated by a mass-flow-controller. The gases from the SRM reactor acted as the feed of the membrane module. At lower swept gas flow there was just a small fraction of feed which was carried away trough the membrane. At certain flow of nitrogen it could be observed that more gases leave the permeate exit as the retentate exit. But even at this constellation, there was no enrichment effect. A relocation of the inlet channel of the sweep gas and the feed in lumen or shell site did not make any difference. Inserting the feed in lumen or shell site did not cause any difference of gas composition of permeate and retentate in respect of hydrogen and carbon monoxide concentration.

As per theoretical calculation the Knudsen diffusion should take place if the pore diameter of the membrane smaller as 50 nm: the calculated free mean path for hydrogen. Doohwan Lee used alumina membrane with an average pore size of 4.5 nm in his measurements

and observed hydrogen selectivities over He, CH_4, CO and CO_2 [9]. But even the experiments with the denser ceramic membrane (d_p = 0,9 nm) in our study and different ways of creating driving force for the diffusion, no difference in respect of hydrogen and carbon monoxide concentration was observed in retentate and permeate. The product gases and the swept gas (nitrogen) permeated through the membrane in all cases.

The reason of this negative results could be the asymmetry of the membrane pore and the pore size distribution. The Knudsen diffusion was made with the assumption that the pore has a long cylindrical form and the pore of membrane has a small pore size distribution.

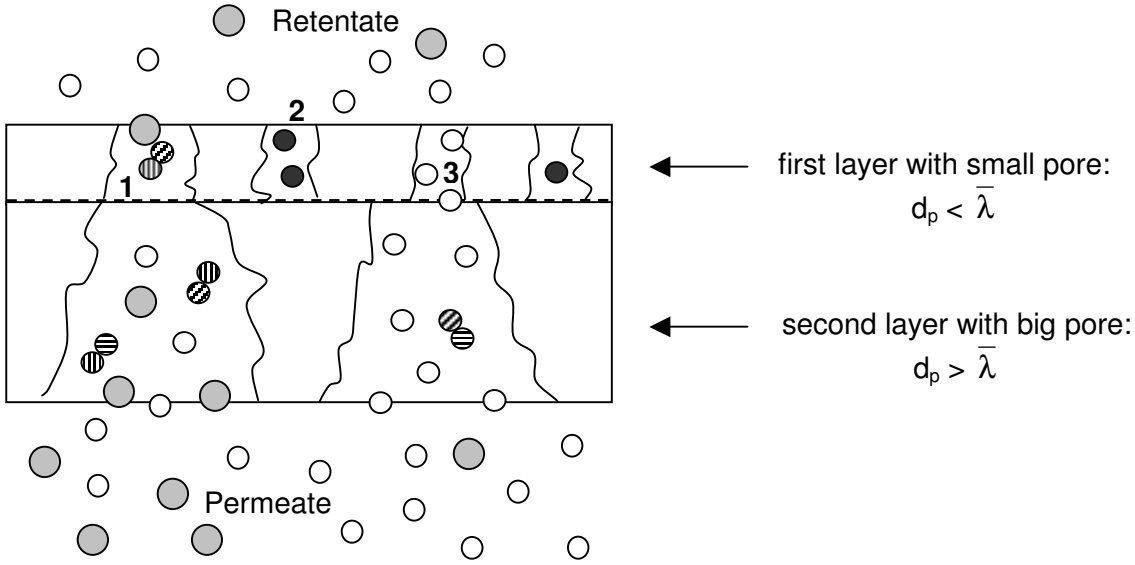

Figure 2.2.12: Diffusion in a cross section of a membrane of a dense layer wiht small pores and a support layer with bigger pores.

○ = light gas molecule

● = heavy gas molecule

= collusionof gas molecules

Since there are some pores with $d_p > \bar{\lambda}$ or the pores exhibit an asymmetry the gas molecules could undergo Brownian motion in this

area (1) and the occured diffusion does not cause any enrichment. Knudsen diffusion occured just if the pore has a diameter smaller than mean free path of the molecules along the whole pore (2). If the fraction of the pores which ensure a Knudsen diffusion does not exist in major amount, an enrichment effect could not be expected.

Another reason could be the lost of partial pressure gradient. If the membrane were porous enough, the back diffusion could occur easily. The diffusion took indeed place, but a quasi equlibrium state would appear and the enrichment effect were shooted down, since the partial pressure gradient disappeared and hence no concentration difference could be observed.

Beside of the improvement of the pore size distribution, we could try to find a more specific membrane which could selectively let pass hydrogen and carbon dioxide through the membrane.

Huang et al [11] embarked another strategy for the purification step: they used a CO_2 selective membrane to increase the CO conversion at WGS by removing the carbon dioxide from the reactant. A polymer membrane containing aminoacid (e.g., 50% wt % lithium glycinate in polyvinylalcohol) was proposed [12] and used as the CO_2 selective membrane reactor. Some Cu/Zn based WGS catalyst in small particle size was filled in the tube and the WGS was carried out at 150°C to reduce the CO content. They calculated in their simulation of the processes in a CO_2-selective WGS membrane reactor and reported a CO concentration less than 10 ppm and a hydrogen recovery of greater than 97% from autothermal reforming syngas. However the applied pressure ratio was quite high: p_{feed}:$p_{swept\ gas}$ = 3:1 and this was still a theoretical calculation with the assumption that CO_2 and H_2 were the only two gases permeating through the membrane.

2.2.4. Outlook

Since the purification step by a dense membrane needs a high pressure and temperature due its low permeance or an chemical aftertreatment as WGS reactor or multiple PROX reactors consume much energy, they are energetically not advantageous. If we consider that the steam reforming of methanol is an endotherm process and the CO concentration at smaller conversion is quite low, we should keep embarking the strategy to develop an autothermal system with membranes with a separation factor over 200 for H_2:CO and impermeability for methanol. Based on the measurement of SRM over MEOH1 at 80% conversion at 250°C we have calculated that already a separation factor of 180 could provide for a CO concentration below 50 ppm. The residual methanol left the membrane device as retentate and can be burned to ensure the authothermal process. Since the required separation factor is just some hundreds, it should be possible to develop inorganic membranes with a sufficient separation factor and an excellent permeability which prevent from a high working pressure. The small pore size distribution and the providing of symmetric cylindrical pore fore are essential requirements.

2.2.5. References

[1] B. Frank, F. Jentoft, H. Soerijanto, J. Kröhnert, R. Schlögl, R. Schomäcker, Steam reforming of methanol over copper-containing catalysts: influence of support material on microkinetics, submitted in Journal of Catalysis.

[2] S. Velu, K. Suzuki, M.P. Kapoor, F. Ohasi, T. Osaki, Selective production of hydrogen for fuel cells via oxidative steam reforming of methanol over CuZnAl(Zr)-oxide catalysts, Applied Catalysis A: General 213 (2001) 47-63.

[3] J. Agrell, H. Birgersson, M. Boutonnet, I. Melián-Cabera, R.M. Navarro, J.L.G. Fierro, Production of hydrogen from methanol over Cu/ZnO catalysts promoted by ZrO_2 and Al_2O_3, Journal of Catalysis 219 (2003) 389-403.

[4] Liwei Pan, Shudong Wang, A compact integrated fuel-processing system for PEMFC, International Journal of Hydrogen Energy 31 (2006) 447-454.

[5] O. Pozdnyakova, D. Teschner, A. Wootsch, J. Kröhnert, B. Steinhauer, H. Sauer, L. Toth, F.C. Jentoft, A. Knop-Gericke, Z. Paál, R. Schlögl, Prefential CO oxidation in hydrogen (PROX) on ceria – supported catalysts, Part I: Oxidation state and surface species on Pt/CeO2 under reaction conditions, Journal of Catalysis 237 (2006) 1-16.

[6] Kinetische Untersuchungen zum Reforming von Methanol, Diploma Thesis, H. Soerijanto, TU Berlin 2002.

[7] J. Agrell, H. Birgersson, M. Boutonnet, Steam reforming of methanol over Cu/ZnO/Al_2O_3 catalyst: a knietic analysis and strategies for suppression of CO formation, Journal of Power Sources 106 (2002) 249-257.

[8] A. Basile, F. Galluci, L. Paturzo, Hydrogen production from ethanol by oxidatiove steam reforming carried out in a membrane reactor, Catalysis Today 104 (2005) 251-259).

[9] D. Lee, Studies on hydrogen Selective Silica Membranes and the Catalytic Reforming of CH_4 with CO_2 in a Membrane Reactor, PhD Thesis, Faculty of Virginia Polytechnic Institute and State University (May 9, 2003).

[10] K. Malek, M.O. Coppens, Knudsen self- and Fickian diffusion in rough nanoporous media. Journal of Chemical Physics, 2003. **119**(5): p. 2801-2811.

[11] J. Huang, L El-Azzami, W.S. W. Ho, Modeling of CO_2-selective water gas shift membrane reactor for fuel cell, Journal of Membrane Science 261 (2005) 67-75.

[12] W.S.W. Ho, Membranes comprising aminoacid salts in polyamine polymers and blends, US Patent: 6,099,621 (2000)

3. CO free Hydrogen Production from Ammonia over Zirconia Oxynitride

3.1. Introduction

Zirconium oxynitrides exhibit a remarkable catalytic activity in the decomposition of ammonia without formation of hydrazine during extended time on stream. The results presented show for the first time a direct correlation between the onset of ion conductivity as a bulk property, a modified electronic structure of the surface, and the catalytic performance of a heterogeneous catalyst.

Hydrogen constitutes one of the promising candidates as an energy carrier in the quest for a replacement of fossil fuels particularly in mobile applications. The future use of hydrogen to generate power in one of the various available types of fuel cells appears to be commonly agreed on. Conversely, the proper way of storing hydrogen for mobile application is still being debated. In addition to high-pressure or cryogenic hydrogen, physisorbed hydrogen, or metal hydrides, small hydrogen containing molecules can be employed as hydrogen carriers in an on-board reforming process. The reforming of fossil fuels is economically and ecologically questionable at best. Conversely, methanol, for instance, can be obtained from biomaterials or from methanol synthesis plants being operated at remote locations where hydrogen is available, for instance, from solar energy plants. Thus, methanol is often regarded as being a suitable replacement for fossil fuels. However, the major disadvantage of using carbon containing hydrogen storage molecules is the formation of carbon monoxide during the reforming process. Because the latter acts as a fuel cell poison, it needs to be removed in down-stream gas purification units, which reduces the overall efficiency of the reforming process. Moreover, steam reforming of carbon-containing hydrogen sources results in the formation of the greenhouse gas carbon dioxide which posses additional ecological concerns.

As a potential alternative to methanol, ammonia can be used as a hydrogen carrier. [1, 2] Like methanol synthesis, ammonia synthesis is a well-understood, large-scale industrial process that also can be operated at any place where inexpensive hydrogen is available. In principle, the subsequent production of hydrogen by decomposition of ammonia is a particularly clean process that yields only hydrogen and nitrogen. However, many of the known metal catalysts for ammonia decomposition produce significant amounts of hydrazine. [3] Hence, similar to carbon monoxide, any hydrazine formed has to be removed in a subsequent gas purification unit. Alternatively, new catalysts need to be developed that possess high catalytic active in ammonia decomposition without formation of hydrazine.

The limited selectivity of common metal catalysts in ammonia decomposition originates from the presence of neighboring actives sites that facilitate the formation of hydrazine. Based on this assumption, we attempted to tailor the selectivity of improved catalysts by rationally seeking new materials that avoid neighboring active sites. Additionally, these materials need to be able to provide nitrogen atoms from the catalyst bulk for the formation of dinitrogen molecules.

Nitrogen-conducting zirconium oxynitrides [4, 5] were chosen as promising new ammonia decomposition catalysts that avoid the presence of neighboring metal sites.

3.2. Experimental

3.2.1. Catalyst Preparation

Zirconium oxynitride pellets were prepared from isostatically pressed commercial zirconia powder nitrided at 1900°C in nitrogen atmosphere for 2 h (graphite heated resistance furnace), resulting in a mixture of nitrogen-free monoclinic ZrO_2 and the ß”-type of zirconium oxynitride phases (~$Zr_7O_{9,5}N_3$) [6]. Subsequently, the material was quenched from a vertical tube furnace from 1300°C (nitrogen atmosphere) in water. X-ray analysis after quenching shows a reduced

amount of monoclinic zirconia and the metastable ß'-phase of zirconium oxynitride (~$Zr_7O_{11}N_2$). [7] For the catalysis testing described here a sample consisting of 51 wt-% ZrO_2 and 49 wt-% β' phase was used. Hot gas extraction of the as-prepared material yielded a total amount of nitrogen of 1.63 wt-% (theoretical 1.62 wt-%). After three month time on stream during ammonia decomposition the material exhibited only a minor decrease in the amount of nitrogen (-0.30 wt-%).

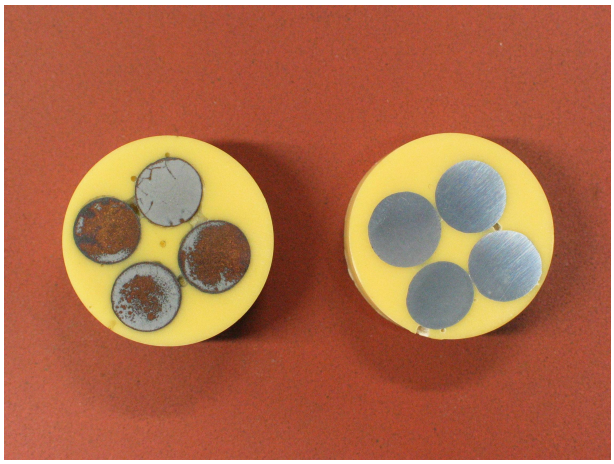

Figure 3.1: The fresh prepared ß" phase of ZrON with impurities on the surface (left picture): gold brown (zirconia nitride) and black particles (carbide compounds; C from the graphite furnace) and the grinded sample on the right picture.

Reaction equation of the nitridation [8] can be described in Kröger-Vink notation as follows:

$$3\ O_O^x + N_2 \rightarrow 2\ N_O' + V_O^{\circ\circ} + 1{,}5\ O_2 \qquad (1)$$

O_O^x = oxygen anion on a regular oxygen lattice

N_O' = nitrogen anion in oxygen lattice with a charge of -1

$V_O^{\circ\circ}$ = oxygen vacany in the anionic sublattice with a charge of +2

3.2.2. In situ XRD

For the high-temperature X-ray diffraction experiments a STOE STADI P diffractometer (CuKα_1-radiation, λ = 0.15406 nm) equipped with a graphite heated resistance furnace was used. The oxynitride powders were filled into capillaries under nitrogen and heated up at a rate of 20 $Kmin^{-1}$. At a given temperature, diffraction data were collected for 15 minutes using a position sensitive detector after an annealing time of 15 minutes.

3.2.3. Catalyst testing

Catalysis measurements of the decomposition of ammonia ($NH_3 \rightarrow 0.5\ N_2 + 1.5\ H_2$, $\Delta H^0 = +46.2$ kJ/mol) were performed at atmospheric pressure in a PFTR reactor (stainless steel) heated to the corresponding reaction temperature. A schematic drawing of the catalysis set-up used is depicted in Figure 5. The reactor temperature was manually increased in steps of 20 K. After each temperature step a spiked increase in conversion was observed followed by a slowly decreasing conversion with time on stream. Steady-state conversion was reached after about 10 min. The conversion data reported here were determined after 20 min time on stream at the corresponding temperature.

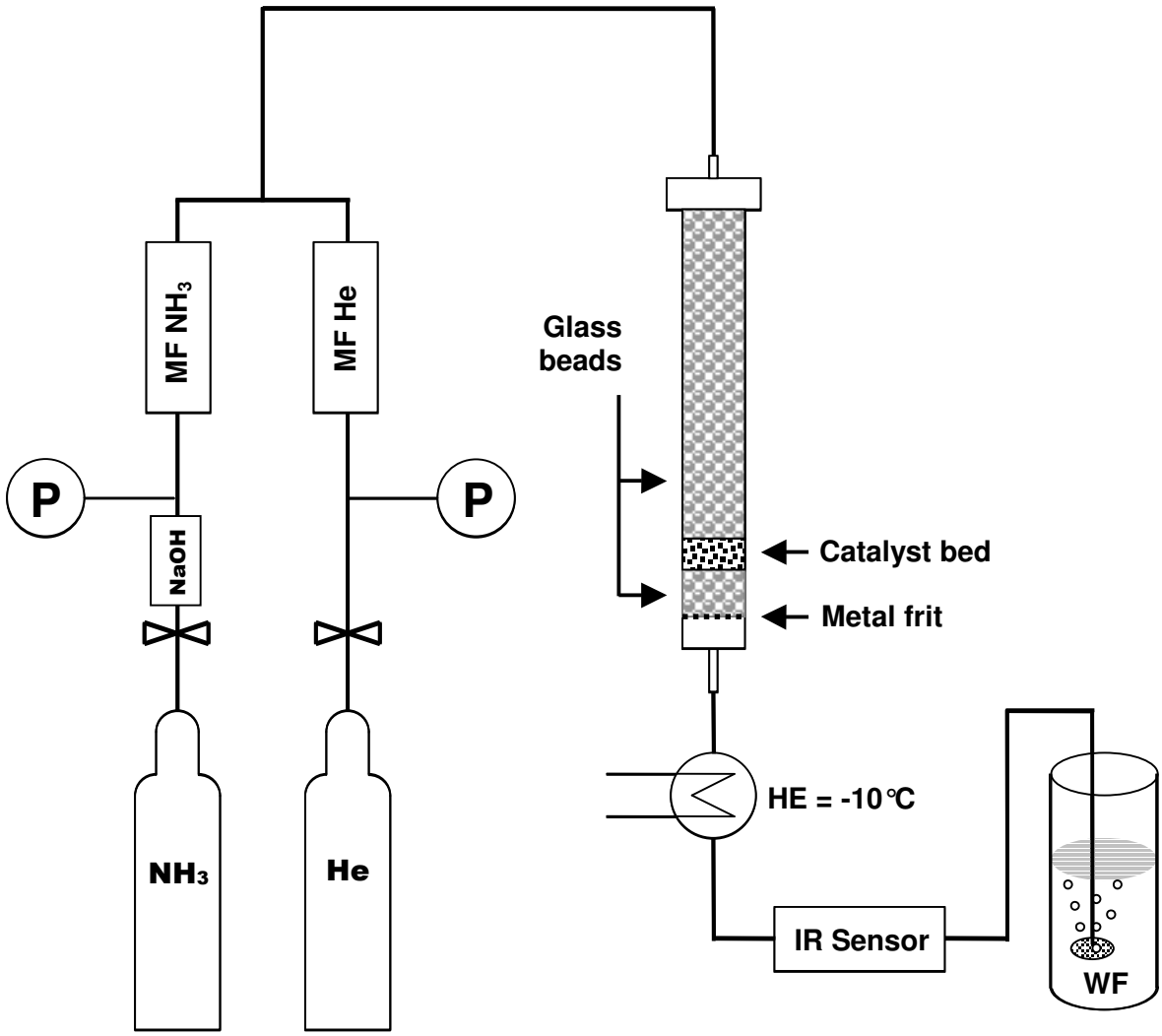

Figure 3.2: Schematic arrangement of experimental set up / P = pressure reducer, MFC = massflow controller, HE = heat exchanger, WF = wash flask, filled with H_2SO_4

The amount of ammonia and helium in the feed was adjusted by massflow controllers (Bronkhorst). This arrangement permits setting different ammonia partial pressures at different flow rates, resulting in different contact times. The massflow controller for ammonia needed a special seal and a reliable pressure reducer of particular precision in order to properly adjust small flow rates of ammonia. The PFTR reactor was mounted into a heating block (brass, 80 mm in diameter, 150 mm length), equipped with six high temperature heating cartridges of 220 Watt and heated to the desired to the desired temperature. The heating block is prepared to accommodate three reactors, enabling measurements with three catalysts under the same conditions within one test series. One reactor loaded with glass beads served as a blank reactor to determine the thermal and reactor contribution to the conversion of ammonia. The second reactor was filled with an iron oxide catalyst (1 g Fe_3O_4 (magnetite) + 2 mol% K_2CO_3 + 4 mol% Al_2O_3; particle size: 0,3 – 1 mm and a BET surface area below ~ 7 m^2/g) which acted as a reference catalyst for ammonia synthesis. This catalyst was prepared as desribed previously [f]. The third reactor was filled with the zirconium oxynitride catalyst (4 g zirconia oxynitride: 0,3 – 1 mm particles and a BET surface area below ~ 0.9 m^2/g). Glass beads were placed above and below the catalyst bed to ensure that the feed gases and the catalyst powder possess the same preset temperature in the reaction zone.

To rule out the diffusional limitations, the Weisz modulus, Ψ', considering ammonia as the limiting reactant ws estimated. The Weisz modulus describes the ratio of reaction rate to reactant diffusion rate and is defined by:

$$\psi' = L^2 \cdot \frac{m+1}{2} \cdot \frac{r_{eff} \cdot \rho_{cat}}{D_{eff,NH_3} \cdot c_{NH_3}} \qquad (2)$$

$L = 3*10^{-4}$ m (the charasteristic lenght of catalyst particle)

m = 1 (the reaction order of ammonia)

r_{eff} = $1*10^{-4}$ $mol.s^{-1}.kg^{-1}$ (the measured reaction rate)

ρ_{cat} = 6000 $kg.m^{-3}$ (the catalyst densitiy)

D_{eff,NH_3} = $1*10^{-6}$ $m^2.s^{-1}$ (the effective diffusitiy of ammonia)

c_{NH_3} = 0.14 $mol.m^{-3}$ (the concentratuion of ammonia)

With an effective rate of $1*10^{-4}$ $mol.s^{-1}.kg^{-1}$ estimated for 600°C and the data given above, a Weisz modulus of 0.386 was calculated. This indicated that rection proceeded slower than diffusion of ammonia and hence no mass-transfer limitations needed to be considered neither at 600°C nor at the lower temperatures.

The outlet gases were cooled to -10°C to assure that the product stream of different experiments are at the same temperature before they reach the ammonia sensor (Binos IR detector, Rosemount). Afterwards the outlet gases were washed with sulfurid acid. 4-(Dimethylamino)-benzaldehyde was added to test for hydrazine in the reaction product. Even after five weeks of time on stream, no hydrazine was detectable. During this time 2.25 mol of ammonia were passed through the reactor. The detection limit for the hydrazine assay is 0.0005 mg/L, which means formation of <0.4 ppm of hydranzine.

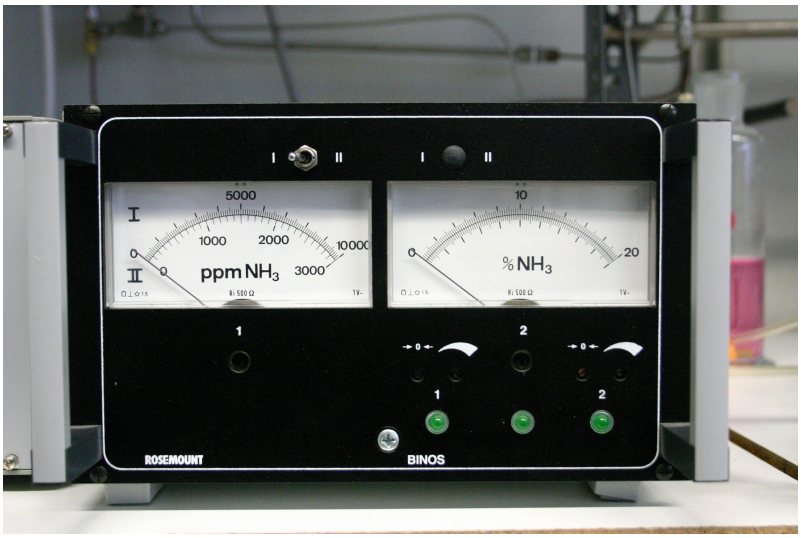

Figure 3.3: Binos IR detector, Rosemount, with two measurement ranges: 0 – 10.000 ppm (I) and 0 – 3.000 ppm (II) which has more accuracy in lower ppm region. A discontinuity of the plotted points on some diagrams was originated by switching between these two measurement ranges.

3.2.4. X-ray photoelectron spectroscopy (XPS)

XPS measurements were performed in a modified LHS/SPECS EA200 MCD system equipped with facilities for XPS (Mg K_α 1253.6 eV, 168 W power) and UPS (He I 21.22 eV, He II 40.82 eV). For the XPS measurements a fixed analyser pass energy of 48 eV was used resulting in a resolution of 0.97 eV FWHM of the Ag $3d_{5/2}$ intensity. The binding energy scale was calibrated using Au $4f_{7/2}$ = 84.0 eV and Cu $2p_{3/2}$ = 932.67 eV. The base pressure of the UHV analysis chamber amounted to 10^{-10} mbar. The ZrON catalyst was deposited on a stainless steel sample holder with minimized exposure to air. The sample was heated to the corresponding measuring temperatures at a rate of 1 K/s. Quantitative data analysis was performed by subtracting a Shirley background [9] and using empirical cross sections. [10]

3.3. Result of catalyst testing and catalyst characterization

Nitrogen-conducting zirconium oxynitrides [4, 5] are promising new ammonia decomposition catalysts that avoid the presence of neighboring reduced metal sites. The combination of an appropriate intrinsic reactivity towards nitrogen and the high resistance towards reduction makes this group of materials promising candidates for ammonia catalysts. Here we describe first catalysis studies linking the catalytic behavior in the decomposition of ammonia to the onset of nitrogen mobility in the bulk structure of a zirconium oxynitride catalyst.

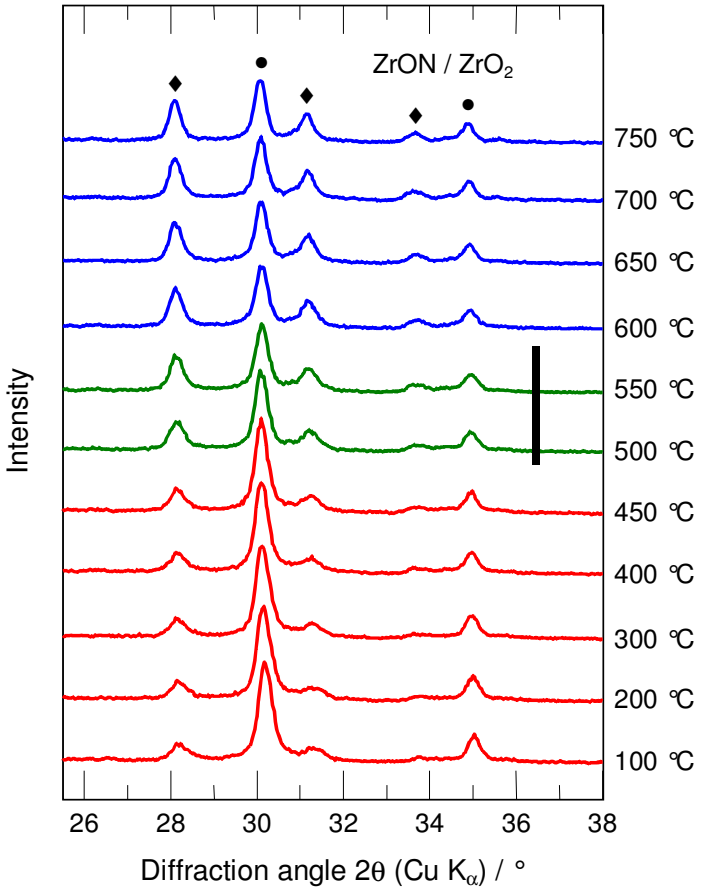

Figure 3.4: Evolution of XRD patterns measured during thermal treatment of a mixture of zirconium oxynitride (•) and ZrO_2 (♦) in the temperature range from 100°C to 750°C. The phase change from the β´ ZrON phase to the β´´ ZrON phase is indicated (bar).

X-ray analysis of the as-prepared material shows a mixture of monoclinic zirconia and the metastable ß'-phase of zirconium oxynitride (~$Zr_7O_{11}N_2$) (Figure 3.4). This material was used for catalysis testing and characterization and is referred to as ZrON in the following. The conversion of ammonia as a function of temperature measured during ammonia decomposition (feed 4100 ppm NH_3) on a conventional iron catalyst (mostly Fe_3O_4), the ZrON catalyst (heating and cooling), and the blank reactor (glass beads) is depicted in Figure 3.5. The iron oxide catalyst showed an onset of activity in the decomposition of ammonia at ~340 °C. Conversely, measurements of the as-prepared ZrON yielded no detectable activity below 550 °C. However, upon increasing the reaction temperature further, the zirconium oxynitride exhibited a jump in activity of ammonia decomposition at a temperature of ~ 550 °C (Fig. 3.5). At reaction temperatures above ~550 °C the activity of the material was similar to that of a conventional iron catalyst. The dynamics of the jump in activity at ~550 °C is shown in the inset of Fig. 3.5. Upon subsequently cooling down to ambient temperature, the ZrON catalyst showed a continuous decrease in ammonia conversion.

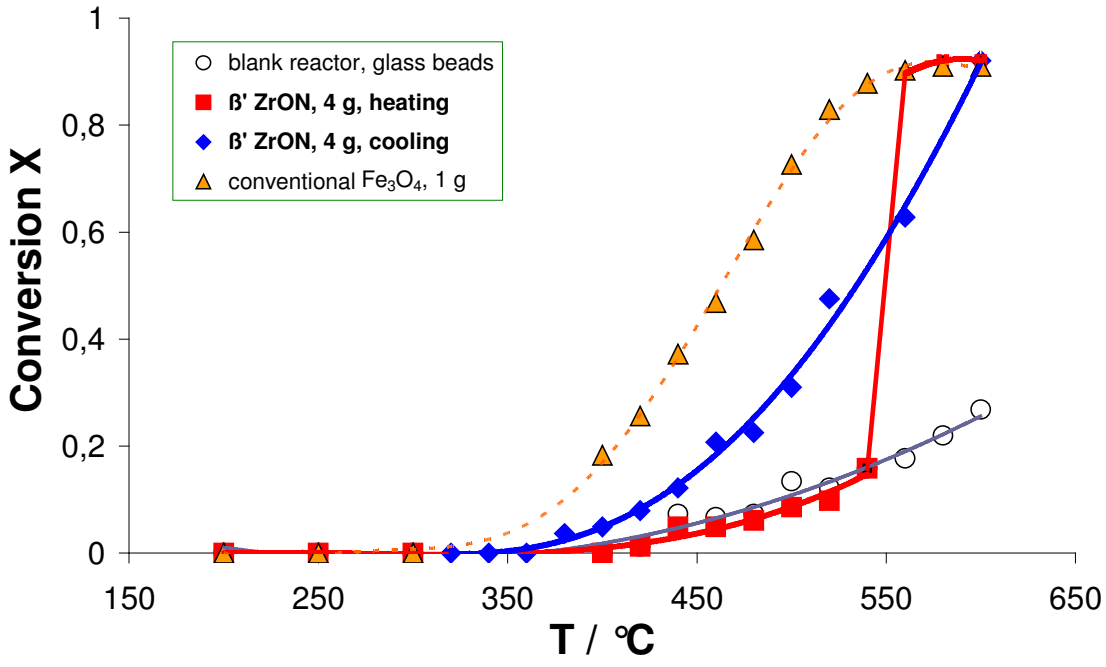

Figure 3.5: Evolution of ammonia conversion as a function of temperature during ammonia decomposition (feed 50 ml/min He with 4100 ppm NH_3) on Fe_3O_4, ZrON (heating and cooling), and blank reactor (glass beads).

Compared to the conventional iron oxide catalyst, the sudden onset of catalytic activity of ZrON at ~550°C does not correspond to a regular increase in activity with increasing reaction temperature. Because of the endothermic nature of the ammonia decomposition reaction, an ignition behavior of the reactor can be ruled out. Hence, rapid bulk structural changes have to be assumed as origin of the catalytic activity observed. As known from our high-temperature XRD work, reheating the as-prepared metastable mixture of nitrogen-poor ß'-phase ($Zr_7O_{11}N_2$) and nitrogen-free monoclinic ZrO_2 in nitrogen results in a further demixing to the nitrogen-rich ß"-phase ($Zr_7O_{9.5}N_3$) and an increased amount of m-ZrO_2 at 550°C (Figure 3.4). [7] Structurally, the ß'- and ß''-phases can be described as anion-deficient fluorite types with ordered anion vacancies, whereas the ß'-phase is strongly disordered. [11, 12] The β" ZrON phase contains a larger amount of nitrogen ions in the lattice than the β´phase, accompanied by an increased amount of vacancies in the oxygen sublattice. [12, 13] Apparently, the phase demixing requires an increased mobility of nitrogen ions in the ZrON structure to enable migration of nitrogen ions and the formation of β" ZrON and ZrO_2. Therefore, the change from the β' to the β" ZrON phase is a suitable indicator for the onset of nitrogen ion conductivity in the ZrON catalyst studied.

The sudden onset of catalytic activity in ammonia decomposition on ZrON corresponds very well to the phase change from the initial β' phase to β" ZrON (Figure 3.5). Apparently, the β´ phase exhibits only negligible activity in ammonia decomposition while the β´´ ZrON phase possesses a considerably activity similar to that of a conventional iron catalyst. It may be envisaged that the β" phase exhibits an increased nitrogen mobility compared to the β' phase, in addition to the increased amount of nitrogen in the β" phase. Both may be a prerequisite for the β" phase to function as an active catalyst for ammonia decomposition. Hence, the reduced amount and mobility of nitrogen in the initial β' phase is not sufficient to merit a detectable catalytic activity.

X-ray diffraction studies have shown, that the β´´ phase persists upon cooling and does not change back to β´ *ZrON*. [7] This metastability of the β´´ *ZrON* phase is nicely reflected in the conversion of ammonia during the cool-down period (Figure 3.5). Even below the phase demixing temperature, the increased amount of nitrogen and its mobility in the β´´ *ZrON* phase resulted in an improved activity compared to the β´ phase. Moreover, the ammonia conversion on β´´ ZrON exhibited a more regular behavior as a function of the decreasing temperature. Subsequently increasing the temperature under reaction conditions resulted in a regular increase in activity of the catalyst that coincided with the cooling curve of the first temperature cycle.

In order to determine the activation energy of ammonia decomposition on ZrON catalysts, the partial pressure of ammonia in the feed was varied and the conversion of ammonia was determined as a function of temperature. The ammonia conversion over ZrON at a given temperature and residence time was independent of the ammonia partial pressure (Figure 3.6). It can be assumed that the ZrON catalyst was not saturated under the applied conditions and, hence, the results obtained indicate a first order reaction.

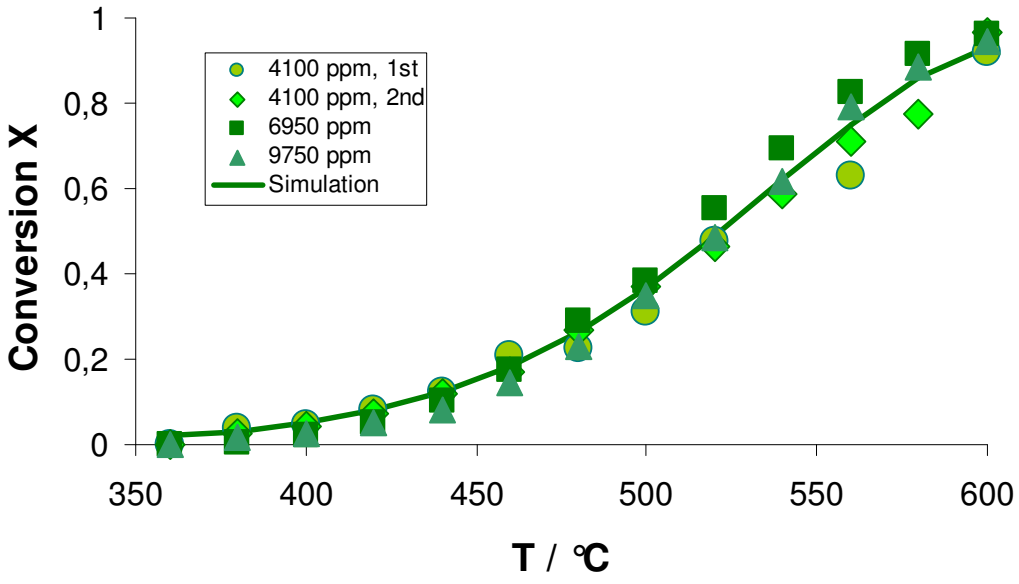

Figure 3.6: Conversion of ammonia on 4 g ZrON measured at various feed concentrations. The solid line represents a refinement of a first order reaction kinetics according to eqn. 1 to the data obtained for 6950 ppm NH_3 in the feed.

For a first order reaction the solution of the material balance of a PFTR gives the following equation for the conversion:

$$X = 1 - e^{(-c_{kat} \cdot k + k_{uncat}) \cdot \tau} \quad (3.a)$$

$$X = 1 - e^{-\left(k \cdot e^{\frac{-E_{A,ZrON}}{RT}} + k_{glass} \cdot e^{\frac{-E_{A,glass}}{RT}} \right)} \quad (3.b)$$

$$\text{with } X = \frac{(p_{NH_3,0} - p_{NH_3})}{p_{NH_3,0}} \quad (4)$$

Assuming a temperature dependency of the rate constant according to the Arrhenius equation:

$$k = k_0 \cdot e^{(-E_A / RT)} \quad (5)$$

The apparent activation energy E_A can be determined by fitting eqn. 3.b to the conversion data as function of temperature (Figure 3.6). An apparent activation energy of 106 ± 10 kJ/mol was obtained at 400-550 °C. This value is in good agreement with activation energies assumed for ion conductivity in zirconium oxynitride based materials [1]. For the uncatalysed reaction, an activation energy of 70 ± 10 kJ.mol^{-1} was calculated from the conversion data. Moreover, the apparent activation determined corresponds well with the expected and previously reported values of 120 kJ.mol^{-1} [13]. On one hand, the similiar activation energies indicate a similiar rate-determining step of the reaction on ZrON and reduced metal caltalysts. On ohter hand, the absence of detectable amounts of hydrazine is indicative of a mechanism of ammonia decomposition on ZrON that varies from that of conventional reduced-

metal catalysts. This corroborates the correlation between onset of catalytic activity and nitrogen mobility in the bulk of the ZrON catalyst as a new mechanistic concept for this class of materials. Details on the role of the anion vacancies an anion mobilitiy in the material for kinetics of the decomposition of ammonia will be investigated in the kinetic study.

In addition to bulk structural properties, the electronic structure of the surface of the ZrON catalyst as a function of temperature was studied by X-ray photoelectron spectroscopy (XPS). The Zr 3d doublet exhibited only minor changes in shape and position during heating and cooling. However, a detailed peak profile analysis revealed an abrupt broadening of the Zr 3d peak at ~550°C and a shift in binding energy (Figure 3.7), possibly due to changes in differential charging of the surface.

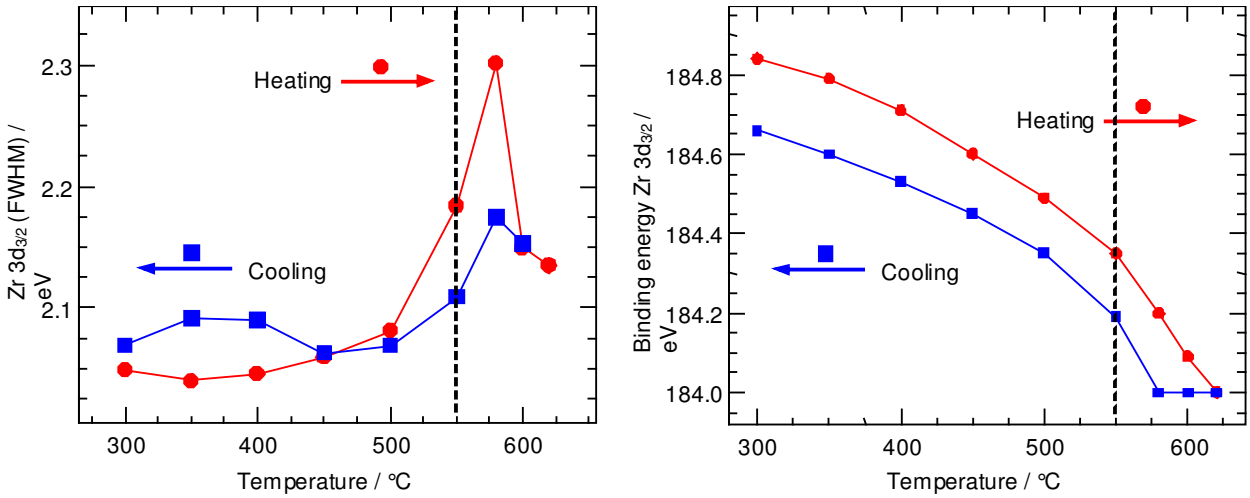

Figure 3.7: Evolution of width (left) and position (right) of XPS Zr $3d_{3/2}$ peak of β' ZrON during heating and subsequent cooling. The dashed line indicates the onset of the phase change from β´ ZrON to β´´ ZrON and catalytic activity.

The corresponding change in the electronic structure of the ZrON catalyst coincided with the onset of catalytic activity (Figure 3.5) and nitrogen ion mobility of β" ZrON (Figure 3.4). The increasing and decreasing Zr 3d peak broadening observed as a function of temperature indicates a differential charging and a transition state of the ZrON

surface structure. These effects accompany the phase change from β' ZrON to the characteristically ordered β" ZrON.

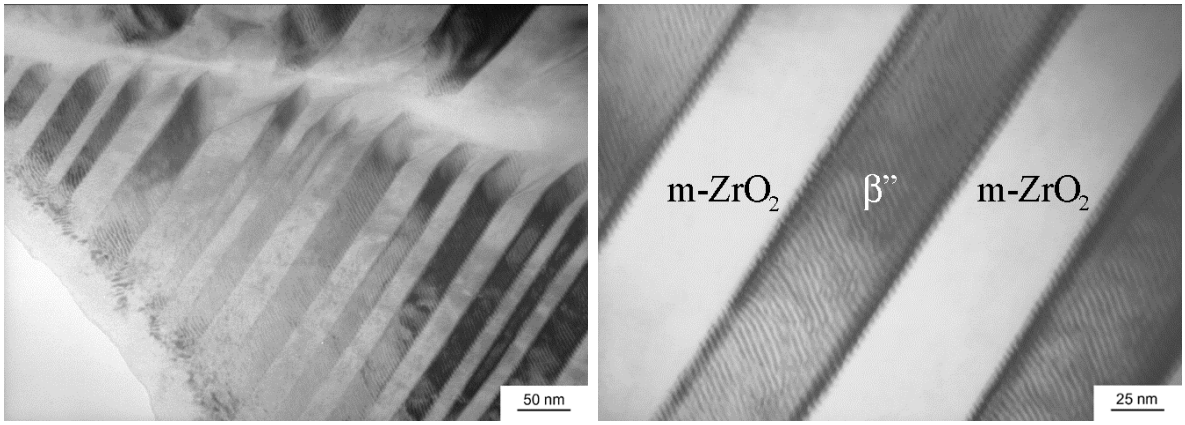

Figure 3.8: Bright-field TEM images show the coexistence of the monoclinic ZrO_2 phase and the modulated b" phase.

Subsequently, the resulting surface structure persists (Figure 3.7) and retains its catalytic activity even at temperatures below 550 °C (Figure 3.5). Moreover, a quantitative analysis of the XPS data revealed an increasing amount of nitrogen at the surface of the ZrON material after heating to 600°C (Figure 3.9 and Table 3.1).

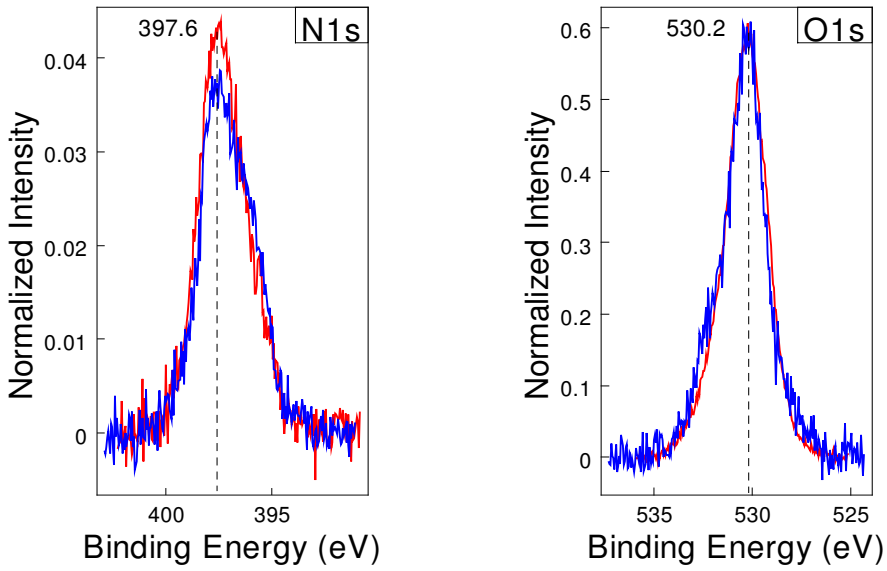

Figure 3.9: XPS of O1s and N1s at 200°C (blue curves) and at 600°C (red curves) of ß' sample, charging corrected with BE of ZrO_2 Zr $3d_{5/2}$ at 182,2 eV as standard. The

amount of nitrogen at the surface increased while the amount of oxygen slightly decreased (-4%).

T	O (atom%)	N (atom%)	Zr (atom%)	O/Zr	O/N
200 °C (u)	55.02	6.02	21.83	2.52	9.14
620 °C	55.5	7.9[a]	24.1	2.3	7.0
200 °C (d)	50.8	7.0	23.1	2.2	7.2

Table 3.1: Surface composition (atom%) of ZrON material obtained from XPS measurements (O 1s, N 1s, Zr 3d), before (u) and after (d) thermal treatment between 200 and 620 °C.

[a] Measured at 600 °C

Apparently, the dynamic behavior of the surface of the ZrON catalyst under reaction conditions accompanies the phase change in the ZrON material at ~550°C. Hence, the formation of the nitrogen rich β´´ ZrON phase is especially detectable at the surface confirming the assumption of nitrogen mobility and β´´ phase formation as prerequisites for activity of ZrON in ammonia decomposition. It may be envisaged that the phase change from β´ to β´´ phase results in the formation of characteristic lattice defects at the surface of the catalyst. In a corresponding schematic mechanism, these defects constitute the active sites for the dissociative adsorption of ammonia. Subsequently, a dinitrogen molecule is formed together with a nitrogen atom from the lattice of the *ZrON* catalyst. Finally, the thus generated vacancy in the nitrogen sublattice is replenished by nitrogen diffusion from the bulk or ammonia from the gas phase (Figure 3.10).

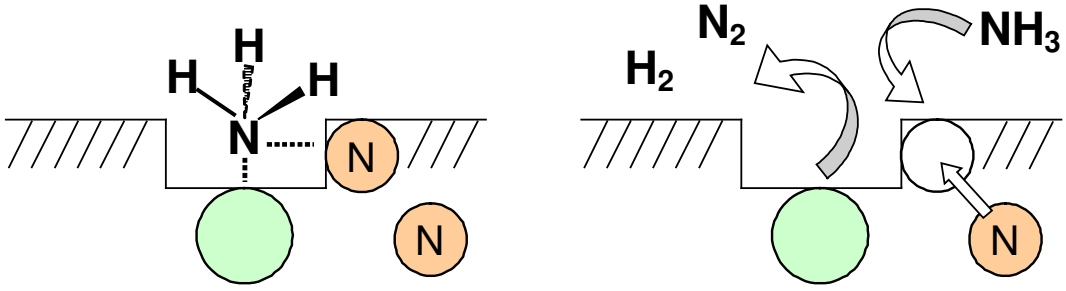

Figure 3.10: Schematic representation of the decomposition of ammonia on a zirconium oxynitride catalyst.

3.5. Kinetic study

For a kinetic analysis the residence time of the gases at preset concentrations and fixed temperatures was varied. The ammonia and helium flux were separately adjusted by two massflow controllers (Figure 3.2). This arrangement allowed to set different ammonia partial pressures at different flow rates. For this purpose we calibrated in advance the flow controller of helium and ammonia. Ammonia partial pressures/ concentrations of 4600 ppm, 7400 ppm & 9900 ppm at room temperatures were adjusted and checked with the ammonia detector. During these measurements 4 g ß" ZrON and the experimental set up as described in catalyst testing (Figure 3.2) were used. The measurement was started at 400 °C with the lowest pair of helium & ammonia flow rates and the highest residence time respectively. The first series of measurements were carried out at 400 °C and subsequently at temperatures in elevated 50 K increment.

3.6. Result of kinetic study

The quenched sample of ZrON showed a sudden activity increase after phase transition. This jump in NH_3 conversion dissapeared after some cycles of heating and cooling and it was not just keeping its activity, it rather showed an even increasing activity with time (Figure 3.11). After three months time on stream, it was as active as the conventional iron catalyst, even although the zirconia oxynitride has less specific surface area. This result is indeed a good feature for possible application, but since it became better and was changing with time, it was not suitable for kinetic study.

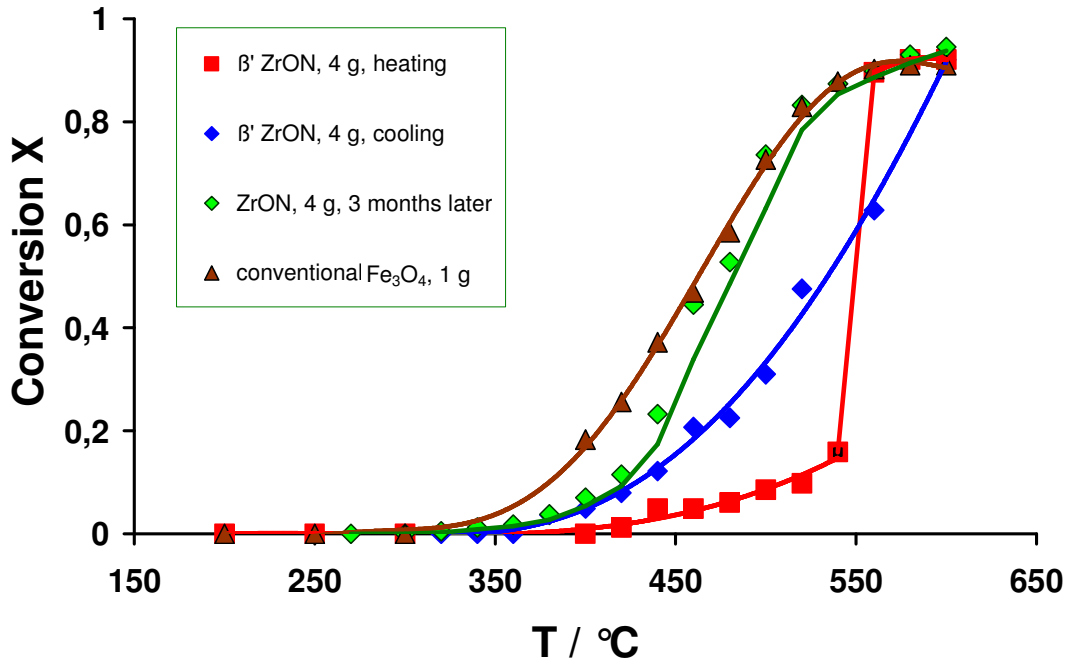

Figure 3.11: Conversion of ammonia decomposition of 4 g quenched ZrON at the first activation, first cooling and after three months time on stream.

Since the ß”-phase of ZrON is the active one, the kinetic measurements were carried out over 4 g ß”-phase of zirconia oxynitride (BET surface area: 0,958 m²/g) which was obtained by the same preparation procedure as described above but after heating to 1900 °C, it was not quenched but cooled down slowly to room temperature in order to maintain the ß” phase of ZrON. So prepared ß” phase of ZrON showed a good stability and gave an excellent reproducibility during a period of some months of the measurement respectively.

The conversion of the ammonia decompostion increased with longer contact time and increasing temperatures. We clearly see the difference in the gradients of ammonia partial pressure at short contact time at 450 °C and 500 °C in Figure 3.12.

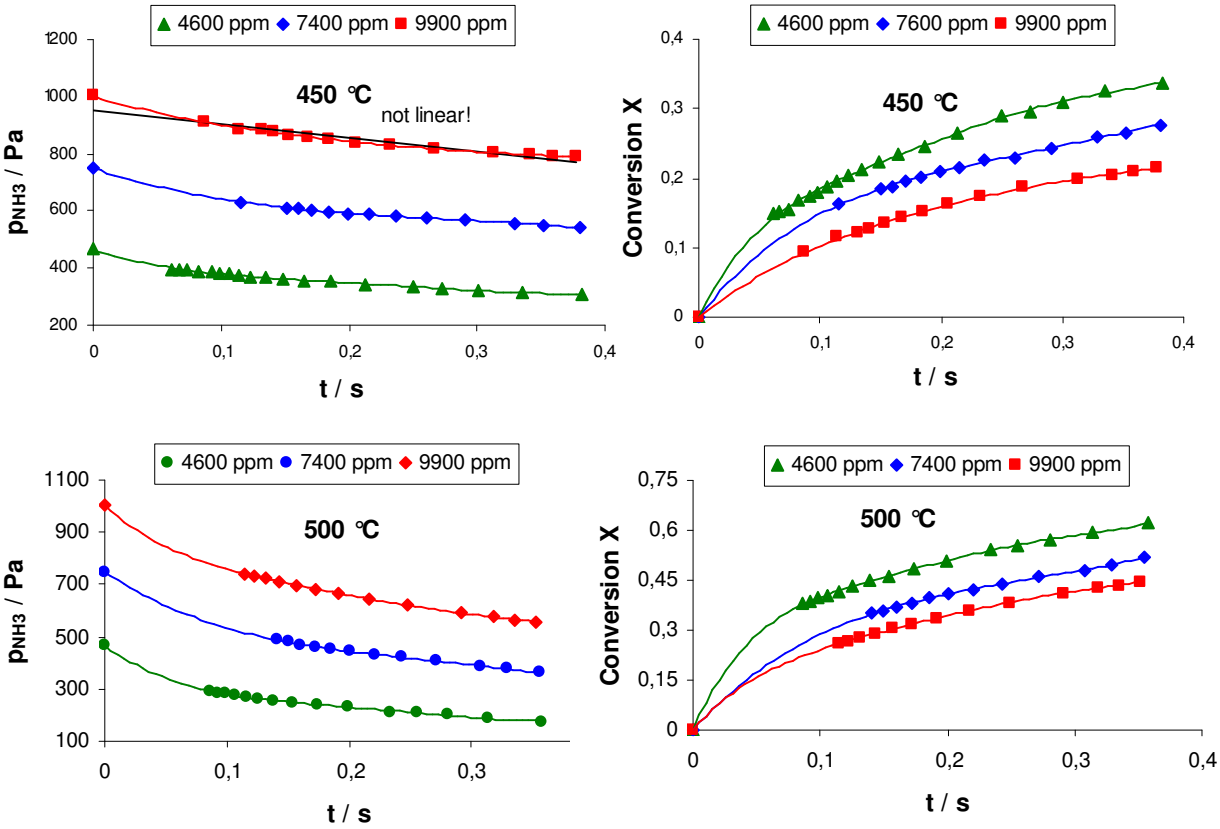

Figure 3.12: Evolution of ammonia partial pressure (left diagram) and conversion of ammonia (right diagram) at 450 °C and 500 °C in its depedency on contact time over 4 g ß" ZrON at three different initial concentration of ammonia.

An unusual aspect was observed in the plot of reaction rates as a function of ammonia partial pressures. Normaly the reaction rates would fall on to one curve independently of the start concentration. But this can be seen only at the diagram at 550 °C (Figure 3.13). At lower temperatures the reaction rates decrease sharply after some ammonia is converted. This phenomenon made a differential analysis of the kinetic data impossible. There must be an explanation why the reaction rate at the different initial concentrations showed such behaviour. Since the reaction rates dropped sharply after some feed was converted, one of the product gases must inhibit the reaction, for example by occupying the active site of the catalyst. An addition of nitrogen has almost no effect on the conversion, but an addition of hydrogen decreases the activity distinctly.

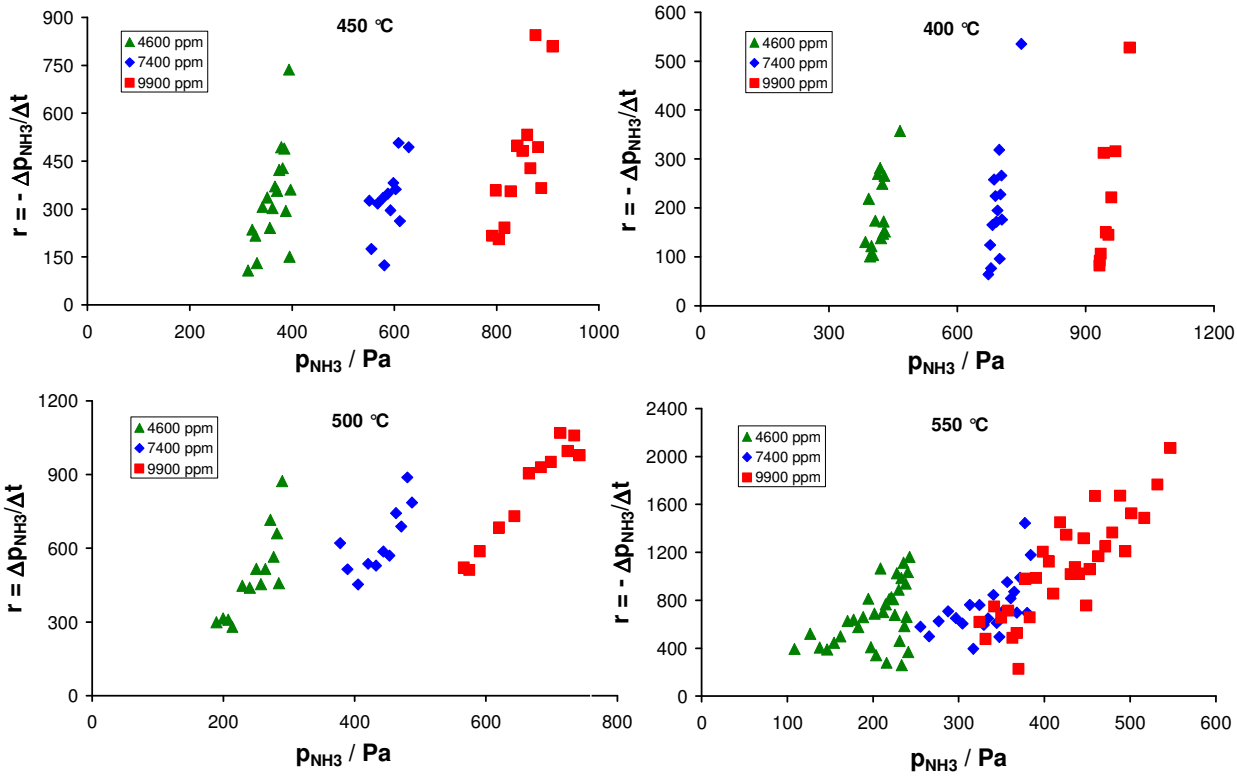

Figure 3.13: Reaction rates of ammonia decomposition over 4 g ß" ZrON at various reaction temperatures, calculated from$\Delta p/\Delta t$

3.7. Reaction mechanism

XPS measurements indicated the mobility of nitrogen from the bulk of the ZrON to the surface. The nitrogen content of the catalyst in the first series of experiment under ammonia flow did not present an eminent decrease (just ~0.30 wt-%), even though the catalyst had undergone reaction conditions over 600 °C. But the later investigation on ß"-phase of ZrON showed that the catalyst lost its nitrogen, significantly: the fresh sample for the kinetic study contained 54 mol-% ß"-phase (2,70 wt% nitrogen) and after three weeks heating at 550 °C under 10 mL/min helium, it contained just 30 mol-% ß"-phase (1,49 wt% nitrogen). These two facts indicated that:

1. The nitrogen from the bulk moves definitely to the surface.
2. There must be a nitrogen exchange between embedded nitrogen in the catalyst and adsorbed nitrogen species from the ammonia

cracking which keep the nitrogen content of the catalyst stable under reaction condition.

3.7.1. The role of anion vacancies, nitrogen concentration and ion conductivity

Both phases of zirconia oxynitrides contain monoclinic zirconia Zr_7O_{14} and bevan structure $Zr_7O_8N_4$, which contains two vacancies (Figure 14). The nitrogen poor ß' phase ($Zr_7O_{11}N_2$) is just an irregular stack of both structures and the nitrogen rich ß" phase ($Zr_7O_{9.5}N_3$) can be described as a randomly arranged stack of three bevan clusters and one monoclinic zirconia:

ß' phase: $Zr_7O_{11}N_2 = (Zr_7O_8N_4 + Zr_7O_{14})/2$

ß" phase: $Zr_7O_{9,5}N_3 = (3.[Zr_7O_8N_4] + Zr_7O_{14})/4$

Since the vacancies occupy an oxygen lattice sites and have a carge of +2, it would be denoted as $\left(V_O^{00}\right)$. Including this Kröger-Vink notation into the description, the ß-phases should be written as following chemical formula:

ß phase : $Zr_7O_8\left(N_O^{'}\right)_4\left(V_O^{00}\right)_2$

ß' phase : $Zr_7O_{11}\left(N_O^{'}\right)_2\left(V_O^{00}\right)$

ß" phase : $Zr_7O_{9.5}\left(N_O^{'}\right)_3\left(V_O^{00}\right)_{1.5}$

A special fact which should be considered in a closer inspection of the ß" ZrON is the location of the two anion vacancies which are not neighbouring, as can be seen at the Figure 3.14. Formally the nitrogen ion has a negative charge and the vacancy is a cation with a positive charge of +2. In the thesis of Dirk Nädele [14] it is described that one vacany is surrounded by two nitrogen anions. In reaction equations it

should be written as $\left(N_O^{'}\right)_2\left(V_O^{00}\right)_1$ in consideration of the position of nitrogen and vacancy which in both cases replace an oxygen. Therefore the Bevan structure should be described correctly by an empirical formula: $Zr_7O_8\left(N_O^{'}\right)_4\left(V_O^{00}\right)_2$. But it must be considered that morpologically there are two separate $\left(N_O^{'}\right)_2\left(V_O^{00}\right)_1$ structures in each Bevan unit (Figure 3.14). The most prefered arrangement of the vacancies is a linear chain of $\left(V_O^{00}\right)$-Zr-$\left(V_O^{00}\right)$ along [111] direction, which is the case at Bevan structure [7, 16].

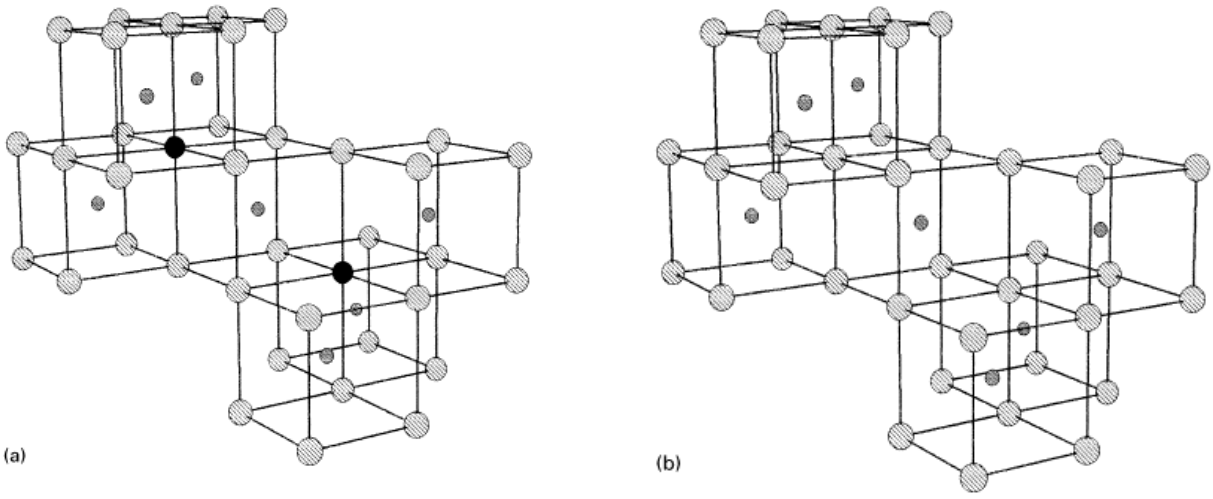

Figure 3.14: Units of ß phases: a) Bevan cluster: $Zr_7O_8N_4$ (Zr_7X_{12}) and b) monoclinic zirconia unit: Zr_7O_{14}. Small spheres: zirconium ions, big spheres: anions, dark spheres: vacancies. **[15]**

Although both ß'- and ß"-phase of ZrON contain monoclinic zirconia and Bevan structure, the ß' phase did not show any activity and only after phase transition to ß"-phase a conversion jump in ammonia decomposition was observed. There must be a reason why the ß'-phase of ZrON is inactive and the ß"-phase of ZrON is active for ammonia decomposition. One reason could be the better ion conductivity of ß"-phase or the higher local nitrogen concentration in ß" structure. Since in the ß"-phase there are at least two bevan structures existing side by

side, we must also investigate, if a high local concentration of vacancies also plays a distinct role.

In order to examine this questions two new samples were investigated, which have a different specification: one sample with a high nitrogen and vacancy concentration (Zr_2ON_2) and one sample with less nitrogen concentration and less vacancy concentration but with a high ion conductivity (nitrided zirconia with Y_2O_3 as doping agent).

3.7.1.1. Catalyst preparation & characterization

Sample 1: Zr_2ON_2 (yellow sample)

ZrO_2 powder (Alfa, Puratronic: 99.978%) was placed in a corrundum vessel and heated in a furnace to 1100°C under an ammonia stream of 40 l/h at ambient pressure for at least 15 h. A yellow powder with a composition of 92 wt-% Zr_2ON_2 and 8 wt-% impurity (other phases, mostly ß-phase) would be gained. Since there is a vacancy in each structure unit, we could denote this sample as $Zr_2ON_2[\ ]_1$.

Nitrogen content of fresh sample: 9.74 wt-%. A latter determintaion of the used sample gave an nitrogen content of 10.56 wt-% and an increase of the fraction of ß-phase to 12 wt-%.

Sample 2: NF14 ($Zr_{0.88}Y_{0.12}O_{1.72}N_{0.15}$)

A coprecipitated powder of zirconia with 6 mol-% Y_2O_3 was heated to 900°C and ammonolyzed in an ammonia stream of 15 l/h. A hot gas extraction gave a nitrogen content of 1.727 wt-%. The outcome of the calculation gave an empirical formula of $Zr_{0.88}Y_{0.12}O_{1.72}N_{0.15}$

Since Ytrium have an ionic charge of +3 and Zirconium have an ionic charge of +4, each cation substitution produces a vacancy in the structure:

$$Y_2O_3 \xrightarrow{ZrO_2} 2Y'_{Zr} + 3O_O^x + V_O^{00} \qquad (6)$$

O_O^x = oxygen anion on a regular oxygen lattice

Y'_{Zr} = Ytrium in zirconium lattice with a charge of -1

V_O^{00} = oxygen vacany in the anionic sublattice with a charge of +2

But even this sample contains much less anion vacancies in comparison to Zr_2ON_2, the NF14 shows a better ion conductivity, about three to four orders of magnitudes larger, because in contrast to Zr_2ON_2 which has an ordered vacancy structure, the anion vacancies in the NF4 are highly disordered as a result of the Ytrium-doping. In the habilitation thesis of Prof. Lerch it was reported that NF14 has following values for its electrical conductivity:

T	σ
500 °C	~ $8*10^{-5}$ S/cm
560 °C	~ $3*10^{-4}$ S/cm
620 °C	~ $10^{-2,9}$ S/cm

Table 3.2: Electrical conductivity of NF14 at different temperatures

3.7.1.2. Catalyst pretreatment

Since a catalyst powder would be carried out from the reactor and damage the IR sensor, it must be peletized before use. The powder was filled in a metal stamp (Figure 3.15, left) and pressed under 100 bar into a thin pellet, which then was crushed into small particles. After sieving (Figure 3.15, rights) a fraction of catalyst particles of 200 – 300 µm was obtained and this fraction was used for the further catalyst characterization and BET measurements.

In this pretreatment process it was noticed that the Zr_2ON_2 was harder to peletize because it tended to produce crumbly particles. A slight increase of the surface area of the used Zr_2ON_2 sample might be a

result of surface extension due to crumbling effect after mechanical and thermal treatment in the reactor.

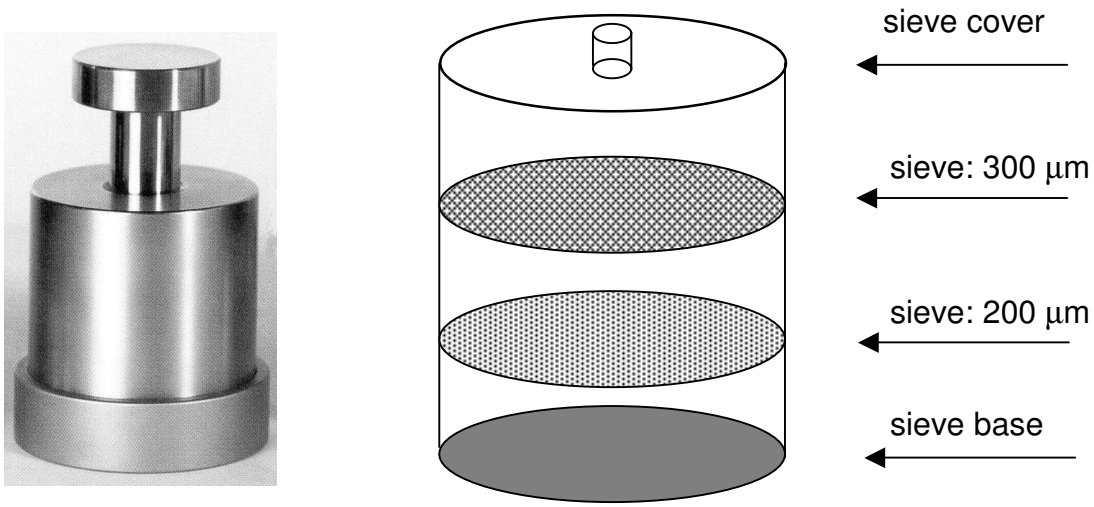

Figure 3.15: Metal stamp for production of catalyst pellets (left picture) and metal sieves (right picture) for selection of a particle size

Sample	BET area of fresh sample	BET area of used sample
Zr_2ON_2	3.39 m^2/g	3.49 m^2/g
NF14	8.37 m^2/g	8.07 m^2/g

Table 3.3: BET data of tested catalyst. Particle size: 200 -300 µm

Sample	N content of fresh sample	N content of used sample
Zr_2ON_2	9.74 wt-%	10.56 wt-%
NF14	1.73 wt-%	1.54 wt-%

Table 3.4: Nitrogen content from hot gas exrtraction of investigated camples

3.7.2.3. Result of catalyst testing and mechanistic study

Both new catalysts were not active under 450°C. At higher temperatures they became active. The yellow sample (Zr_2ON_2) was more active than the grey sample (NF4). A high ion conductivity is hereby not a proper criteria for the activity of the catalyst.

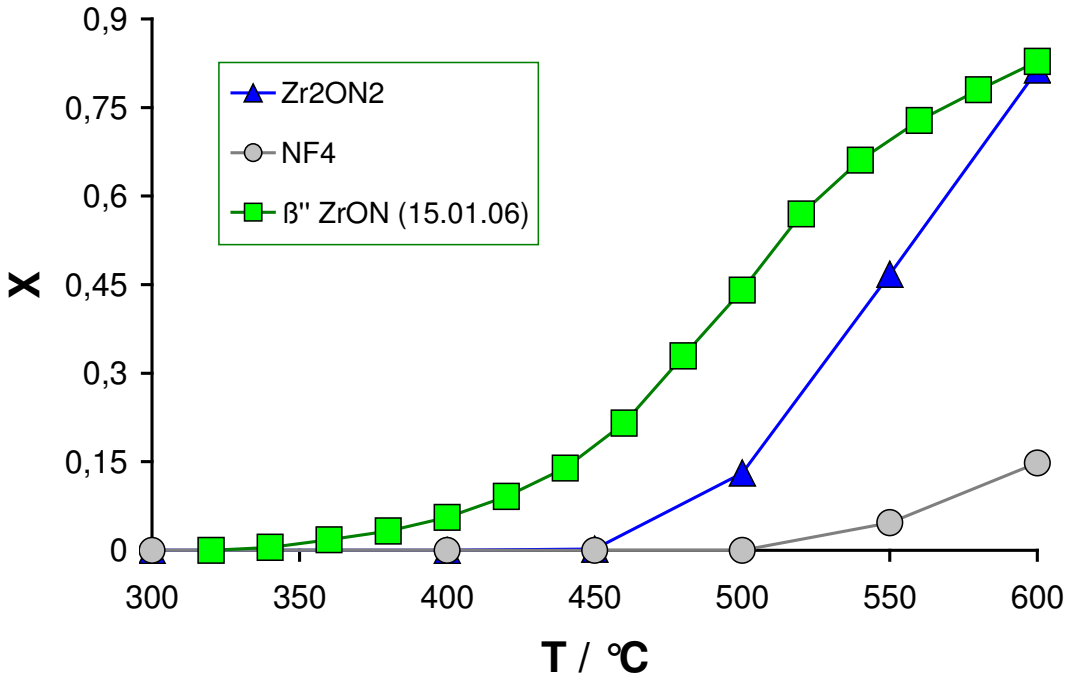

Figure 3.16: Conversion of NH_3 decomposition over three different catalysts. Feed concentration of ammonia: 4000 ppm

The assumption of nitrogen exchange in the process (see arguments in chapter 3.7.) was supported by the fact that the more active sample Zr_2ON_2 exhibited an increased nitrogen content than NF4 which has a better conductivity (see table 3.4). The TPR study in the next section backed up also this hypothesis. A high nitrogen content in the bulk is therefore an important criteria for the catalysis, even if it is not sufficient. A higher nitrogen content in N-doped zirconia does not provide inevitably a better activity because it leads to an increase of the overall activation energy for diffusion [16].

The yellow sample (Zr_2ON_2) which contains more nitrogen than ß" ZrON was indeed less active (see Figure 3.16). The ß"-phase of ZrON is the most active species among the studied samples, although it had the lowest specific surface area with just about 1/3 of the value of Zr_2ON_2 and with its 2,7 wt% much less nitrogen than Zr_2ON_2 (9,74 wt% nitrogen).

Assuming that the anion mobility in the more dissordered ß" ZrON was better than in the more ordered vacancy structure in Zr_2ON_2, the key feature for the ammonia decomposition is the density of mobile nitrogen anion of the catalyst.

3.7.2. TPR study

To revise the assumptions and to verify the proposed kinetic model a TPR study was carried out over 2,65 g of ß" ZrON. The catalyst was heated with a temperature ramping of 5 K/min under a gas mixtrure of 5 % hydrogen in helium with a total flow rate of 50 ml/min. At 850°C the temperature was held isothermal for 30 minutes, then the heating was switched off and the temperature was cooled down to room temperature. The m/z (mass-to-charge ratio) values of all species in the isotherm period were quite constant.

If the reaction involves the nitrogen from the bulk of the catalyst, ammonia must be formed under hydrogen flow. And indeed ammonia was detected in the outlet gas mixture. An increasing NH_3 formation at temperatures over 400 °C is seen In Figure 3.17 and it decreased again at temperatures around 650 °C.

For a better facility of inspection the m/z 17 and 16 were denoted just as NH_3 and NH_2 respectively. In fact they contain a small fraction of OH^+ and O^+, respectively. The signal m/z 32 is attributed to oxygen. Since the m/z 30 ($N_2H_2^+$) and 31 ($N_2H_3^+$) were negligible and the m/z 32 in the whole range between 400°C and 850°C showed no increase, it concluded that no hydrazine was produced and the m/z 32 could be attributed only to oxygen. It should be considered here that in consequence of the use of silicon tube which connected the glass reactor

with the gas supply (5% H_2 in helium), some air was inserted into the reaction system. It is the reason why some oxygen and nitrogen were registered already at room temperature.

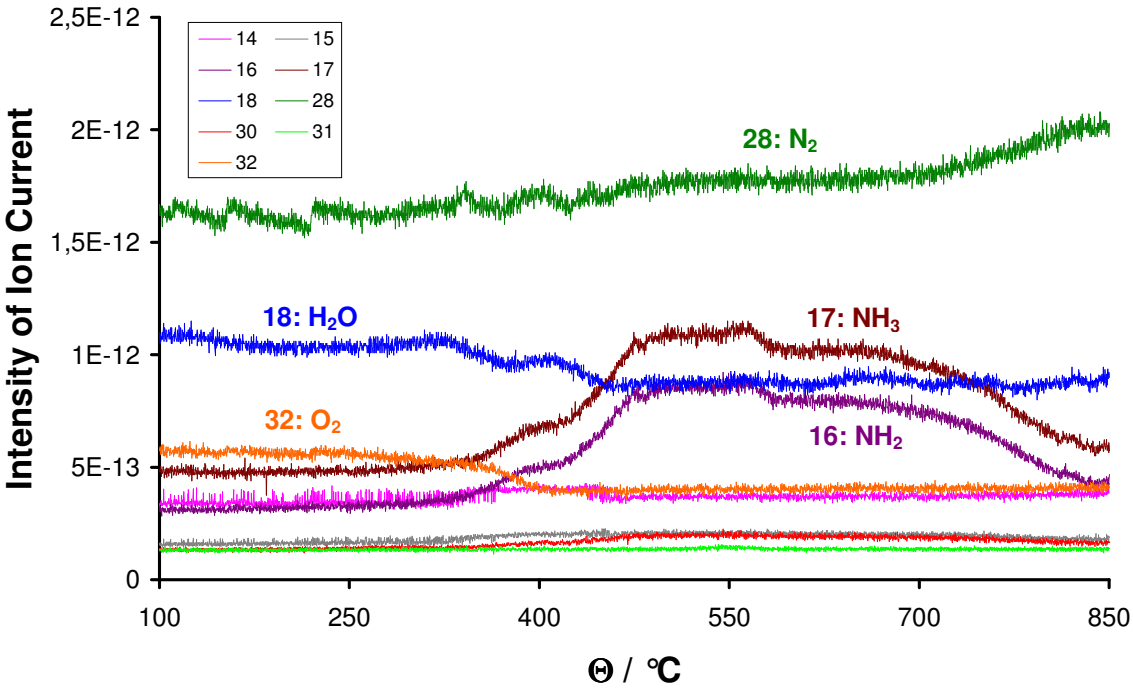

Figure 3.17: TPR of ß" ZrON with 5% H_2 and a temperature heating ramp of 5K/min

The development of the signals during the temperature ramping in Figure 3.17 and 3.18 shows that the oxygen intensity decreased as ammonia begann to be produced over 400℃. Oxygen probably replaced the leaving nitrogen which reacted with hydrogen to produce ammonia or at higher temperatures left the lattice as nitrogen molecules. Thermodynamically the decomposition of ammonia to nitrogen is favoured at higher temperatures and indeed less ammonia was detected and more nitrogen was registered in product gas at higher temperatures.

The development of the water signal during the TPR showed a clear tendency which was counter current to the developtment of ammonia. As the nitrogen from the bulk reacted with hydrogen to produce ammonia and in consequence a formally positive vacancy was created, the negative hydroxyl group which was derived from water

would easily occupied the generated vacancy. In the extreme case this process could destroy the catalyst, if all nitrogen in the structure would be replaced by oxygen. Water is therefore definetively a poison for this process.

The increase of the signal of ammonia species after the switch-off of the heating device (marked by the arrow in Figure 3.18) could be explained with a thermodynamic reason. In contrast: the obtained signals of ammonia species which showed a plateau between 450 °C and 560 °C (see Figure 3.17) could not be explained by pure thermodynamics or Langmuir-Hinselwood kinetics. This result indicated that an unusual process occured which could include an exchange of nitrogen with the bulk.

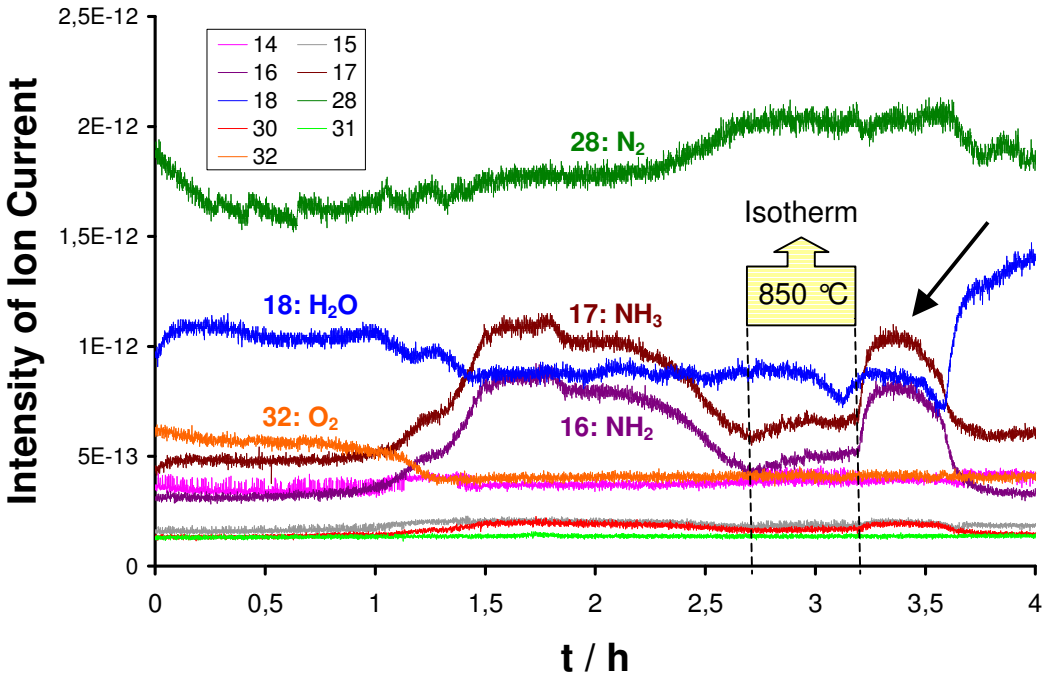

Figure 3.18: Chronogical development of investigated species at TPR study. The heating device was switched off after the isotherm. The increase of ammonia species next to first cooling down phase is pointed by an arrow.

The final evidence that the observed reaction included a nitrogen exchange with the bulk nitrogen, an extra experiment with SSITKA (steady-state isotopic transient kinetic analysis) still needs to be done.

3.8. Reaction kinetics

Based on the previous results, a mechanistic kinetic model was developed, which included the vacancy as an important reaction center. In the first step of ammonia decompositon over ZrON, the vacancy which formally has a charge of +2 would be occupied by ammonia. Following reaction steps were suggested:

R-0 : $NH_{3(g)} + * \rightleftharpoons *\text{-}NH_3$

R-I : $N_O^{'}V_O^{oo} + NH_{3(g)} \rightleftharpoons N_O^{'}(H_3N)_O^{oo}$ ➔ r_1

R-II : $N_O^{'}(H_3N)_O^{oo} \rightleftharpoons N_O^{'}(H_2N)_O^{o} + H^+$

R-III : $N_O^{'}(H_2N)_O^{o} \rightleftharpoons N_O^{'}(HN)_O^{x} + H^+$

R-IV : $N_O^{'}(HN)_O^{x} \rightleftharpoons (N_O N_O)^{''} + H^+$

R-V : $(N_O N_O)^{''} + H^+ \rightleftharpoons (N_O N_O)^{'} + 0.5\ H_{2(g)}$

R-VI : $(N_O N_O)^{'} + H^+ \rightleftharpoons (N_O N_O)^{x} + 0.5\ H_{2(g)}$

R-VII : $(N_O N_O)^{x} + H^+ \rightleftharpoons (N_O N_O)^{o} + 0.5\ H_{2(g)}$

$\sum_{i=II}^{VII} R-i$: $N_O^{'}(H_3N)_O^{oo} \rightleftharpoons (N_O N_O)^{o} + 1.5 H_{2(g)}$ ➔ r_2

R-VIII: $(N_O N_O)^{o} \rightarrow N_{2(g)} + (V_O V_O)^{o}$ ➔ r_3 (rds)

R-IX : $(V_O V_O)^{o} + NH_{3(g)} \rightleftharpoons (V_O(H_3N)_O)^{o}$ ➔ r_4

R-X : $(V_O(H_3N)_O)^{o} \rightleftharpoons (V_O(H_2N)_O)^{x} + H^+$

R-XI : $(V_O(H_2N)_O)^{x} \rightleftharpoons (V_O(HN)_O)^{'} + H^+$

R-XII : $(V_O(HN)_O)^{'} \rightleftharpoons (V_O N_O)^{''} + H^+$

R-XIII: $(V_O N_O)^{''} + H^+ \rightleftharpoons (V_O N_O)^{'} + 0.5\ H_{2(g)}$

R-XIV: $(V_O N_O)^{'} + H^+ \rightleftharpoons (V_O N_O)^{x} + 0.5\ H_{2(g)}$

R-XV : $(V_O N_O)^{x} + H^+ \rightleftharpoons (V_O N_O)^{o} + 0.5\ H_{2(g)}$

$\sum_{i=X}^{XV} R-i$: $(V_O(H_3N)_O)^{o} \rightleftharpoons V_O^{oo} N_O^{'} + 1.5\ H_{2(g)}$ ➔ r_5

The physisorption of ammonia at the catalyst surface (equation R-0) could not be excluded but it is not an issue of kinetics description because this species would not be incorporated in the reaction steps toward nitrogen production. For the kinetic calculation we could summarise the reaction steps R-II until R-VII as preequilibrium into a rate equation r_2 which represents a step by step formation of hydrogen. The next reduction of hydrogen ion and its formation to hydrogen (R-X until RXV) is abstracted to rate equation r_5. Following reaction steps are formulated for kinetics calculation:

r_1: $N_O^{'} V_O^{oo} + NH_{3(g)} \rightleftharpoons N_O^{'} (H_3N)_O^{oo}$ (7)

r_2: $N_O^{'} (H_3N)_O^{oo} \rightleftharpoons (N_O N_O)^{o} + 1.5 H_{2(g)}$ (8)

r_3: $(N_O N_O)^{o} \xrightarrow{(rds)} N_{2(g)} + (V_O V_O)^{o}$ (9)

r_4: $(V_O V_O)^{o} + NH_{3(g)} \rightleftharpoons ((H_3N)_O V_O)^{o}$ (10)

r_5: $((H_3N)_O V_O)^{o} \rightleftharpoons N_O^{'} V_O^{oo} + 1.5\ H_{2(g)}$ (11)

The resulting rate equations are:

$$r_1 = k_{1,f} \cdot p_{NH_3} \cdot c_{(N_O V_O)^o} - k_{1,r} \cdot c_{(N_O (H_3N))^{oo}} \quad (12)$$

$$r_2 = k_{2,f} \cdot c_{(N_O (H_3N))^o} - k_{2,r} \cdot c_{(N_O N_O)^o} \cdot p_{H_2}^{1.5} \quad (13)$$

$$r_3 = k_3 \cdot c_{(N_O N_O)^o} \quad (14)$$

$$r_4 = k_{4,f} \cdot c_{(V_O V_O)^o} \cdot p_{NH_3} - k_{4,r} \cdot c_{((H_3N)_O V_O)^o} \quad (15)$$

$$r_5 = k_{5,f} \cdot c_{((H_3N)_O V_O)^o} - k_{5,r} \cdot c_{(N_O V_O)^o} \cdot p_{H_2}^{1.5} \quad (16)$$

The reactions r_1, r_2, r_4 and r_5 are in equilibirium state, therefore: $r_1=r_2=r_4=r_5=0$. The irreversible reaction r_3 is the slowest step and acts as rate determining step (rds): $r = r_3 = k_3 \cdot c_{(N_O N_O)^o}$

For the reactions r_1, r_2, r_4 and r_5 the following equilibrium constants are defined:

$$K_1 = \frac{k_{1,f}}{k_{1,r}} = \frac{c_{(N_O (H_3N))^o}}{p_{NH_3} \cdot c_{(N_O V_O)^o}} \rightarrow c_{(N_O (H_3N))^{oo}} = c_{(N_O V_O)^o} \cdot p_{NH_3} \cdot K_1 \quad (17)$$

$$K_2 = \frac{k_{2,f}}{k_{2,r}} = \frac{c_{(N_O N_O)^o} \cdot p_{H_2}^{1.5}}{c_{(N_O (H_3N))^o}} \rightarrow c_{(N_O N_O)^o} = \frac{c_{(N_O (H_3N))^o} \cdot K_2}{p_{H_2}^{1.5}} \quad (18)$$

$$K_4 = \frac{k_{4,f}}{k_{4,r}} = \frac{c_{((H_3N)_O V_O)^o}}{c_{(V_O V_O)^o} \cdot p_{NH_3}} \rightarrow c_{((H_3N)_O V_O)^o} = c_{(V_O V_O)^o} \cdot p_{NH_3} \cdot K_4 \quad (19)$$

$$K_5 = \frac{k_{5,f}}{k_{5,r}} = \frac{c_{(N_O V_O)^o} \cdot p_{H_2}^{1.5}}{c_{((H_3N)_O V_O)^o}} \rightarrow c_{(N_O V_O)^o} = \frac{c_{((H_3N)_O V_O)^o} \cdot K_5}{p_{H_2}^{1.5}} \quad (20)$$

The material balance of the active site is:

$$c_{\left(N_O^{'} V_O^{oo}\right)_t} = c_{\left(N_O^{'} V_O^{oo}\right)} + c_{N_O^{'} (NH_3)_O^{oo}} + c_{(N_O N_O)^o} + c_{(V_O V_O)^o} + c_{((NH_3)_O V_O)^o} \quad (21a)$$

$$c_{\left(N_O^{'}V_O^{oo}\right)_t} = \frac{c_{(N_ON_O)^o} \cdot p_{H_2}^{1.5}}{p_{NH_3} \cdot K_1 \cdot K_2} + \frac{c_{(N_ON_O)^o} \cdot p_{H_2}^{1.5}}{K_2} + c_{(N_ON_O)^o}$$

$$+ \frac{c_{(N_ON_O)^o} \cdot p_{H_2}^{3}}{p_{NH_3}^{2} \cdot K_1 \cdot K_2 \cdot K_4 \cdot K_5} + \frac{c_{(N_ON_O)^o} \cdot p_{H_2}^{3}}{p_{NH_3} \cdot K_1 \cdot K_2 \cdot K_5} \qquad (21.b)$$

$$c_{\left(N_O^{'}V_O^{oo}\right)_t} = c_{(N_ON_O)^o} \cdot \left(\frac{p_{H_2}^{1.5}}{p_{NH_3} K_1 \cdot K_2} + \frac{p_{H_2}^{1.5}}{K_2} + 1 + \frac{p_{H_2}^{3}}{p_{NH_3}^{2} K_1 \cdot K_2 \cdot K_4 \cdot K_5} + \frac{p_{H_2}^{3}}{p_{NH_3} K_1 \cdot K_2 \cdot K_5} \right) \qquad (21.c)$$

The insertion of equation 21.c into the rate law of the rds gives following rate equation for the ammonia decomposition over ZrON:

$$r = k_3 \cdot c_{(N_ON_O)^o} \qquad (14)$$

$$r = k_3 \cdot \frac{c_{\left(N_O^{'}V_O^{oo}\right)_t}}{\left(\frac{p_{H_2}^{1.5}}{p_{NH_3} \cdot K_1 \cdot K_2} + \frac{p_{H_2}^{1.5}}{K_2} + 1 + \frac{p_{H_2}^{3}}{p_{NH_3}^{2} \cdot K_1 \cdot K_2 \cdot K_4 \cdot K_5} + \frac{p_{H_2}^{3}}{p_{NH_3} \cdot K_1 \cdot K_2 \cdot K_5} \right)} \qquad (22.a)$$

$$r = \frac{k_3 \cdot c_{\left(N_O^{'}V_O^{oo}\right)_t} K_1 \cdot K_2 \cdot K_4 \cdot K_5 \cdot p_{NH_3}^{2}}{\left(p_{H_2}^{1.5} \cdot p_{NH_3} \cdot K_4 \cdot K_5 + p_{H_2}^{1.5} \cdot p_{NH_3}^{2} \cdot K_1 \cdot K_4 \cdot K_5 + p_{NH_3}^{2} \cdot K_1 \cdot K_2 \cdot K_4 \cdot K_5 + p_{H_2}^{3} + p_{H_2}^{3} \cdot p_{NH_3} \cdot K_4 \right)} \qquad (22.b)$$

$$r = \frac{k^{'} \cdot K_1 \cdot K_2 \cdot K_4 \cdot K_5 \cdot p_{NH_3}^{2}}{\left(p_{H_2}^{1.5} p_{NH_3} K_4 \cdot K_5 \cdot (1 + p_{NH_3} \cdot K_1) + p_{NH_3}^{2} K_1 \cdot K_2 \cdot K_4 \cdot K_5 + p_{H_2}^{3} (1 + p_{NH_3} \cdot K_4) \right)} \qquad (22.c)$$

The temperture dependency of the rate constant and equilibrium constants are given by following Arrhenius and Van't-Hoff equations:

$$k = c_{\left(N_O' V_O^{oo}\right)_t} \cdot k_{3,0} \cdot e^{\left(-\frac{E_{A,3}}{RT}\right)} = k_0 \cdot e^{\left(-\frac{E_{A,3}}{RT}\right)} \quad (23)$$

$$K_1 = K_{1,0} \cdot e^{\left(-\frac{\Delta H_1}{RT}\right)} \quad (24)$$

$$K_2 = K_{2,0} \cdot e^{\left(-\frac{\Delta H_2}{RT}\right)} \quad (25)$$

$$K_4 = K_{4,0} \cdot e^{\left(-\frac{\Delta H_4}{RT}\right)} \quad (26)$$

$$K_5 = K_{5,0} \cdot e^{\left(-\frac{\Delta H_5}{RT}\right)} \quad (27)$$

The previous sets of experimental data were fitted by the rate equation 22.c. The obtained rate constants in the measured temperature range were plotted in an Arrhenius diagram (Figure 3.19) to get the activation energy of the reaction. The calculation gave an activation energy $E_{A,3}$ of 70 ± 10 kJ/mol for ammonia decomposition over ß" of ZrON.

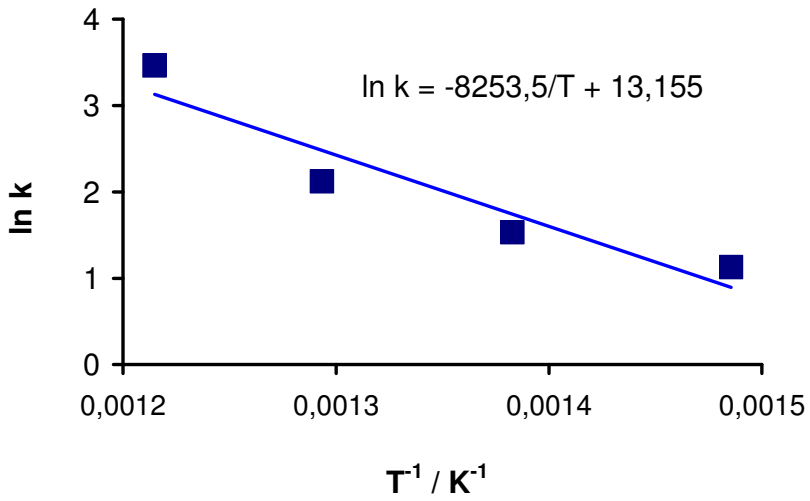

Figure 3.19: Arrhenius diagramm of reaction constant k_3

In order to estimate the reaction enthalphies of the equlibrium reactions, the obtained equilibrium constants K_1, K_2, K_4 and K_5 were plotted in Van't Hoff diagramm in Figure 3.20.

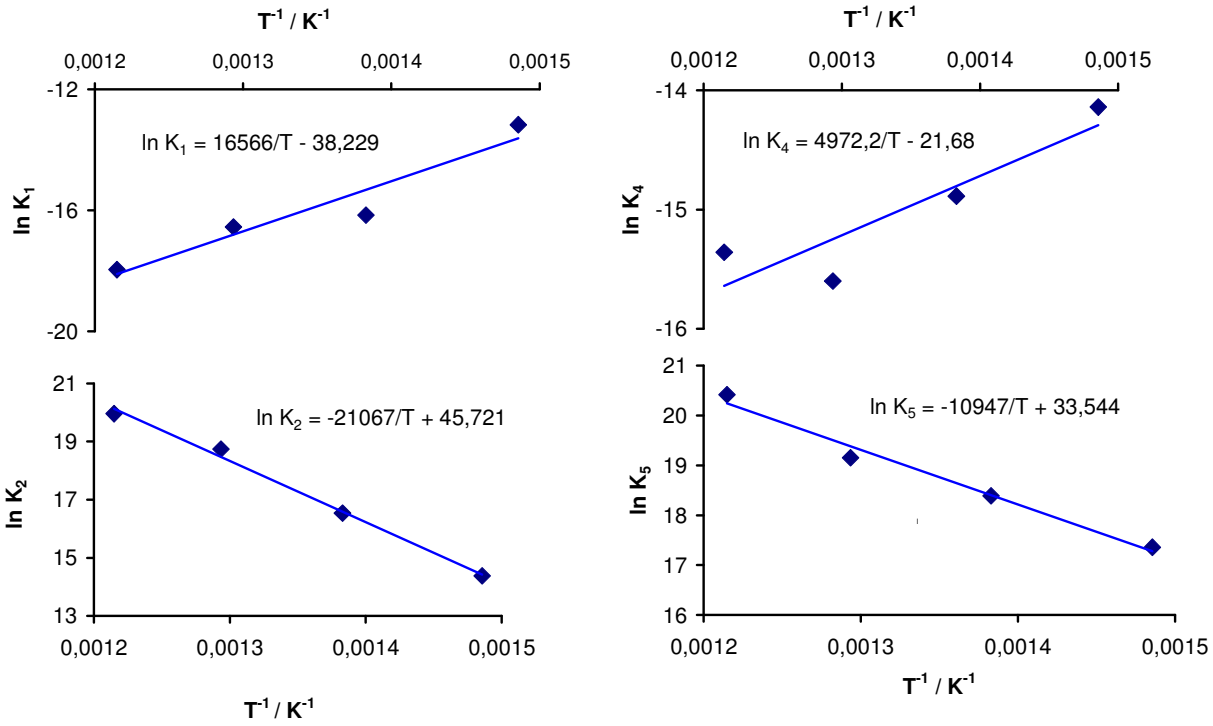

Figure 3.20: Van't Hoff plots of equlibrium contants in a temperature range between 400 °C and 550 °C

The calculation gives following data for the reaction enthalpies:

ΔH_1 = -138 ± 20 kJ/mol

ΔH_2= 175 ±10 kJ/mol

ΔH_4 = -41 ± 20 kJ/mol

ΔH_5 = 91 ± 10 kJ/mol

In order to determine the effective activation energy, the natural logaritm of calculated rates for different temperatures was plotted ersus the reciprocal of temperture in Kelvin. The effective activation energy

then could be calculated from the slope in the Arrhenius diagramm (Figure 3.21).

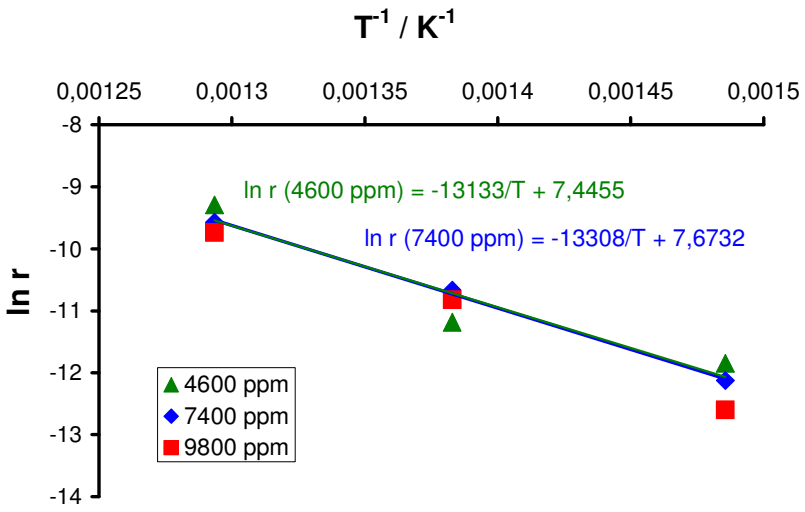

Figure 3.21: Arrhenius diagramm for the determination of effective activation energy at 10% conversion over temperatures between 400 °C and 500 °C

The reaction rates were calculated from the experimental data within the investigated temperature range and three different initial partial pressures of ammonia and the obtained plots gave an effective activation energie $E_{A,\,eff}$ = (110 ± 10) kJ/mol.

An energy profile of the reaction is constructed from the obtained thermodynamic data and the activation energy. A graphical determination of activation energy based on the obtainend values from the reaction simulation by Madonna showed an effective activation energy of 106 kJ/mol (Figure 3.22).

It must be mentioned here that the value pairs fo K_1 - K_2 and K_4 – K_5 could be mathematically described as exotherm – endotherm or endotherm – exotherm, which leaded to different values but the sum of (ΔH_1 + ΔH_2) and (ΔH_4 + ΔH_5) would not change much. But it is physically reasonable to decribe the desorption of hydrogen as an endotherm process.

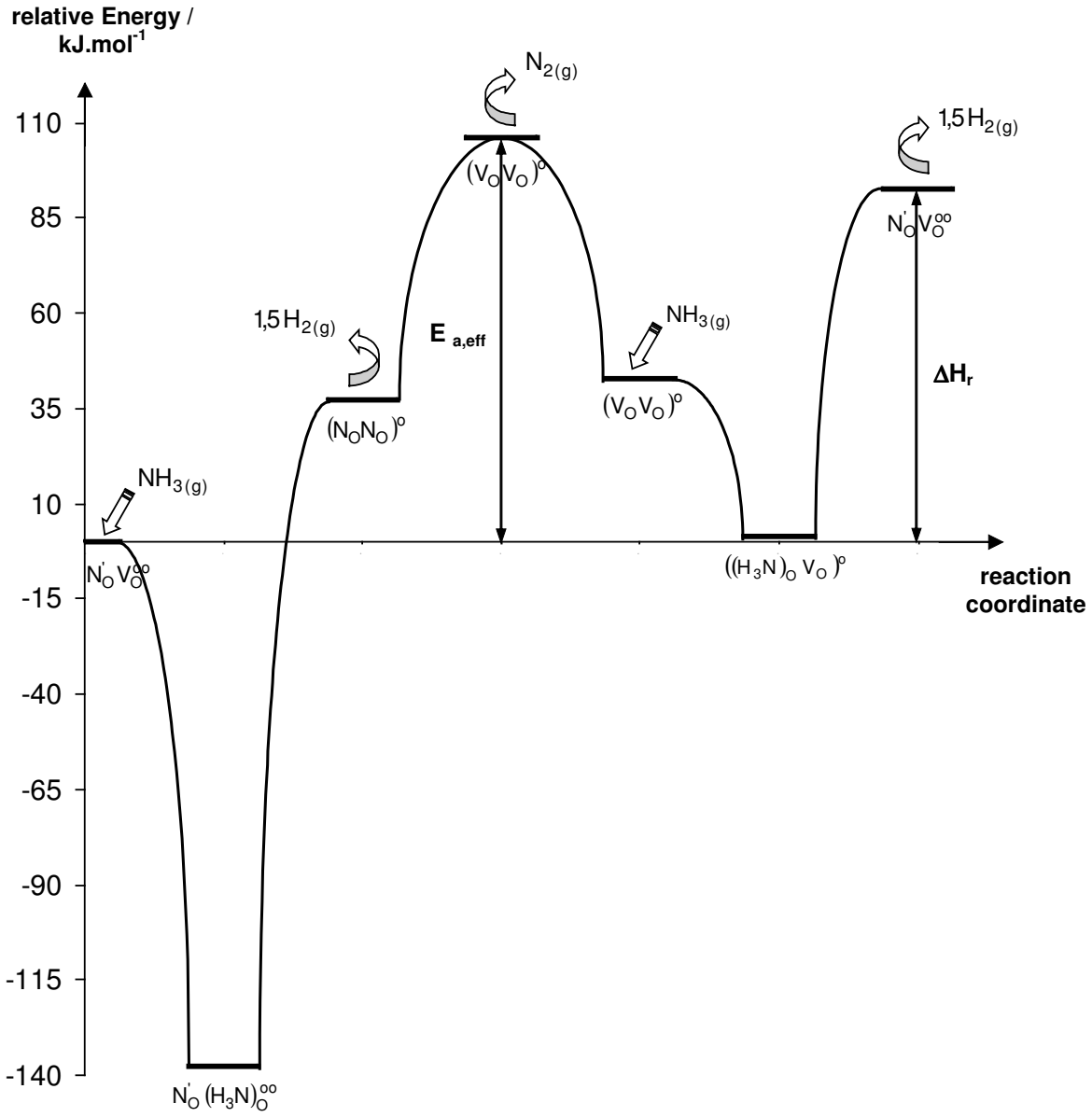

Figure 3.22: Energy diagram of ammonia cracking over ZrON catalyst with $E_{a,\ eff}$ = 106 kJ/mol and ΔH_r = 92.4 kJ/2 mol NH_3

As mentioned in chapter 3.7.1. there are two nitrogen and one vacany in neighbouring circumstances as a unit: $\left(N_O^{'}\right)_2\left(V_O^{00}\right)_1$, as also described in the thesis of Dirk Nädele [14]. Thomas Bredow found in his theoretical investigation that the most stable configuration in the nitrogen rich supercell has a structure as desribed in Figure 3.23.

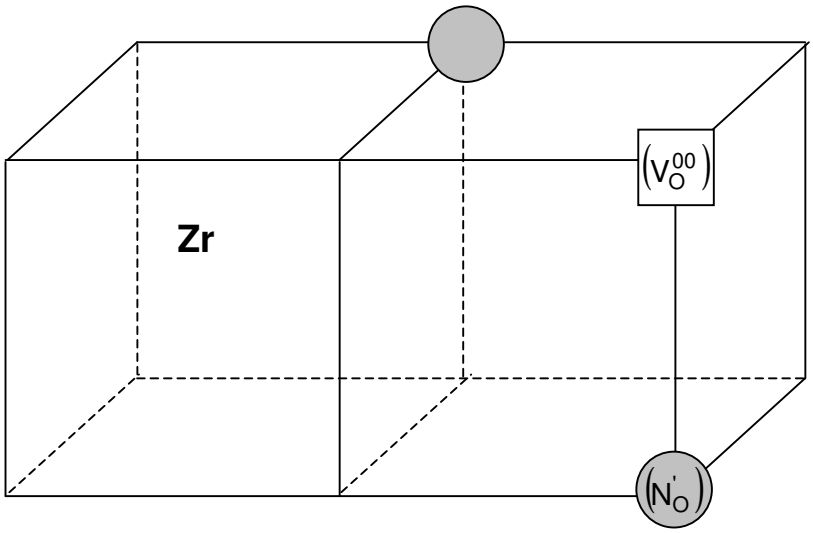

Figure 3.23: Most stable configuration of $(N_O')_2(V_O^{00})_1$ for the supercells $Zr_8O_{13}N_2$ with ○ = (N_O') and □ = (V_O^{00})

Since just one of the nitrogen is included in the reaction, just one nitrogen and one oxigen vacancy is written in the reaction scheme in the energy diagramm of ammonia decomposition due to a better clarity. The nitrogen which is included in the reaction must be the one which is located further to zirconia and has a weaker bond to zirconia, respectively.

Thomas Bredow reported in his theoretical investigation that the formation of two neighbouring oxygen vancancies is thermodynamically not favoured, but they can exist under strong reducing conditions.[16] This is the case in the investigated reaction system.

3.9. Conclusion

In summary, the zirconium oxynitride studied showed a remarkable catalytic activity in the decomposition of ammonia. Compared to conventional metal containing catalysts, the ZrON catalysts exhibited no formation of hydrazine during extended time on stream. The sudden increase in activity at ~550°C coincides with the onset of nitrogen ion conductivity in the material and the phase change from the initial ß' phase to the nitrogen rich β" ZrON phase. An addition of nitrogen does

not influence the conversion, but an adddition of hydrogen has a distinctive inhibition effect to the reaction. Moreover, an apparent activation energy of 110 ± 10 kJ/mol agrees well with the activation energy of ion mobility in zirconia based materials. The dramatic change in activity is also correlated to a rapid change in the electronic structure of the surface that accompanies the formation of the more active β" ZrON phase. The results presented show for the first time a direct correlation between the onset of ion conductivity as a bulk property, a modified electronic structure of the surface, and the catalytic performance of a heterogeneous catalyst.

3.10. References

[1] (a)S.F. Yin, B.Q. Xu, X.P. Zhou, C.T. Au, *Appl. Catal. A: General* 2004, *277*, 1-9.

(b)T.V. Choudhary, C. Sivadinarayana, D.W. Goodmann, *Chem. Eng. J.* 2003, *93*, 69-80.

[2] C.H. Christensen, T. Johannessen, R.Z. Sorensen, J.K. Norskov, Towards an ammonia-mediated hydrogen economy?, Catalysis Today 111 (2006) 140-144.

[3] G. Ramis, L. Yi, G. Busca, M. Turco, E. Kotur, R.J. Willey, *J. Catal.* 1995, *157*, 523-535.

[4] J. Wendel, M. Lerch, W. Laqua, J. Solid State Chem. 142 (1999) 163-167.

[5] M. Kilo, A.M. Taylor, C. Argirusis, G. Borchardt, M. Lerch, O. Kaitasov, B. Lesage, PCCP 6(13) (2004) 3645-3649.

[6] M. Lerch, J. Am. Ceram. Soc., 79 (10), (1996), 2641-2644

[7] M. Lerch, O. Rahäuser, J. Mat. Sci. 32 (1997), 1357-1363.

[8] S. Gutzow, M. Lerch, Nitrogen incorporation into pure and doped zirconia, Ceramic Internaional 2005, doi: 10.1016/j.ceramint.2005.08.007

[9] D.A. Shirley, High-resolution X-ray photoemission spectrum of the valence bands of Gold, Phys. Rev.. B: Solid State 5 (12) (1972) 4709-4714.

[10] Briggs and Seah “Practical Surface Analysis” second edition, Volume1-Auger and X-ray Photoelectron Spectroscopy, Wiley, 1990 pp.635-638 (Appendix 6).

[11] A.T. Tham, C. Rödel, M. Lerch, D. Wang, D.S. Su, A. Klein-Hoffman, R. Schlögl, Cryst. Res. Techn., 39 (5), (2004), 421-428.

[12] A.T. Tham, C. Rödel, M. Lerch, D.S. Su, A. Klein-Hoffman, R. Schlögl, Cryst. Res. Techn., 40(3), (2005), 193-198.

[13] G. Papapolymerou, V. Bontozoglou, *J. Mol. Catal.* **1997**, *120*, 165.

[14] D. Nädele, In situ-Elektronenmiskroskopie und –Röntgenbeugung: Die Reaktionen des Zirconiumdioxids mit Wasser und Ammoniak, Dissertation, Fakultät für Chemie und Pharmazie der Eberhard-Karls-Universität Tübingen, 2002.

[15] Lerch, J. of Mat. Sci. Lett. 17 (1998), 441-443.

[16] T. Bredow, Theoretical investigation of nitrogen substitution in cubic zirconia, Physical Review B **75**, 144102 (2007)

4. Summary

The most appropriate system for on board hydrogen production is the steam reforming methanol due its advantages regarding to the high hydrogen content of methanol, the absence of C-C bond in the reactants and the moderate reaction temperature. Copper based catalysts are known as active and quite selective candidate. In this study steam reforming of methanol (SRM) was investigated over $Cu/ZrO_2/CeO_2$ (CZC) catalysts prepared via a novel synthetic method based on co-precipitation and polymer templating. This mesoporous catalyst is very active, it needs no activation period, and because of its porosity there is no diffusion limitation. Structural characterization of the samples was performed by N_2 adsorption-desorption, N_2O decomposition, and X-ray diffraction. The variation of the Cu loading resulted in an increased Cu crystallite size and a decreased specific surface area of the active particles. Catalytic investigations were carried out in a fixed bed reactor at 10^5 Pa, by applying a $CH_3OH:H_2O$ = 1:1 ratio. The samples with Cu contents higher than 5 % exhibited good long-term stabilities and low CO levels during continuous operation. The kinetic model suggested for the transformation involved the reverse water-gas shift (RWGS) and methanol decomposition (MD), in addition to the SRM reaction. Kinetic measurements were accomplished in the temperature range 503-573 K and the experimental results could be well modelled. The highest methanol conversions and the lowest CO levels were observed in the temperature range 523-543 K. The apparent activation energies for the individual reactions were found to depend on the Cu content of the catalyst. Since the influence of mass transport limitations on the kinetic data could be excluded, it was established that the variation of the Cu concentration in the precursor material altered the microstructure of the Cu particles and, accordingly, the active Cu surface, which resulted in the formation of significantly different catalysts.

Steam reforming of methanol is an endotherm process and the hydrogen production by SRM over copper based catalysts has still a

problem in respect of the undesirable production of carbon monoxide. These two aspects need to be solved and must be taken into account if we want to produce hydrogen on board for mobile application. A process approach must be developed which is capable to run the processes autothermaly and reduce the carbon monoxide content to a tolerable limit for the platinum electrodes of the fuel cells. Since a chemical solution due to minimizing the CO content is not existent and an effort in this direction has no promising perspective, a new reactor concept which could solve the problems technically was proposed. A membrane reactor is tested in this study and investigated. In order to design an autothermal reactor, the membrane should be able to separate the product gases and the residual methanol, which is burned to produce the heat needed for evaporation of the reactants and for energy demand of the endothermal SRM. Furthermore the membrane must be able to reduce the CO content of the produced hydrogen or surpress the production of CO to the tolerable limit. Since dense metall membrane need much energy to separate the hydrogen from other gases and Knudsen diffusion could not provide for a sufficient enrichment of hydrogen, a ceramic membrane must be developed which exhibits the property between dense metal membrane and Knudsen membrane.

Another strategy to counter the CO problem is finding another hydrogen carrier without carbon content. Ammonia is an excellent candidate since this cheap chemical is available in sufficient amount and it can be produced eco-friendly. Furthermore the decomposition of ammonia has in the era of emmissions trading additionaly an advantage since it produces no CO_2. However the formation of hydrazine during ammonia decomposition must be excluded, otherwise it must be separate from the hydrogen bevor feeding it into fuel cell. Since the formation of hydrazine could not be excluded at ammonia decomposition over metal based catalysts, a new kind of non metal based catalyst was proposed and tested. Four different zirconia oxynitrides were prepared and investigated in this study: ß' ZrON, ß" ZrON, Zr_2ON_2 and $Zr_{0.88}Y_{0.12}O_{1.72}N_{0.15}$ (Y_2O_3 dopped zirconia oxynitride).

The long term study of ß-phase ZrON showed no hydrazine formation. The kinetic study in the temperature range 673-823 K and the comparison of different zirconia oxynitrides indicate that nitrogen from the bulk is involved in the reaction mechanism and the structure of the catalyst plays a distinct role. The activity of ZrON is based on the mobility of nitrogen ion of the catalyst in certain molecular structure. The most active catalyst is the ß" ZrON which has a high nitrogen content in the suitable structure which allows anion mobility. A high ion conductivity or a high nitrogen content solely is not a sufficient criterium for a good activitiy. Hydrogen and water have an negative effect to the reaction since hydrogen inhibits the reaction and water decreases the anion mobility by destroying the oxygen vacancies.

Since ß" ZrON produces no hydazine and it showed a comparable high activity as conventional catalyst even the ZrON has less specific surface area, it is interesting to optimize the catalyst by fuhrter investigation.

5. Appendix

5.1. Madonna – Simulation (450 °C) / mechanistic model:

{ NH3 <==> 0.5N2 + 1.5H2 }

r1=k3*c_Vac_t*K1*K2*K4*K5*NH3_1^2/(H2_1^1.5*NH3_1*K4*K5*(1+NH3_1*K1)+NH3_1^2*K1*K2*K4*K5+H2_1^3*(1+NH3_1*K4))

r2=k3*c_Vac_t*K1*K2*K4*K5*NH3_2^2/(H2_2^1.5*NH3_2*K4*K5*(1+NH3_2*K1)+NH3_2^2*K1*K2*K4*K5+H2_2^3*(1+NH3_2*K4))

r3=k3*c_Vac_t*K1*K2*K4*K5*NH3_3^2/(H2_3^1.5*NH3_3*K4*K5*(1+NH3_3*K1)+NH3_3^2*K1*K2*K4*K5+H2_3^3*(1+NH3_3*K4))

k3=4.8
K1=0.0097
K2=0.47
K4=0.0347
K5=3
c_Vac_t=0.00385

INIT NH3_1=0.0046598 , INIT NH3_2=0.0074962, INIT NH3_3=0.0100287
INIT H2_1=0, INIT H2_2=0, INIT H2_3=0
INIT N2_1=0, INIT N2_2=0, INIT N2_3=0

d/dt(NH3_1)=-r1
d/dt(H2_1)=1.5*r1
d/dt(N2_1)=0.5*r1

d/dt(NH3_2)=-r2
d/dt(H2_2)=1.5*r2
d/dt(N2_2)=0.5*r2

d/dt(NH3_3)=-r3
d/dt(H2_3)=1.5*r3
d/dt(N2_3)=0.5*r3

METHOD RK4

STARTTIME = 0, STOPTIME=0.43, DT = 0.00002

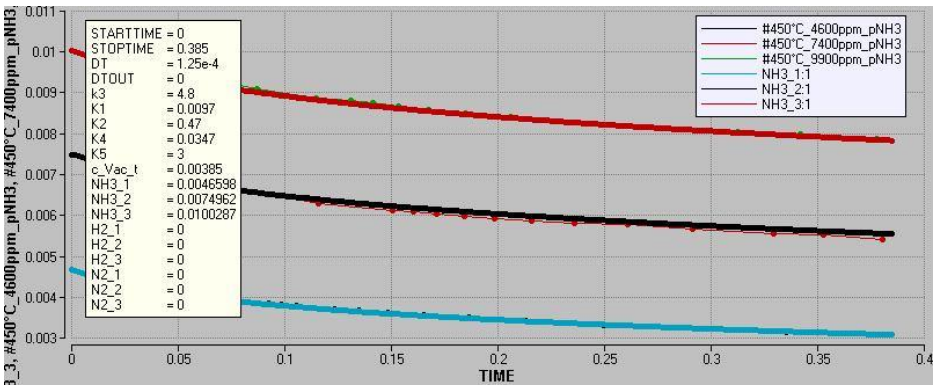

5.2. List of Abbreviations & Greek Symbols

5.2.1. List of Abbreviations

AFC: Alkaline Fuel Cell

BET : Stephen **B**runauer, **E**mmet & Erward **T**eller

BJH : Barrett, Joyner, Halenda

BtL: Biomass to Liquid

CarboPLOT P7: the CP-CarboPLOT P7 column is specially designed for the separation of N_2, O_2, CO, CO_2 and C1-C2 hydrocarbons

c_i = concetration of component i [$mol.L^{-1}$]

CRM: Combined Reforming of Methanol

CZC : $Cu/ZrO_2/CeO_2$

$D_{eff,i}$: effective diffusity of gas i [$m^2.s^{-1}$]

DME: Dimethylether

DMFC : Direct Methanol Fuel Cell

d_i : molecule diameter of gas i

d_p : pore diameter of membrane

DRIFT : Diffuse Reflection Infrared Transform

E_A : activation energy

E_k : the kinetic energy

FC: Fuel Cell

FWHM : the full width at half maximum

GC : gas chromatograph

HPLC : high pressure liquid chromatography

k : reaction constant

k_0 : pre-exponential faktor of reaction constant

k_f : rate constant of forward reaction

k_r : rate constant of reward reaction

K_i : adsoption or desorption constant of species i

L : charasteistic length of catalyst particle (d/4)

^{mi} : reaction order of species i

mari : most abundant reaction intermediates (on the catalyst surface)

MCFC : Molten Carbonate Fuel Cell

MD: Methanol Decomposition

MeOH : Methanol

MS : mass spectrometry

n_i = reaction order or mol of component i
OSRM : Oxidative Steam Reforming of Methanol
PAFC : Phosphoric Acid Fuel Cell
PEMFC : Polymer Electroliyte Membrane Fuel Cell
PFR : Plat-Fin Reformer
PFTR: Plug Flow Turbular Reactor
p_i : partial pressure of gas i
PID : proportional-integral-derivative (in control systems)
POM : Partial Oxidation of Methanol
ppm : parts per million
PSD : position sensitive detector of a X-ray diffractometer
r : reaction rate
RFC : reactive frontal chromatography
RMD: Reverse Methanol Decomposition
RME: Rapeseed Methyl Esther
RSRM: Reverse Steam Reforming of Methanol
RWGS: Reverse Water Shift Gas Reaction
SOFC : Solid Oxide Fuel Cell
SRM : Steam Reforming of Methanol
STOE Stadi P : powder diffractometer system of Stoe & Cie GmbH
t : time [s]
TCD : thermal conductivity detector
WGS : Water Shift Gas Reaction
X : conversion
XFA : X-ray fluorescence analysis
XPS : X-ray photoelectron spectroscopy
XRD : X-ray diffraction
Z_s : number of missing neighbours of an atom on the surface

5.2.2. List of Greek Symbols

$*$: free active site

ν_i : stochiometric coefficient of component i

η : efficiency

θ_i : coverage of species i

κ_0 : structure factor

Θ : angel

φ_i : the volume fraction of i

τ : retention time

ψ : Weisz modulus

ρ : density [$kg.m^{-3}$]

$\overline{\lambda}$: mean free path

σ : cross section of the molecule

$\alpha_{i,j}$: separation factor of gas j from gas i

$ß_i$: enrichment factor of gas i